國立臺灣大學電機資訊學院光電工程學研究所

博士論文

Department or Graduate Institute of Photonics and Optoelectronics
College of Electrical Engineering and Computer Science
National Taiwan University

Doctoral Dissertation

以廣義高斯常數使用於深紫外光學微影之成像與照明系統設計

Extreme Ultraviolet Lithography Projector and Illuminator Design with Generalized Gaussian Constants

蕭立人
Li-Jen Hsiao

指導教授：林晃巖 教授
Advisor: Prof. Hoang-Yan Lin

中華民國 108 年 7 月
July 2019

doi:10.6342/NTU201901098

國立臺灣大學博士學位論文

口試委員會審定書

以廣義高斯常數使用於深紫外光學微影之
成像與照明系統設計

Extreme Ultraviolet Lithography Projector and Illuminator Design with Generalized Gaussian Constants

本論文係蕭立人君（學號 D01941028）在國立臺灣大學光電工程學研究所完成之博士學位論文，於民國 108 年 3 月 25 日承下列考試委員審查通過及口試及格，特此證明

口試委員：

（指導教授）

所　長

Acknowledgements

To dad, thank you for the your constant support and encouragements over these long years. For the discussions, chats, and banters. And, for our coffee times.

To Prof. Lin, my advisor, teacher, and friend, thank you for taking me under your wing when I came to Taiwan. It was an honor and an enjoyment to be a part of your lab.

To my lab mates (before me), thank you guys for the many tips that made my daily PhD life much easier than I had first thought. Thank you guys for welcoming me into this small family that we call lab. (And for the short while that we gymmed together.) The time I spent here is an irreplacible part of my life, and I will treasure it always.

To my lab mates (after me), thank you guys for helping making the lab an enjoyable place to be. I wish you guys good luck in your studies, and that you would enjoy this lab part of your Master/PhD life as much as I had.

Li-Jen Hsiao

Feb. 2019

(To my fellow hunters Queen, 68, and Jemon, thank you for the adventures from 2G, P3, XX, to World. It has been a fun journey!

るー)

doi:10.6342/NTU201901098

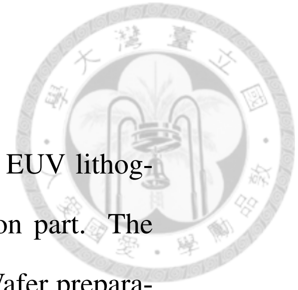

Abstract

This study aims to develop a systematic design procedure for the EUV lithography (EUVL) tools, for both the projection part and the illumination part. The optical lithography is a complex process encompasses many stages. Wafer preparation, resist coating, pre-exposure bake, exposure, post-exposure bake, etching, and metrology. Through analysis using generalized Gaussian constants (GGC), relationships between optical properties and requirements can be obtained, and can be used to help ensuring that optical system properties required for the tool are upheld during the design process.

The GGC is closely related to the ABCD matrix method, however over and above, it is also useful in analyzing the whole system as a combination of smaller subsystems, which can then again be broken down into even smaller subsystems to any degree desired. This abstraction of raw lens data into optical properties of the sub-systems at arbitrary level of abstraction is a great help in analyzing the inter-subsystem relations, which are easily lost in the raw expansion of the ABCD matrix of even a slightly larger optical system. In fact, the development of GGC was initially intended for purpose of zoom lens design and analysis, where inside the complex optical system the optical elements are constantly moving in relation to one another. This analytic power lends itself well to optics design of other applications, such as this case of EUVL projection systems.

As verification of the design method, this study demonstrates an eight mirror 0.4 NA projector, and its illuminator. In addition to the use of commercial design software, a simple Monte Carlo random walk algorithm is also deviced for the purpose of integrating the use of GGC into existing design software.

Keywords: EUV, lithography, imaging, non-imaging, optical system design

doi:10.6342/NTU201901098

中文摘要

此研究的主要目的爲開發及系統化極紫外光波段之光刻機之成像及照明系統的設計。 光刻爲一系列頗複雜的流程的組合。 其中，最爲關鍵的部分之一爲曝光這一步驟。曝光機的成像品質，於其成品的製程密度與解析度甚至於此製成的生產效率中間，存在直接的影響與關係。 然而，曝光機之光學系統特性，及其參數之間，存在著許多複雜且繁瑣之關係，導致於此光學系統不易分系，也不易設計。因此，此研究最爲核心的目的，爲研究及開發某一系統化之分析方法，以達到簡化此光學系統之設計之目的。 此研究核心之關鍵，爲將廣義高斯常數應用於光刻機之分析及設計上。 通過廣義高斯常數，眾多複雜且繁瑣之光學特性及光學系統之間之聯繫能以之表達及簡化，而將所有關係結合並簡化後，從中所導出之數學關係式可用於與商用光學設計軟體之結合，以達到幫助分析及設計簡化。

原理上，廣義高斯常數與光學分析中常用之 ABCD 矩陣極爲相似，唯一最大不同爲當以 ABCD 矩陣進行光學系統分析時，計算其矩陣及將其展開時，其難度及複雜性與其光學系統中光學元件之數量呈指數增長，因此，不適用於較爲複雜之光學系統分析。 而相較於 ABCD 矩陣，廣義高斯常數適用於表達及分析由多數光學系統組合所形成之相對複雜之光學系統，而其又可將之分解成更小之光學系統看待。 此廣義高斯常數之特性，可隨心將多數光學系統視爲一總光學系統，或是將一光學系統拆開以多數小光學系統看待，可適用於分析或推導個別光學元件之參數及整體光學系統特性之關係。

廣義高斯常數之最初用途爲變焦光學系統之分析及設計，其中通常有複數多件光學元件所組成之組合，及其爲配合不同使用狀況而改變位置及光學特性。 而將之強大分析能力應用於極紫外光刻機之分析及設計爲此研究之重要關鍵之一。 此研究之成果之一爲某一 0.4 數值孔徑之極紫外光刻機之反射式成像光學系統之分析與設計，以及其照明光學系統之分析與設計。 設計過程中所用之光學設計軟體中包含市售光學設計軟體，及一簡單 Monte Carlo 優化演算法將廣義高斯常數與市售光學設計程式結合使用以達成協助光學設計之目的。

關鍵字: 極紫外，光刻，成像光學系統，非成像光學系統，光學系統設計

doi:10.6342/NTU201901098

Contents

1 Introduction **14**

1.1 Lithography Overview . . . 14

1.1.1 Evolution of Lithographic Systems . . . 16

1.1.2 Lithography Systems . . . 23

1.2 Aerial Image Formation . . . 27

1.2.1 Partial Coherence . . . 30

1.3 Resolution . . . 34

1.3.1 Resolution Limit . . . 36

1.3.2 Resolution Enhancement Techneques . . . 39

1.4 EUV Lithography . . . 47

1.4.1 Extreme Ultraviolet Source . . . 48

1.4.2 Mirror Optics . . . 50

1.5 EUV Lithographic Tool Design . . . 58

1.5.1 Projector Design . . . 58

1.5.2 Illuminator Design . . . 60

2 Mathematical Methods **66**

2.1 Gaussian Bracket . . . 66

2.1.1 Definition . . . 66

2.1.2 Identities . . . 67

2.2 Generalized Gaussian Constants . . . 69

2.2.1 Definition . . . 69

2.2.2 Relationship to the Matrix Method . . . 69

2.2.3 GGC and Optical System Properties . . . 70

2.2.4 GGC in Mirror Systems for EUV . . . 75

2.3 Numerical Optimization . . . 76

2.3.1 Commercial Opical Design Software . . . 76

2.3.2 GGC Integrated Optimization . . . 80

doi:10.6342/NTU201901098

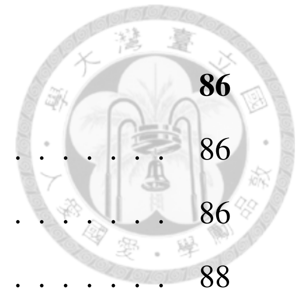

3 Projection Tool Design 86

3.1 Optical System Properties . . . 86

3.1.1 Telecentricity . . . 86

3.1.2 Magnification . . . 88

3.1.3 Mask-Wafer Conjugate . . . 89

3.1.4 Total Tract Length . . . 90

3.2 Number of Mirrors . . . 90

3.2.1 Notes on the Aperture Stop Position . . . 91

3.2.2 Mirror Pair Concept . . . 91

3.2.3 Multiple mirror pair expansion . . . 92

3.2.4 Mask and Wafer Side Working Distance . . . 94

3.2.5 Subsystem Magnifications . . . 94

3.3 Monte Carlo Random Walk Kernel . . . 95

3.3.1 Demonstration: Four-Mirror System . . . 98

3.3.2 Brief Note on Solution Convergence and Computation Time . . . 99

3.4 Eight-Mirror System . . . 102

3.4.1 Optical System Optimization . . . 103

4 Illuminator Design 109

4.1 Illumination Optics System Properties . . . 109

4.1.1 Pupil Matching . . . 109

4.1.2 Field Lens and Mask Position . . . 109

4.1.3 Grid Source NA and Exposure Field Width . . . 111

4.1.4 Illumination Optics NA and Collimated Plasma Source Beam Size 112

4.1.5 Pupil Pitch Size . . . 113

4.1.6 Number of Array Elements . . . 113

4.2 Illumination System Design . . . 114

4.2.1 First Order Analysis . . . 114

4.2.2 Resolving Obstructions . . . 115

4.3 Reflective Illuminator System Embodiment . . . 118

doi:10.6342/NTU201901098

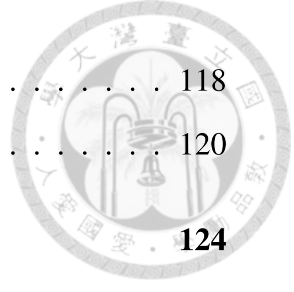

4.3.1 Illuminator Design Result 118

4.4 Illuminator Projector Integration 120

5 Conclusion **124**

6 References **125**

7 Appendices **130**

7.1 GGC Implementation into MATLAB 130

7.2 GGC Implementation into Code V 131

7.3 GGC Implementation into Zemax 134

doi:10.6342/NTU201901098

List of Figures

1 Basic structure of a lithography system. 15

2 A conventional projection lens is a complex optical system, often consisting of more than 20 to 30 lenses. 15

3 Early iterations of lithography projections. 17

4 Further developments with increasing NA, for higher resolution. 18

5 Introduction of aspheric lenses to reduce the number of lenses, and immersion techniques are employed to further increase NA (even beyond 1.0 NA), ... 19

6 The lens-mirror hybrid catadioptric systems. Intentional back-reflected paths using mirrors and beam-splitters are introduced to reduce chromatic aberration and Petzval curvature. 19

7 Further developments on the catadioptric systems sacrifice portions of the imaged field to eliminate the need for beam-splitters. 20

8 A one to one reduction ratio reflective lithographic projector curtesy of Perkin-Elmer, 1986. The intended feature size to be printed are on the order of 1 3 μmm. [1] 22

9 Completely reflective system designed to cater to the short wavelength EUV light source. [2] 23

10 An early iteration of a lithographic projector. 23

11 Telecentricity. **(a)** Image space telecentricity. **(b)** Object space telecentricity. 24

12 Double telecentricity. An optical system is double telecentric in the special case that it is both telecentric in the image space and in the object space. 25

13 The performance of optical systems in the case that the object is deviated from its designed position. **(a)** Generic non-telecentric system. **(b)** Object space telecentric system. 25

doi:10.6342/NTU201901098

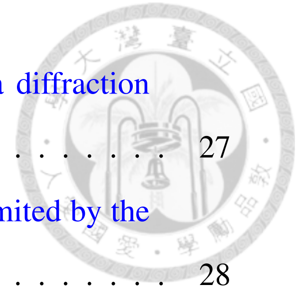

14 Light striking a binary mask of lines and spaces forming a diffraction pattern. 27

15 The maximum order of diffraction collected by the lens is limited by the physical size of the lens, which acts as an aperture. 28

16 The resulting electric field of the aerial image, of an illuminated binary mask through a lens. 29

17 The intensity profile of the aerial image. 29

18 The diffraction pattern formed by coherent illumination. 30

19 The diffraction pattern formed by partially coherent illumination. 30

20 The effect of partial coherence on resolution limit. **(a)** The aperture is able to capture the $\pm 1^{st}$ order diffraction completely. **(b)** The $\pm 1^{st}$ order diffraction moves further apart with finer mask pitch, some of the $\pm 1^{st}$ order information are lost causing degradations in the reconstructed aerial image. **(c)** At this mask pitch, the $\pm 1^{st}$ order diffraction almost moves outside the aperture completely, aerial image reconstruction of even finer mask pitch is impossible. The resolution limit. 32

21 A drawing of a simple gate device. Here, the CD would be how thin the walls can be made, and the pitch resolution would be how small one single unit can be printed. 34

22 A drawing of a grating device of lines and spaces of equal width. In this case, the CD and pitch resolution are closely related, with $\Lambda = 2 \cdot CD$. . . . 35

23 A simple diagram of an optical lithography exposure. Light from a source is redistributed onto the mask by the illuminator (the condensor lens). The illuminated mask is then picked up by the projector (the objective lens) and imaged onto the wafer. 36

24 Wave optics representation of the lithographic process. 37

25 To convey the pattern across, the NA of the optical system (given by $NA = \sin\theta_{max}$) must be large enough such that the $\pm 1^{st}$ order diffraction are collected. 37

doi:10.6342/NTU201901098

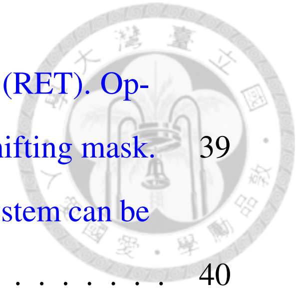

26 The three major types of resolution enhancement techniques (RET). Optical proximity correction, off-axis illumination, and phase-shifting mask. 39

27 Off-axis illumination. The imaging resolution of an optical system can be doubled simply by tilting the angle of the illumination optics. 40

28 Using a phase shifted mask effectively doubles the periodicity of the mask pattern. 41

29 Optical proximity correction makes minor adjustments to the mask such that the imaged pattern stays the same to the pattern intended as much as possible. 42

30 the location of the $\pm 1^{st}$ order diffraction shifts according to the local pitch of the mask pattern illuminated. 44

31 The forbidden pitch, where the 1st order diffraction is at the center of the pupil, with maximum OPD. 45

32 Comparison between off-axis illumination and phase shift mask. 45

33 If the imaging target is immersed, the effective NA in air is enhancd by a factor almost equal to the refractive index of the the immersion medium/fluid. 47

34 Basic schematic of EUV generation. 49

35 A mechanism to prevent (or reduce the amount of) byproducts of the EUV source from entering and contaminating the lithographic optical system. [3] 50

36 Thermal expansion of Schott's Zerodur. 51

37 Thermal expansion of Corning's ULE. 52

38 Reflection spectrum of the 40 Mo/Si multilayer coating. [4] 53

39 Anuglar reflection distribution of the 40 Mo/Si multilayer coating. [4] . . 53

40 Candidates of the reflection depth offset. **(a)** Without the multilayers, the reflection occurs at the surface interface. **(b)** At the bottom of the multilayers. **(c)** At the top of the multilayers. **(d)** Somewhere inside the multilayers. 54

doi:10.6342/NTU201901098

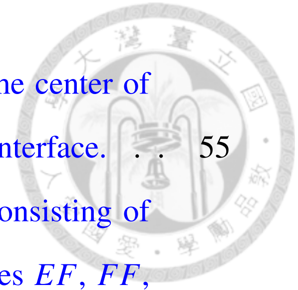

41 The reflections of the EUV light over a multilayer stack. The center of the reflection lies inside the stack towards the air-multilayer interface. . . 55
42 Basic configuration of the lithographic projection system, consisting of two subsystems separated by an aperture stop. The quantities EF, FF, BF, and thc are the effective focal length, front focal length, back focal length, and thickness of the two subsystems respectively. 60
43 A diagram of an illuminator in Kohler illumination configuration with a matching imaging optical system. 61
44 Effect of the partial coherence RET. **Top:** Coherent illumination. **Bottom:** Partially coherent illumination. Broadened diffraction spot allows the limit of the ± 1 order to be collected at a larger angle (i.e. higher resolution). 62
45 A diagram of the Kohler integrator configuration. 64
46 A diagram of the ringfield mirror array, or fly eye reflector. 64
47 The effective focal length, back focal length, and front focal length of an optical system. 71
48 Illustration of a finite conjugate optical system. 73
49 **Upper**: The paraxial representation of an optical system formulated with GGC. **Lower**: The exact same optical system represented using reflective elements. 75
50 Example of a solution space with two local minima. 81
51 Flow diagram of the Monte Carlo random walk algorithm. 84
52 Defocus on a non-telecentric system causes blurring and image shift, while on a telecentric system only blurring occurs. 87
53 A subsystem can be further expanded into multiple mirror pairs, represented by the individual lens modules. **Upper**: Expansion into two mirror pairs. **Lower**: Three mirror pair expansion. 93
54 A flow diagram of the Monte Carlo random walk algorithm. 96

doi:10.6342/NTU201901098

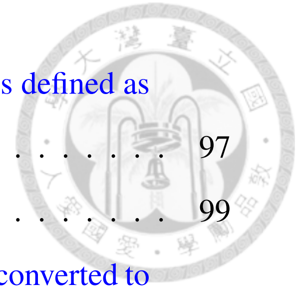

55 The amount of obstruction between a ray bundle and mirror is defined as the angle of the overlapping region. 97
56 The initial state of the four mirror trial run. 99
57 Four-mirror system optimization using Code V. Lens module converted to real mirror surfaces. Lens data and module properties are listed in Table 5. 100
58 Monte Carlo random walk result of an eight-mirror system. 102
59 Initial state of the 8-mirror system, and its spot diagram. The mirror surface profiles at this point is entirely spherical. 104
60 The state of the 8-mirror system after optimization runs, after allowing the conic constants of the surface profiles to vary. 105
61 Layout of an eight-mirror EUVL system. 106
62 The MTF performance of the eight-mirror EUVL system. 107
63 Wavefront aberration of the six defined field positions. **Top Row**: Center, top, and bottom fields on the tangential plane respectively. **Bottom Row**: Center top, and bottom fields at full horizontal mask width. 107
64 The marginal ray angles at the grid source and at the projection tool entrance pupil is related to the magnification of the finite conjugate system formed by the elements in between. 111
65 The illumination NA is directly related to the beam size of the collimated LPP source. 112
66 The number of array elements on the pupil array determines the array pitch and the grid source NA. 113
67 An initial evaluation of the governing equations. 115
68 The amount of obstruction between a ray bundle and mirror is defined as the angle of the overlapping region. [5] 116
69 The same initial evaluation with a 5° tilt introduced. 116
70 Obstruction resolved paraxial layout. The tilt angle required is $\theta_{tilt} = 6.991°$. 117

doi:10.6342/NTU201901098

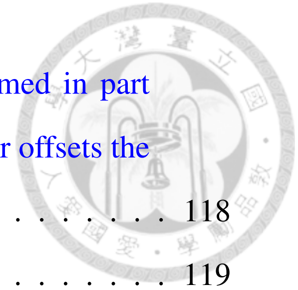

71 Direct conversion from the paraxial result. The lower zoomed in part shows that aberration resultant from the plain spherical mirror offsets the illumination profile from different array elements. 118
72 The aberration corrected illuminator. 119
73 The eight mirror projector design from which the illuminator specifications are derived from. 120
74 The combined system of the illuminator and the projector. 121
75 **Upper**: The resultant ringfield illumination profile at the mask side. **Lower**: The illumination profile at the wafer end. 122

doi:10.6342/NTU201901098

List of Tables

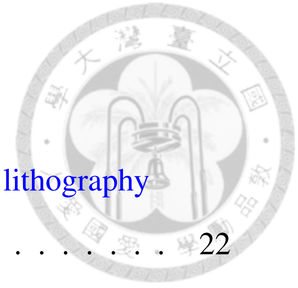

1 The general trend of source wavelength reduction from early lithography history. 22
2 Types of illumination coherence. 31
3 Specification of a EUVL tool design trial run. 97
4 Initial lens module parameters of the optimization run. The four free variables are marked with an asterisk (*), the remaining parameters are dependent. 98
5 Random walk result of the four-mirror system. Left: Lens module properties. Right: Conversion to raw lens data. 99
6 Basic lens data of the eight-mirror system, displaying the radius of curvature R, thickness T, conic constant K, and aspheric coefficients from A_4 to A_{12}. 108
7 RMS wavefront error and Zernike coefficients (tilt and defocus) in wavelength unit. 108
8 A set of specification and initial condition of the illuminator design. 115
9 Initial evaluation of the governing equations using specification and initial conditions provided in Table 8. 115
10 Obstruction resolved illuminator parameters. 117
11 Obstruction resolved illuminator parameters. 119

doi:10.6342/NTU201901098

1 Introduction

1.1 Lithography Overview

The lithography process is a major part of the process chain of the manufacturing of a semiconductor device. Typically in the manufacturing of an integrated circuit chip, lithography can account for up to 30% of its manufacturing cost. As such, the progress in the development of lithography systems is of great interest to the semiconductor industry. [6]

In particularly, the optical lithography systems have received much attention, as historically the technological advancements in semiconductor mass manufacturing are often gated by the progress in optical lithography. In the past when the progress in optical lithography reaches a bottleneck, the industry has attempted to look at the alternative lithography methods to potentially replace optical lithography, such as e-beam and x-ray lithography. After all is considered however, as each of the bottlenecks were overcame the optical lithography quickly regains its place as the most important lithography method, as out of all of them the optical lithography remains the most economical and the most efficient way to mass manufacture semiconductor devices to this day. [7] [8]

The optical lithography process encompasses many stages, usually starting with wafer preparation, then resist coating, pre-exposure bake, exposure, post-exposure bake, etching, and then finishing with metrology. During the exposure stage, light from the source is first redistributed and reshaped by an illuminator before striking the mask. The patterns on the mask, now illuminated, is then picked up by the projection tool, and is transferred

doi:10.6342/NTU201901098

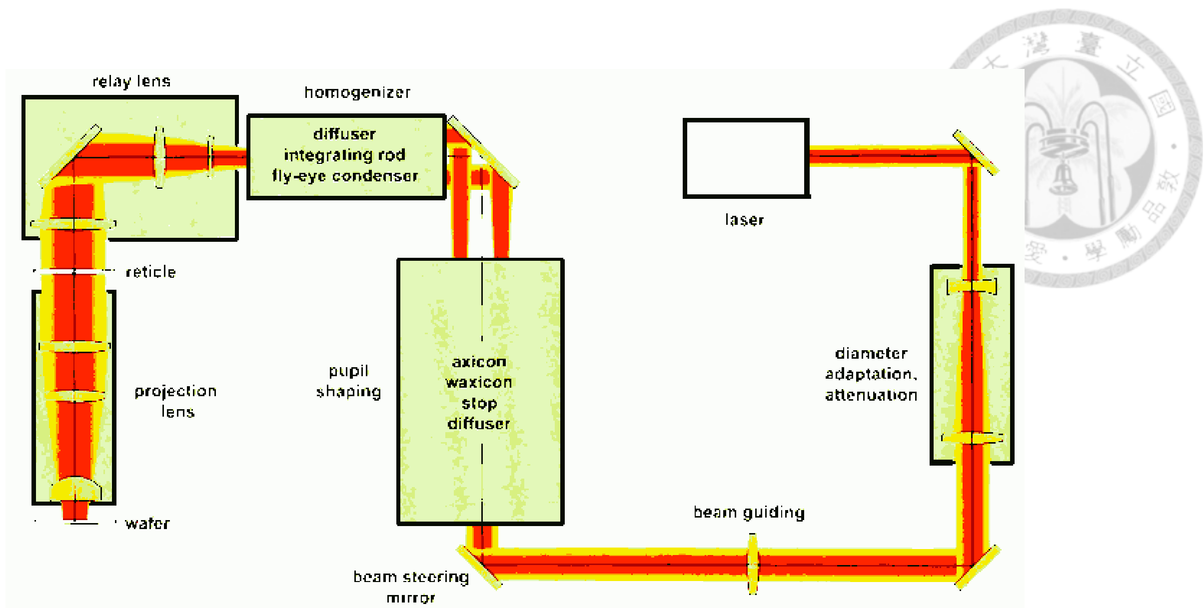

Figure 1: Basic structure of a lithography system.

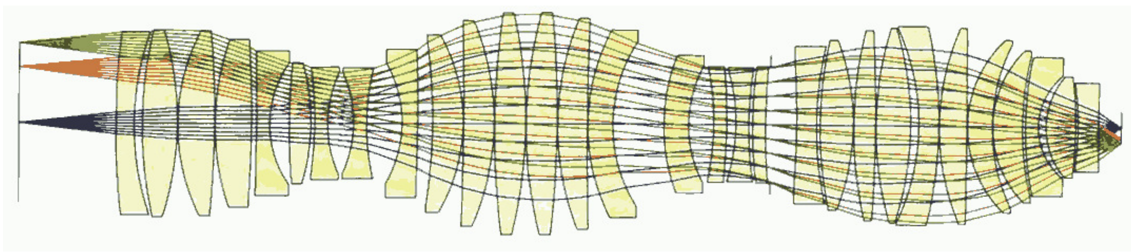

Figure 2: A conventional projection lens is a complex optical system, often consisting of more than 20 to 30 lenses.

to the photoresist coated on the wafer. Figure 1 shows a typical illuminator and projector arrangement, using a laser as the light source.

Figure 2 is a diagram of a conventional lithography projection lens. The lithography projector is an essencial part of optical lithography process, and is conventionally composed of many lenses, spanning well over a meter in length. The designing of a lithography tool, portrayed in many textbooks as the pinnacle of imaging optical system design. The sheer number of optical elements required, coupled with the stringentness of the required imaging quality, all contributes to the overall design difficulty. Despite the difficulty, designers have little choice but to continue to tackle the task, as the design and manufacturing of this projection system will largely determine the resolution and performance of the lithography process.

Aside from the projection tool, other aspects of the lithography also have significant impact on the lithography performance. Regarding the resolution of the lithography pro-

doi:10.6342/NTU201901098

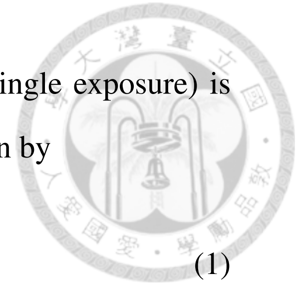

cess, a commonly accepted fact is that the resolution (of a straight single exposure) is determined by the numerical aperture (NA) of the projection tool, given by

$$R = k_1 \frac{\lambda}{NA}. \tag{1}$$

1.1.1 Evolution of Lithographic Systems

Early Developments

The lithographic projection system is a relatively recent development in the field of optical design. Historically, early attempts at designing lithographic projectors results in a high NA but small FOV systems. The wavelengths used are in the blue region of the visible spectrum, where conventional glass materials can be used.

Since its early stages, improvements in the lithography techniques has been partly driven by the extrapolation of Moore's observation in 1965, that the number of components on an integrated circuit chip would double every year reaching roughly 1000 times to what it was by 1975, [9] and indeed for the first decade the semiconductor industry kept up with the trend. However for future decades to come the trend was proven to be too difficult and optimistic for the industry to follow, and Moore himself made adjustments to his observations extrapolated a gentler slopes for future semiconductor manufacturers. [10] [11] Of course, simply by common sense would dictate that Moore's Law cannot continue forever, however as the years advance the market and the industry has seen an ever increasing need for higher lithography resolution.

This need for higher and higher resolution pushed later development towards shorter wavelengths, with increasing NA and FOV, and consequently tighter performance requirements. Among the designs, some special cases exist which are quite insightful in terms of optical system design. In particular, the designs of a field flattener, and the design of a chromatic aberration corrector with only one available glass material. The technology and unerstanding of several aspheres within one system, as well as the principles of catadioptric and mirror systems have been possible as a result of these developments.

More physical optical questions occur during the development of the various gen-

doi:10.6342/NTU201901098

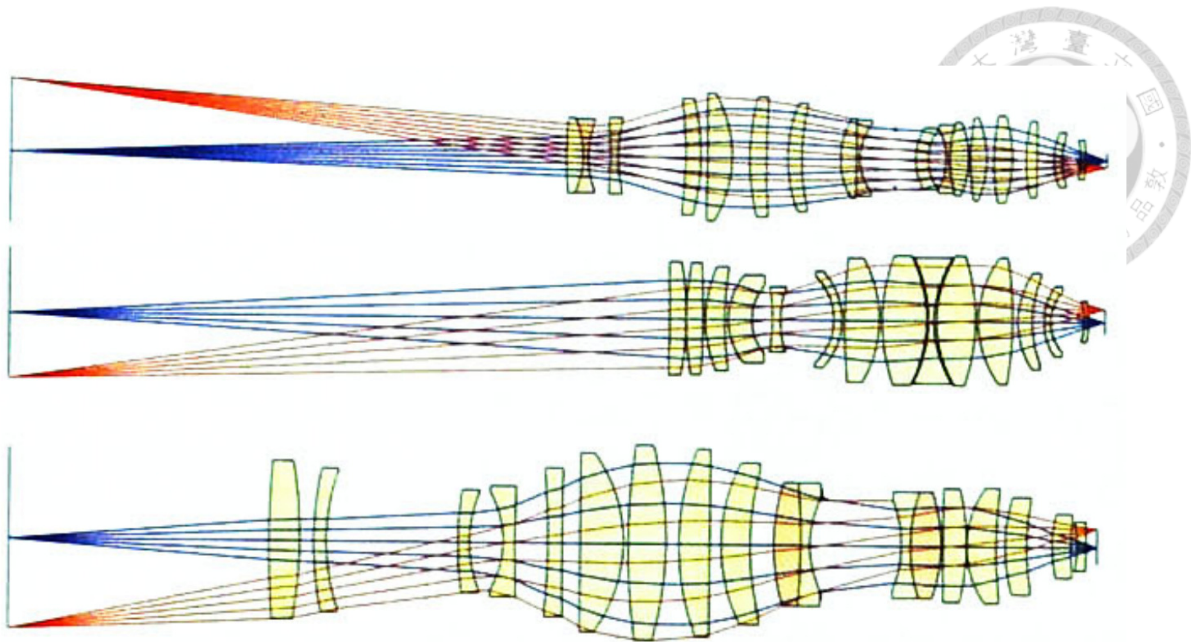

Figure 3: Early iterations of lithography projections.

erations of lithographic systems. The understanding of polarization, the correction and control of birefringence, the theory of simulation for high NA and artial coherent illumination are all developed further within this context. Therefore, although the systems of this type are very situational, they will be discussed in more details.

Figure 3 are some examples of early lithographic projectors. [12] [13] Historically, early projectors consists of a retrofocus photographic lens at the front, and a scaled microscopic lens in the rear. [44-6] The mask side will have a larger field due to the reduction ratio (usually between 0.2 to 0.25), and the wafer side has a smaller field but high NA. Combined together, the two systems forms a complete lithographic system.

Following, in the years of development, the size of the lithography system gradually increased. To enhance the resolution (Equation 1), one possible way is to increase the NA of the projector, as can be seen in Figure 4. [14] [15] However, systems with larger NA generally results in more severe geometric aberrations, which results in the need for lithographic systems to house more and more lenses in the hope to correct the aberrations. To help supressing the aberrations, the angle of refraction at each interface are kept to a minimum, which results in the characteristic smooth bulges and waists in lithographic systems.

doi:10.6342/NTU201901098

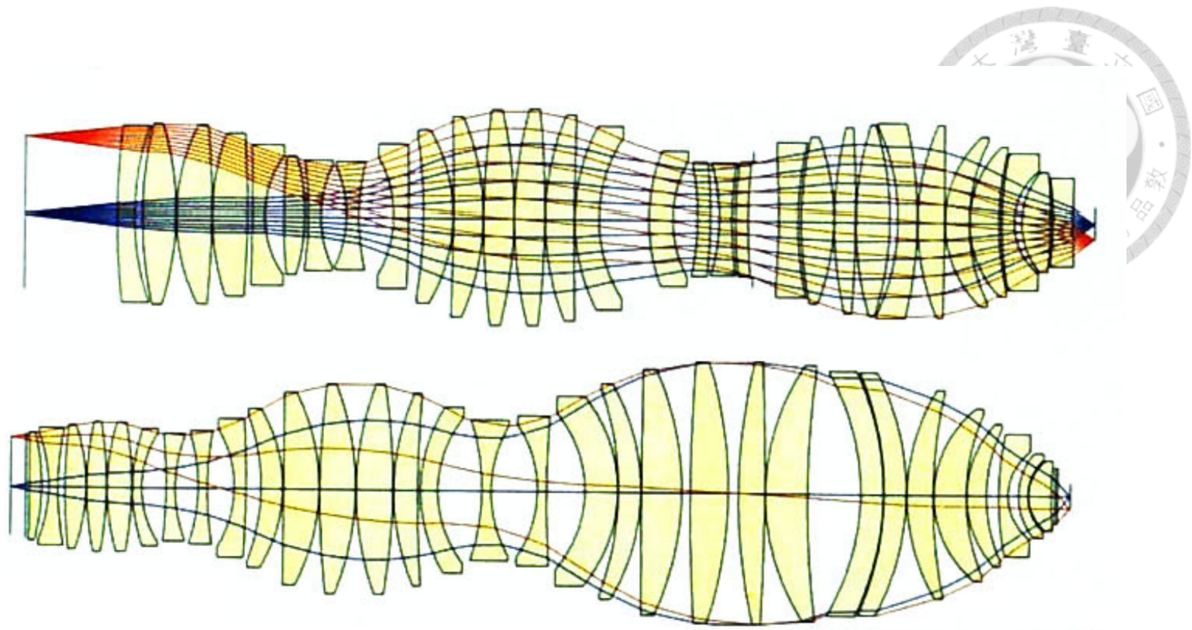

Figure 4: Further developments with increasing NA, for higher resolution.

Aspheric Lenses and Immersion

Beginning around year 2000, the need to reduce the size of the lenses and progress in manufacturing technology allows the inclusion of aspherical surfaces inside the lithographic projection lenses. This considerably reduces the number of lenses required, and the necessary lens diameter of the high NA lenses compared to purely spherical systems of the same NA, as can be seen in Figure 5. [16] With aspheres, the NA of dry systems can be enhanced to roughly 0.95, and if immersion fluids are used (e.g. water), increasing the NA beyond 1.0 is possible. [17]

Catadioptric Systems

Since high NA system leads to large lens diameters in the rear lens groups, problems occur in correcting aberrations and obtaining a good uniformity in the material. Immersion systems are particularly different in their behavior. For this reason, the catadioptric systems, shown in Figure 6, have been introduced. [18] [19] [20] The mirrors help in correcting the Petzval curvature, while the Schupman principle can be used to correct axial chromatic aberrations. The size of the systems can be reduced by a considerable factor, and a NA of 1.35 can be achieved. In Figure 7, a further development upon the catadioptric systems removes the need of a beam splitter cube (which are used at the cost of a 75% decrease

doi:10.6342/NTU201901098

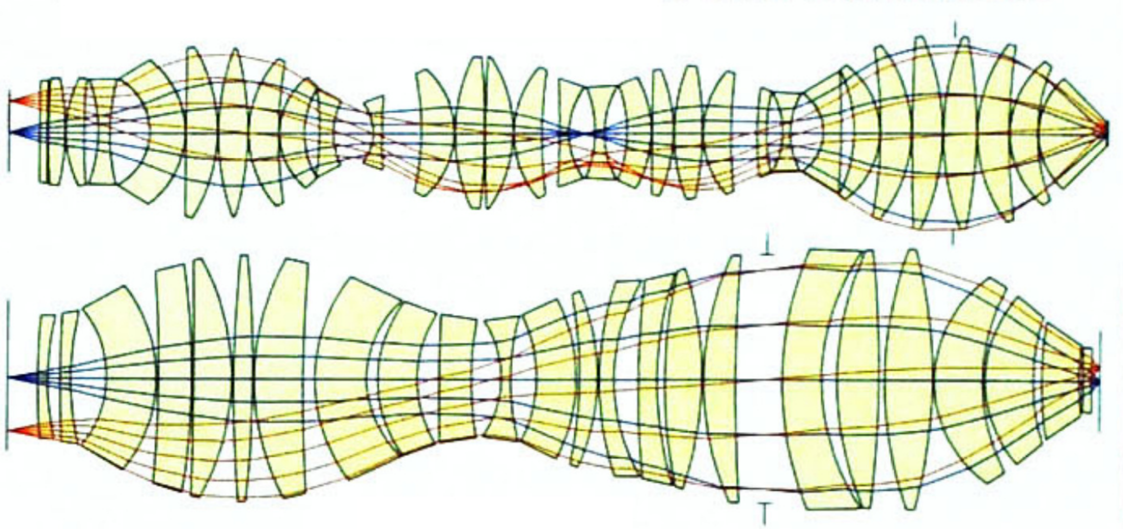

Figure 5: Introduction of aspheric lenses to reduce the number of lenses, and immersion techniques are employed to further increase NA (even beyond 1.0 NA),

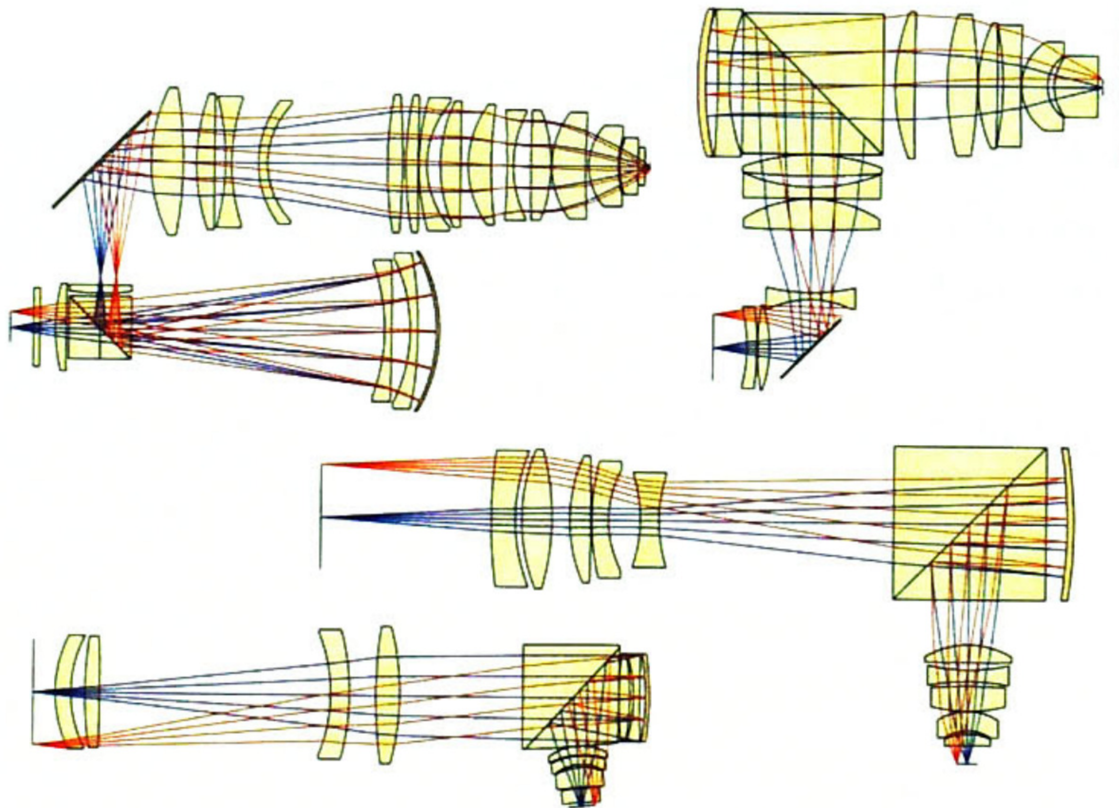

Figure 6: The lens-mirror hybrid catadioptric systems. Intentional back-reflected paths using mirrors and beam-splitters are introduced to reduce chromatic aberration and Petzval curvature.

doi:10.6342/NTU201901098

Figure 7: Further developments on the catadioptric systems sacrifice portions of the imaged field to eliminate the need for beam-splitters.

doi:10.6342/NTU201901098

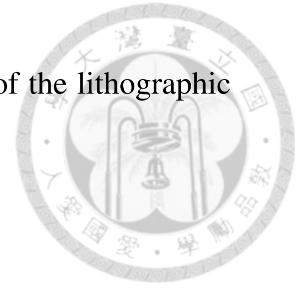

in the aerial image brightness), by trading in half of the usable FOV of the lithographic system. [21] [22] [23] [24]

Reflective Systems

The use of all reflective projection system coupled with a short wavelength source in optical lithography can be dated back over 30 years ago. Figure 8 shows one such early iteration of an all reflective projector, with 1:1 reduction ratio for printing features with size on the order of $\sim 1\ \mu m$. [1]

Table 1 shows a general trend of source wavelength usage from the early history of lithography. For higher resolution, the natural course of action would be to further reduce the wavelength of the light source, since the optical system NA can only be increased to so much, to a maximum of 1 in vacuum or ~ 1.3 by immersion. Following the trend in choosing shorter and shorter wavelengths, the next wavelength after the 193 nm line is the 157 nm line. The problem of using the F_2 laser line at 157 nm wavelength is to be used in projection lithography to obtain a better resolution, only calcium flouride CaF_2 can be used as the transparent material due to the absorptions in other materials.

At 157 *nm*, the corresponding spectral line has a poor efficiency and therefore the line narrowing cannot be achieved as it can for other longer wavelengths. Therefore the need to achromatize the projection lenses has generated some investigation into how to use diffractive elements to correct the system for chromatic aberrations. In principle, this is a possibility, however no current industrial system employs this method. The problem of stray light and the manufacturing of the microstructure tolerances to guarantee the high performance are a severe problem.

Therefore, instead of progressing to the 157 nm lithography, the advent of the immersion method using 193 nm lithography became the next milestone. However, this solution is only temporal, as the NA increase provided by the immersion method is limited. As the search continued for shorter wavelengths, the next possible source discovered is the 13.4 nm line in the EUV region. In the past, the decrease in wavlength has been gradual, however this time the wavelength is an entire magnitude lower from the previous

doi:10.6342/NTU201901098

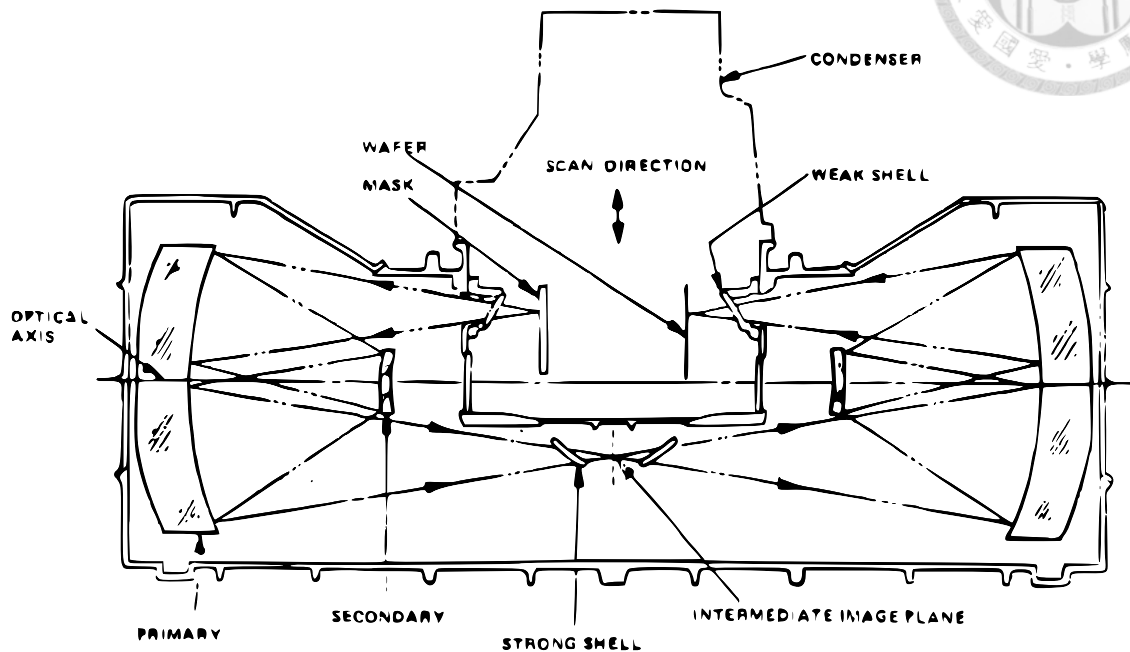

Figure 8: A one to one reduction ratio reflective lithographic projector curtesy of Perkin-Elmer, 1986. The intended feature size to be printed are on the order of 1 3 μmm. [1]

Table 1: The general trend of source wavelength reduction from early lithography history.

Wavelength (*nm*)	Source
405	Hg lamp h-line
365	Hg lamp i-line
248	KrF excimer laser (DUV)
193	ArF excimer laser (VUV)
157	F_2 excimer laser
(193)	In conjunction with immersion technique
13.4	Syncrotron radiation or plasma source (EUV)

 doi:10.6342/NTU201901098

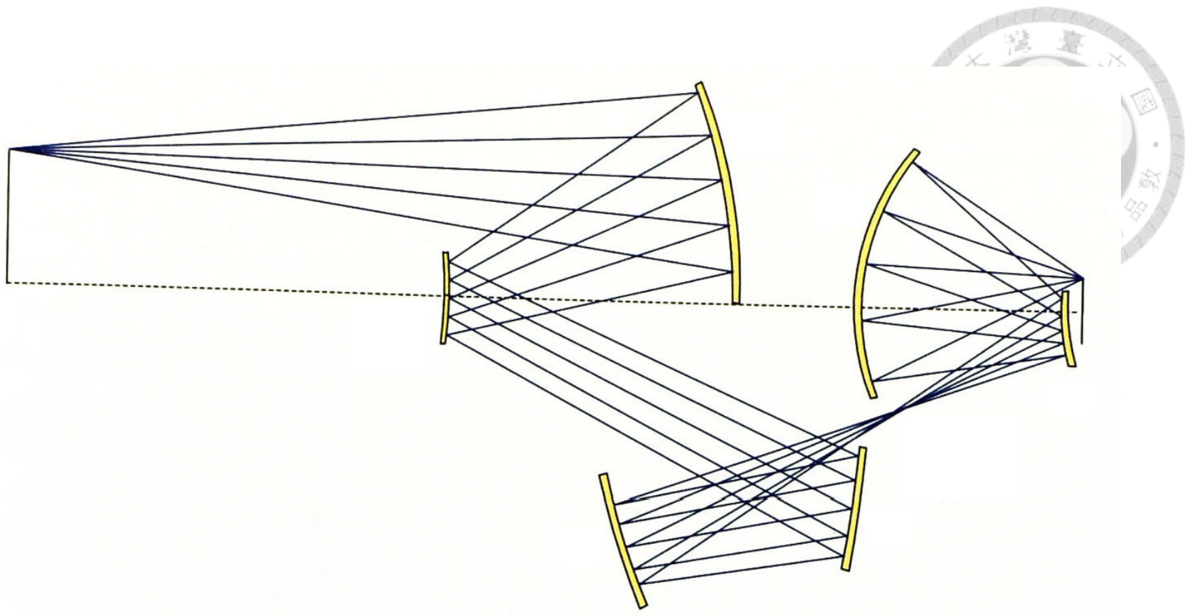

Figure 9: Completely reflective system designed to cater to the short wavelength EUV light source. [2]

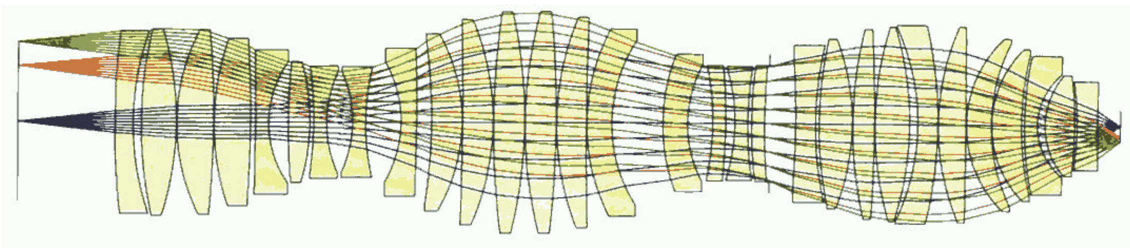

Figure 10: An early iteration of a lithographic projector.

generation.

Due to the high absorption of light in the EUV region exhibited in most mediums, the optical system is forced to use only reflective elements (i.e. mirrors). Figure 9 is an example of such an all reflective optical system. [2] Aside from having only reflective elements, the system must also be placed inside a vacuum environment, since the absorption at the EUV wavelengths is high even in air.

1.1.2 Lithography Systems

The basic operation of a lithography system are as follows. Light from the source is first redistributed and reshaped, by an illuminator system, before striking the mask. The pattern on the illuminated mask is then picked up, by a projector system, and imaged onto the wafer. Shown in Figure 10 is a typical projection lens during the early stage in the history of optical lithography, a complex optical system often consisting of more than 20

doi:10.6342/NTU201901098

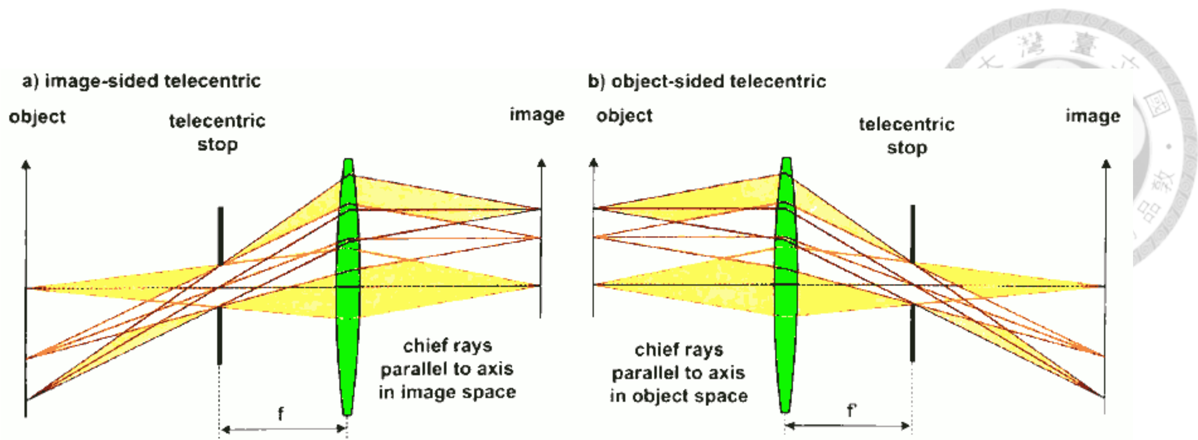

Figure 11: Telecentricity. **(a)** Image space telecentricity. **(b)** Object space telecentricity.

to 30 lenses.

During the manufacturing of a device, overlaying multiple exposures are often needed in lithography processes. Therefore one crucial requirement on the projection system is that, small deviations in the axial direction do not influence the lateral position of the image. This leads to the following conditions:

- Telecentricity in both the mask (object) space, and the wafer (image) space.
- Extremely well corrected distortion aberration in the aerial image.

Telecentricity

There are three types of telecentric systems. Image space, object space, and double telecentricity. An optical system is image space telecentric when the chief rays of the optical system emerge parallel to the optical axis before arriving at the image in the image space. On the other hand, an optical system is object space telecentric when the chief ray from the object is parallel to the optical axis prior to entering the optical system, in the object space. Figure 11 is a diagram showing the setup of the optical system when the optical system is telecentric in the image sapce, and in the object space.

In the special case that the optical system is telecentric in both its image space and object space, the optical system becomes double telecentric. For an optical system to be doubly telecentric, the system must be afocal. The advantage of a telecentric system is that the magnification of the optical system is invariant in the presence of defocusing.

doi:10.6342/NTU201901098

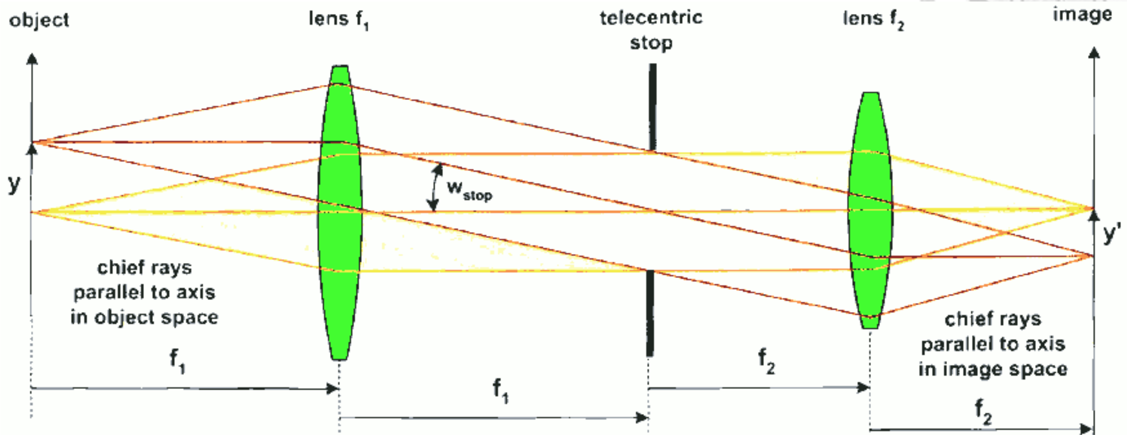

Figure 12: Double telecentricity. An optical system is double telecentric in the special case that it is both telecentric in the image space and in the object space.

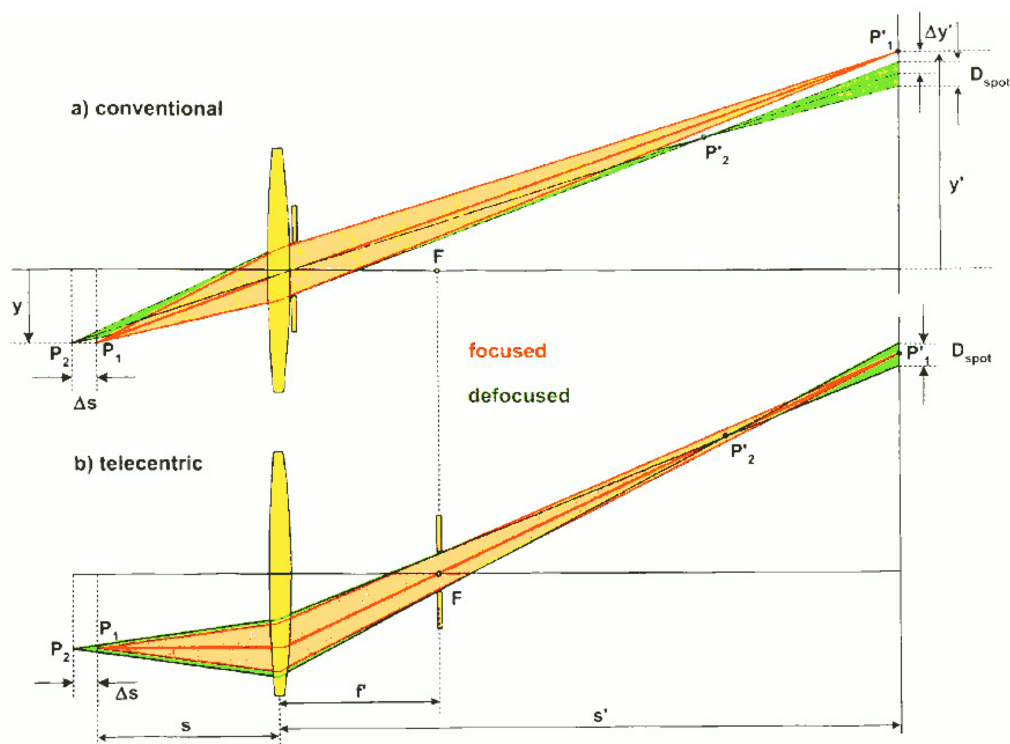

Figure 13: The performance of optical systems in the case that the object is deviated from its designed position. **(a)** Generic non-telecentric system. **(b)** Object space telecentric system.

doi:10.6342/NTU201901098

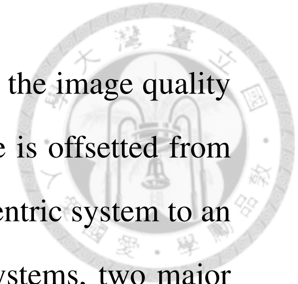

Even if the optical system is designed and manufactured perfectly, the image quality will suffer nonetheless if during operation the object and image plane is offsetted from its designated positions. Figure 13 shows a comparison of a non-telecentric system to an object space telecentric optical system. For non-telecentric optical systems, two major effects of defocus are blurring (image quality degradation) and change in image magnification. If the system is telecentric, then the optical system have one less thing to worry about since the change in the image magnification is eliminated.

doi:10.6342/NTU201901098

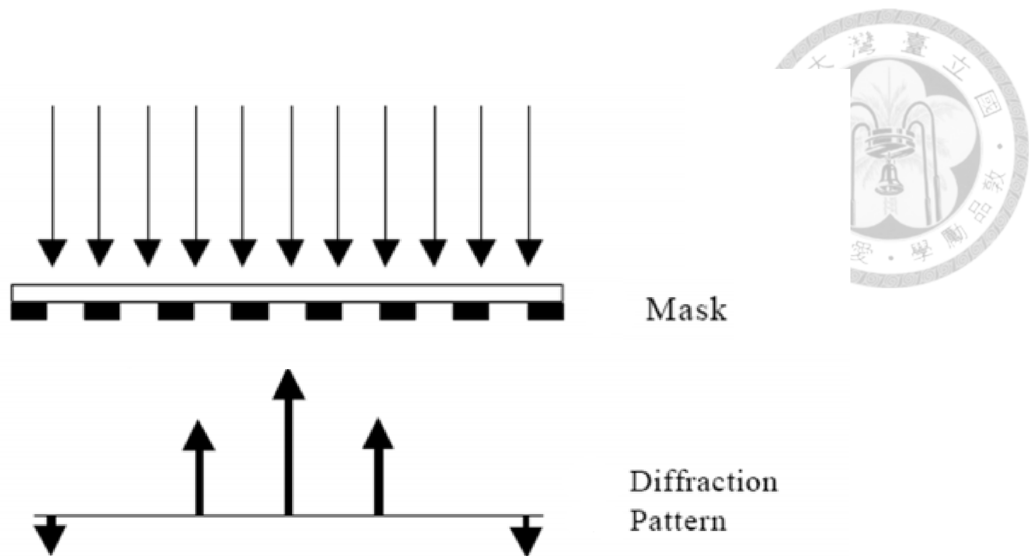

Figure 14: Light striking a binary mask of lines and spaces forming a diffraction pattern.

1.2 Aerial Image Formation

The aim of optical projection lithography, is to print an image of the reticle onto the wafer. To this end, we must first understand how an image is formed in the first place. For a start, consider the simple example of light striking a binary mask pattern of lines and spaces of equal width.

First, as depicted in Figure 14, light from the exposure system strikes the mask, forming a diffraction pattern, given by

$$M(f_x) = \sum_{n}^{\infty} \frac{\sin(\pi w f_x)}{\pi f_x} \delta(f_x - \frac{n}{p}), \tag{2}$$

where f_x is the lateral distance in space perpendicular to the direction of propagation, w is the angular frequency of the phase, p is the pitch of the mask, and n is the order of diffraction. The projection lens then picks up the diffraction pattern.

Due to the finite size of the lens, after passing through it the lens acts as an aperture, effectively limiting the number of the diffraction orders collected, as shown in Figure 15. Typically, when considering the resolution limit, only the 0th order and the $\pm 1^{st}$ order are collected. Therefore, by limiting the diffraction function (Equation 2) to within the $\pm 1^{st}$

doi:10.6342/NTU201901098

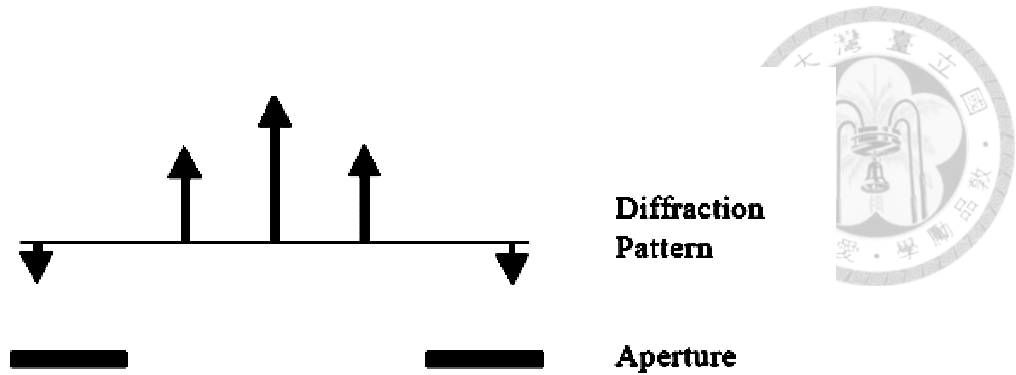

Figure 15: The maximum order of diffraction collected by the lens is limited by the physical size of the lens, which acts as an aperture.

order, the pattern after the aperture is

$$M(f_x) = \frac{\sin(\pi w f_x)}{\pi f_x}\left(\delta(f_x) + \delta(f_x - \frac{1}{p}) + \delta(f_x + \frac{1}{p})\right). \tag{3}$$

After travelling through the lens, the collected diffraction orders then recombines at the image plane and superpositions to form the aerial image, which can be obtained by an inverse Fourier transform of the aperture function (Equation 3), with electric field

$$E(x) = \frac{1}{2} + \frac{2}{\pi}\cos(\frac{2\pi x}{p}) \tag{4}$$

and intensity

$$\begin{aligned} I(x) = & \frac{1}{4} + \frac{2}{\pi}\cos(\frac{2\pi x}{p}) \\ & + \frac{4}{\pi^2}\cos^2(\frac{2\pi x}{p}), \end{aligned} \tag{5}$$

iluustrated in Figures 16 and 17.

doi:10.6342/NTU201901098

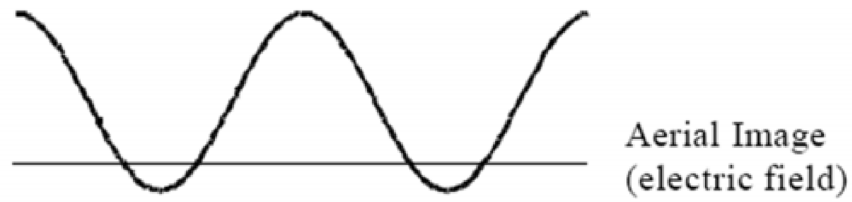

Figure 16: The resulting electric field of the aerial image, of an illuminated binary mask through a lens.

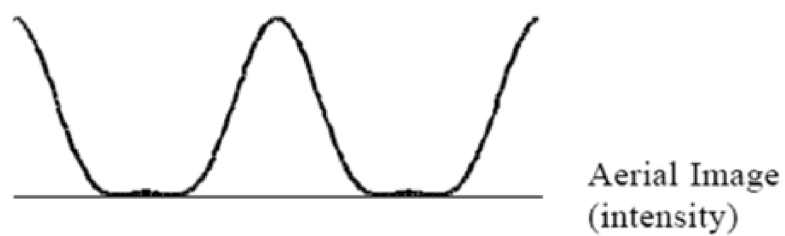

Figure 17: The intensity profile of the aerial image.

doi:10.6342/NTU201901098

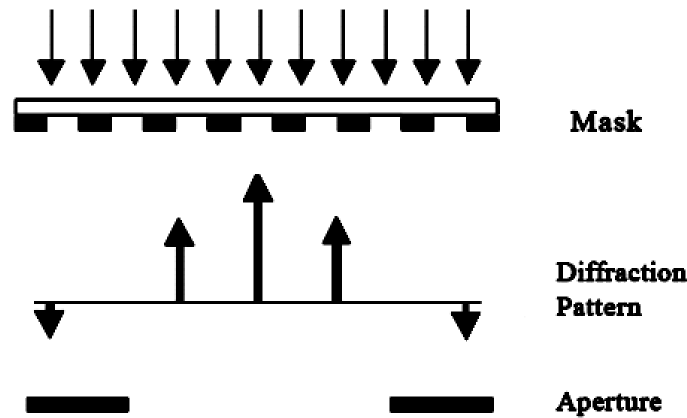

Figure 18: The diffraction pattern formed by coherent illumination.

1.2.1 Partial Coherence

In lithography, the coherence of illumination refers to the range of the angle of the illumination. Different degrees of coherence affects both the resolution and depth of focus of the resultant aerial image. Depicted in Figure 18 is a diffraction pattern resultant from the mask illuminated by a parallel beam of light (coherent illumination), captured by the aperture. If the illumination is partially coherent, the light strikes the mask over a range of angles. This results in a broader diffraction pattern, as can be seen in Figure 19.

The degree of partial coherence is measured by a partial coherence factor σ (also referred to as the pupil filling factor), given by

$$\sigma = \frac{d}{D} \tag{6}$$

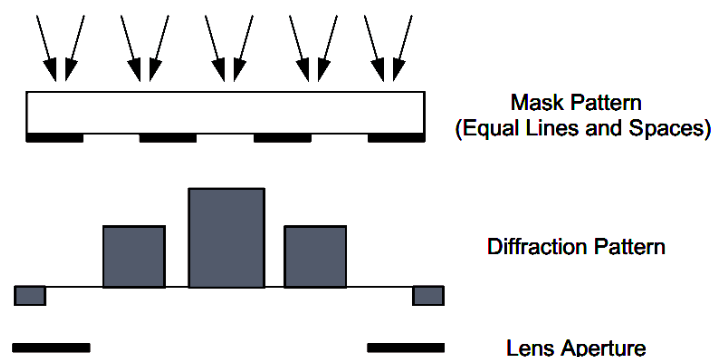

Figure 19: The diffraction pattern formed by partially coherent illumination.

doi:10.6342/NTU201901098

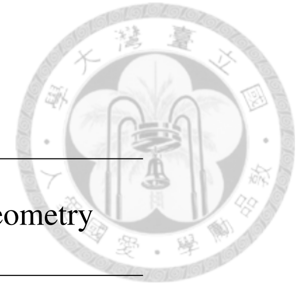

Table 2: Types of illumination coherence.

Illumination Type	Partial Coherence Factor σ	Source Geometry
Coherent	$\sigma = 0$	Point
Partially Coherent	$0 < \sigma < 1$	Finite size and circular
Incoherent	$\sigma \geq 1$	Infinite size

where d is the diameter of the source illumination on the entrance pupil, and D is the diameter of the entrance pupil of the lithographic projector. A partial coherence factor of zero ($\sigma = 0$) means that the illumination is completely coherent, which is possible only with a singular point source. A partial coherence factor between zero and one ($0 < \sigma < 1$) means that the illumination is partially coherent, and that the source is of a circular shape with finite size. A partial coherence factor of one or greater ($\sigma \geq 1$) signifies that the illumination is incoherent. The types of coerence above are also listed in Table 2.

By employing partial coherence, the pitch resolution can be further improved. Consider the case where some amounts of partial coherence σ is present. First, in Figure 19(a), the entrance pupil is sufficiently large that the information necessary to reconstruct an image of the reticle, the 0th and the $\pm 1^{st}$ order diffraction, are collected. Following in Figure 19(b), as the mask pitch becomes finer, the diffraction orders move further apart, and parts of the $\pm 1^{st}$ order diffraction failed to be picked up by the lens entrance pupil, lowering the image constrast. However, the pitch resolution is extended. In Figure 19(c), at this point the $\pm 1^{st}$ order diffraction almost moved completely outside the lens entrance pupil. As such, the reconstruction of the aerial image of even finer mask pitch is impossible, because without the$\pm 1^{st}$ order diffraction, the 0th order contains essentially only a constant level of background energy, therefore no image can be formed. The resolution limit.

Mathematically, the pitch resolution limit of the mask is given by

$$\frac{1}{p} = \frac{NA}{\lambda} \tag{7}$$

doi:10.6342/NTU201901098

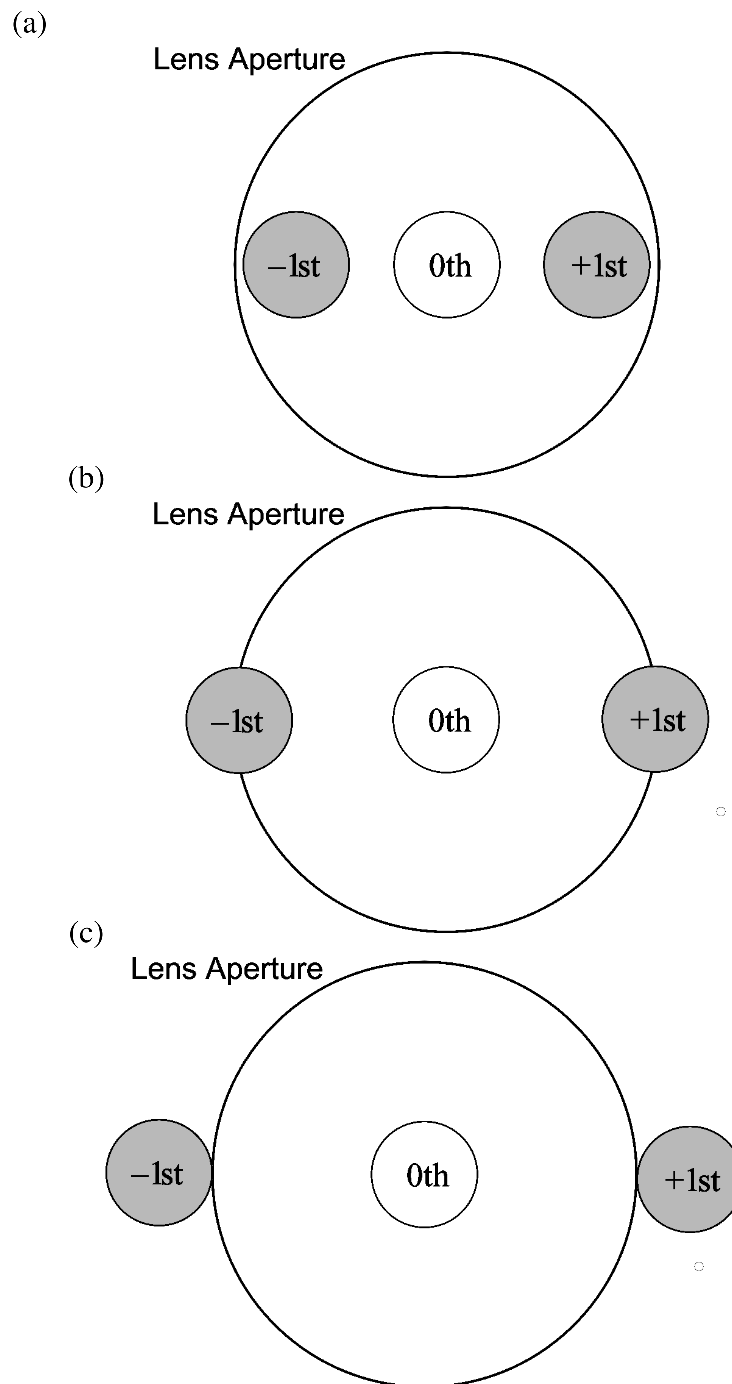

Figure 20: The effect of partial coherence on resolution limit. **(a)** The aperture is able to capture the $\pm 1^{st}$ order diffraction completely. **(b)** The $\pm 1^{st}$ order diffraction moves further apart with finer mask pitch, some of the $\pm 1^{st}$ order information are lost causing degradations in the reconstructed aerial image. **(c)** At this mask pitch, the $\pm 1^{st}$ order diffraction almost moves outside the aperture completely, aerial image reconstruction of even finer mask pitch is impossible. The resolution limit.

doi:10.6342/NTU201901098

under coherent illumination.

For partially coherent illumination, the pitch resolution limit is modified to

$$\frac{1}{p} = (1+\sigma)\frac{NA}{\lambda}, \tag{8}$$

yielding an improvement in the pitch resolution, with increasing value of the partial coherence factor σ.

doi:10.6342/NTU201901098

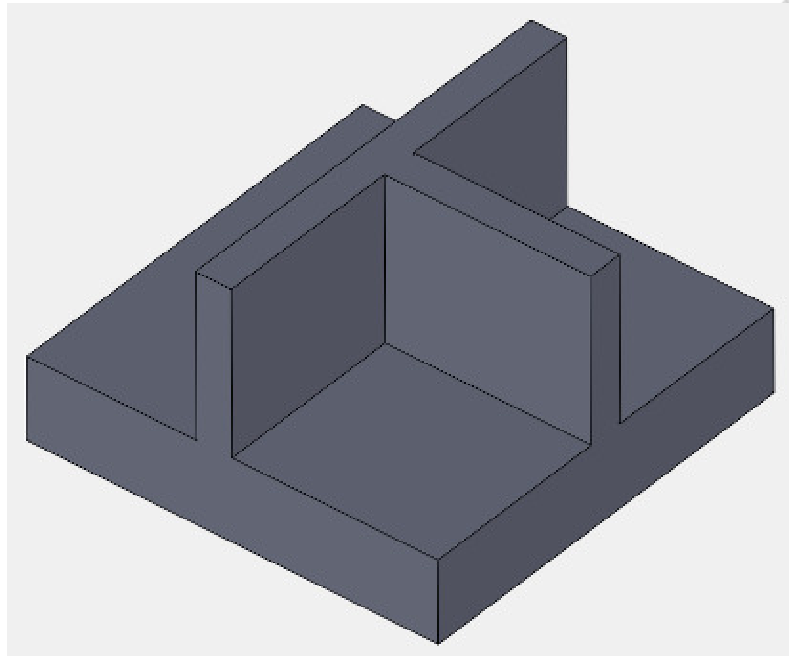

Figure 21: A drawing of a simple gate device. Here, the CD would be how thin the walls can be made, and the pitch resolution would be how small one single unit can be printed.

1.3 Resolution

For lithographers, the term resolution is often ambiguous. In general, two different meanings are often associated with the term resolution. It can either mean how small one individual feature can be made, in which case the proper term to refer to it would be critical dimension (CD); or how many units of repeating pattern that can be printed on the wafer, in which case the proper way to call it would be pitch resolution Λ, though in most cases just simply as the resolution.. While both are important, the distinction between the two must be made clear, because the influence of the two and underlying limitations are very different.

Critical Dimension

The CD is simply, how small lithographer is able to print one single individual feature. Figure 21 is a diagram of a simple gate device. In this case, the CD would be how thin the walls of the device can be made. The CD influences many important electrical functions and properties of the device, such as the drain current, driving voltage, and device efficiency etc. In device manufacturing, as of now, the most limiting factor to the

doi:10.6342/NTU201901098

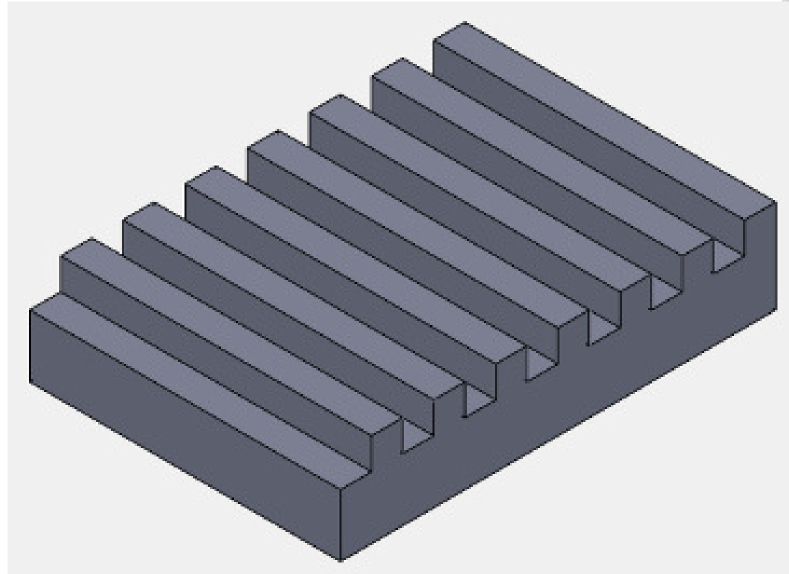

Figure 22: A drawing of a grating device of lines and spaces of equal width. In this case, the CD and pitch resolution are closely related, with $\Lambda = 2 \cdot CD$.

CD of a device feature has been the process control. There are many tricks in printing features with CD well below what the lithography tool is normally capable of. For one single exposure, the resolution is limited by the diffraction limit, as defined previously in Equation 1. However, by combining multiple exposure processes, with techniques such as double imprint, double resist imprint, quadruple imprint etc, features with CD beyond the resolution of a single exposure can be printed. Although, there is a catch, and that is all require extremely high presicion control.

Pitch Resolution

This is the ability of the lithography tool to print repeating features. Or, how many devices can be printed in a finite given area (i.e. one wafer). Figure 22 shows a simple diagram of a grating of equal lines and spaces, in this case the pitch resolution Λ is the size of one repeating unit. The pitch resolution affects aspect of the device directly related to its packaging and manufacturability, such as the cost per function of the device and functions per chip. Here, however, this aspect of the resolution has a hard limit of according to Equation 1

$$R = k_1 \frac{\lambda}{NA} \tag{9}$$

doi:10.6342/NTU201901098

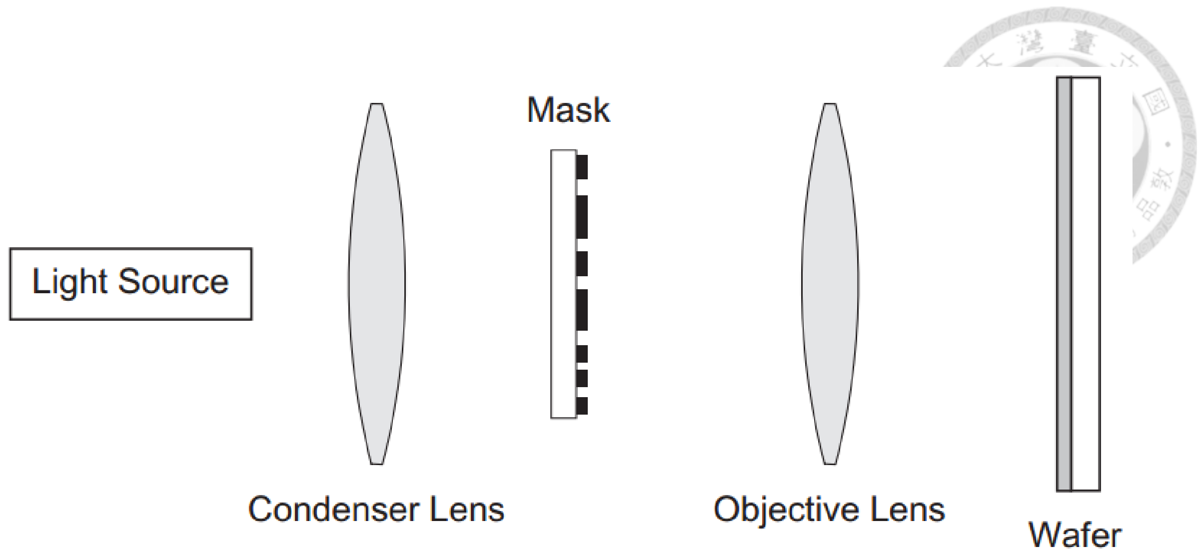

Figure 23: A simple diagram of an optical lithography exposure. Light from a source is redistributed onto the mask by the illuminator (the condensor lens). The illuminated mask is then picked up by the projector (the objective lens) and imaged onto the wafer.

1.3.1 Resolution Limit

The root of the cause of the resolution limit, is due to diffraction. Consider an optical system shown in Figure 23. From the point of view of Fourier optics, when the light from the illuminator strikes the mask, the resultant diffracted field interferes to form a diffraction pattern. The pattern is then received by the projection system, and recombined at the image plane. [25] Figure 24 shows a diagram of the process.

Mathematically, this can be expressed as

$$U(f_x,f_y)_{Image} = \mathscr{F}^{-1}\left[\ A(x',y')_{Lens}\cdot\mathscr{F}\left[\ U(x,y)_{Mask}\ \right]\ \right] \tag{10}$$

where $U(x,y)_{Mask}$ is the mask pattern, $A(x',y')_{Lens}$ is the aperture function of the optical system, and $U(f_x,f_y)_{Image}$ is the resultant imaged field.

Ideally, to perfectly reconstruct the mask pattern, the entire diffracted field from the mask $\mathscr{F}[U(x,y)_{Mask}]$ must be transfered through. To achieve this, however, would require an infinitely large aperture function (or $A(x',y')_{Lens} = 1$) Obviously, this is not possible, nor realistic. Therefore, since the aperture function $A(x',y')_{Lens}$ is finite, during transmission some part of the the diffraction will always be obstructed, causing a lose of higher order information.

doi:10.6342/NTU201901098

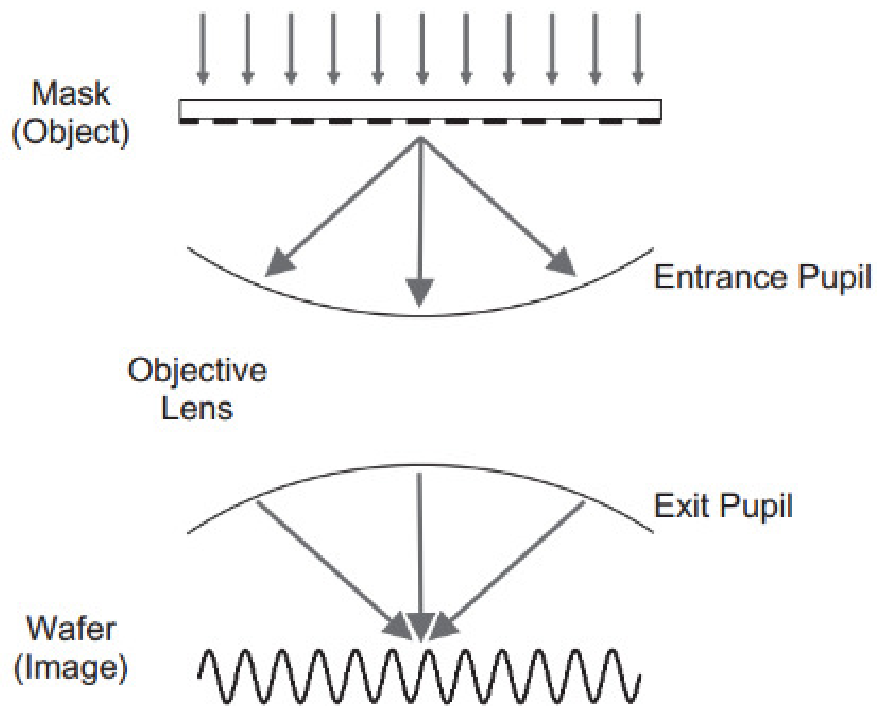

Figure 24: Wave optics representation of the lithographic process.

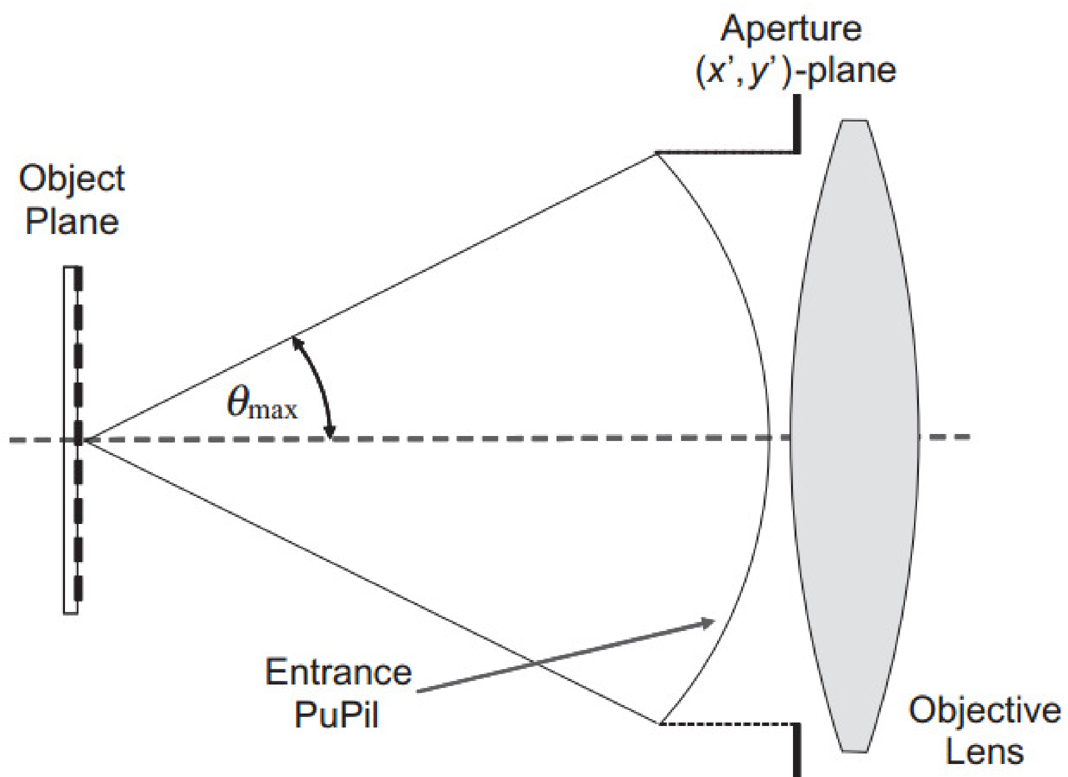

Figure 25: To convey the pattern across, the NA of the optical system (given by $NA = \sin\theta_{max}$) must be large enough such that the $\pm 1^{st}$ order diffraction are collected.

doi:10.6342/NTU201901098

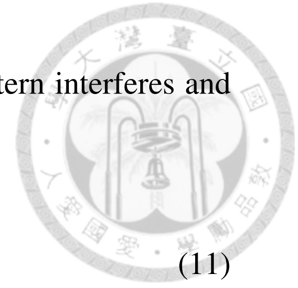

Given some patterns with pitch Λ on the mask, light from the pattern interferes and diffracts into orders given by the well known grating equation

$$\sin\theta_m = \sin\theta_i + \frac{m\lambda}{\Lambda} \tag{11}$$

In the fourier reconstruction of the image, the more orders are present, the more the image reconstructed adhere accurately to the original object

$$u = A_0 + A_1\sin(\alpha) + A_2\sin(2\alpha) + A_3\sin(3\alpha)... \tag{12}$$

However, at least one order of the diffraction must be present in order for information to be conveyed, since the 0th order only carries energy, but contains no information (i.e. DC offset). Therefore, the size of the lens must at least be big enough to collect one order of diffraction, in order for the image to be constructed at all (Figure 25), so

$$\begin{aligned} NA &= \sin\theta_{max} \\ &= \frac{m\lambda}{\Lambda}\ (m=1) \\ &= \frac{\lambda}{\Lambda}, \end{aligned} \tag{13}$$

which can be rearranged to obtain

$$\begin{aligned} R &\equiv Resolution \\ &= \Lambda \\ &= \frac{\lambda}{NA}. \end{aligned} \tag{14}$$

doi:10.6342/NTU201901098

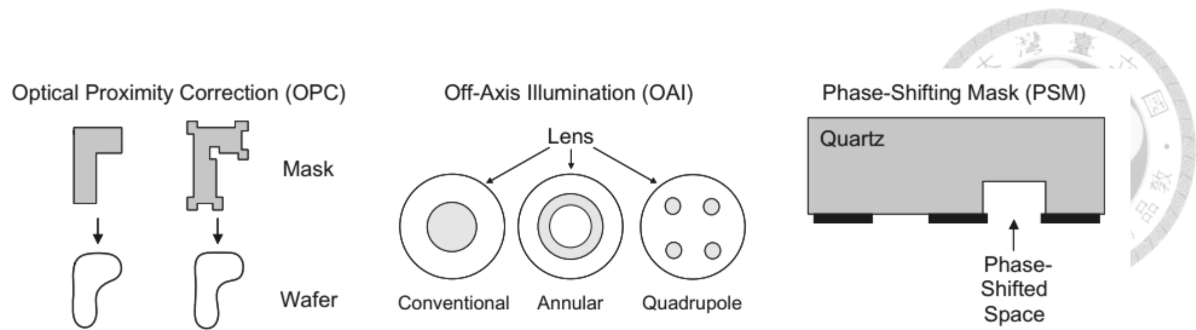

Figure 26: The three major types of resolution enhancement techniques (RET). Optical proximity correction, off-axis illumination, and phase-shifting mask.

1.3.2 Resolution Enhancement Techneques

Recall that the resolution limit previously stated at the beginning

$$R = k_1 \frac{\lambda}{NA} \tag{15}$$

has a different form to the one obtained in the previous section

$$R = \frac{\lambda}{NA}. \tag{16}$$

The two differs by a factor k_1. This parameter k_1 is the Process Parameter, known as such because it is quite literally a parameter that depends on the process. The value of k_1 usually has a lower limit of 1, but over the years researchers have developed tricks to further lower k_1 to as far as 0.5, effectively doubling the resolution to what is normally possible. These tricks are referred to as RET (Resolution Enhancement Techniques).

As of currently, there are three main types of RET in industrial use. Off-axis illumination (OAI), optical proximity correction (OPC), and phase shifting mask (PSM). Each of them is able to enhance the resolution of the aerial image through different physical mechanisms.

doi:10.6342/NTU201901098

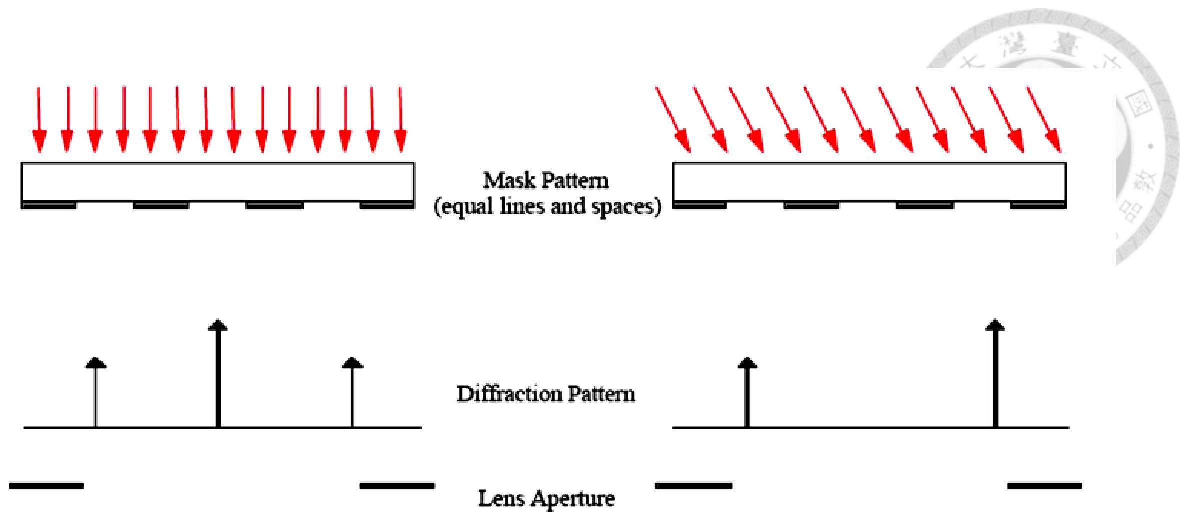

Figure 27: Off-axis illumination. The imaging resolution of an optical system can be doubled simply by tilting the angle of the illumination optics.

Off-Axis Illumination

Recall that previously when defining the resolution limit, the criterion is set such that at least the $\pm 1^{st}$ order diffraction are received by the optical system, since the 0th order contains only background energy but no information. Here, by the same logic, one could argue that only one of the $\pm 1^{st}$ order are necessary for the reconstruction of the image since the two diffraction orders are symmetric. Therefore, one way to improve resolution is to simply tilt the illumination to one side [26], hence the name off-axis illumination, as shown in Figure 27. The resulting diffraction patterns will undergo a shift in one direction. This way, by sacrificing one diffraction order, the available angular space is now twice as large, effectively doubling the resolution.

This method is not without faults, however. Since information of the mask pattern is contained in the $\pm 1^{st}$ order and the 0th order contains only background energy, eliminating one of the $\pm 1^{st}$ order diffraction results in a significant decrease in the contrast of the intensity of the aerial image. Also, since the enhancement of resolution is achieved by tilting the illumination to one side, the enhancement is therefore in one direction only. These demerits must be taken into consideration if OAI is to be utilized.

doi:10.6342/NTU201901098

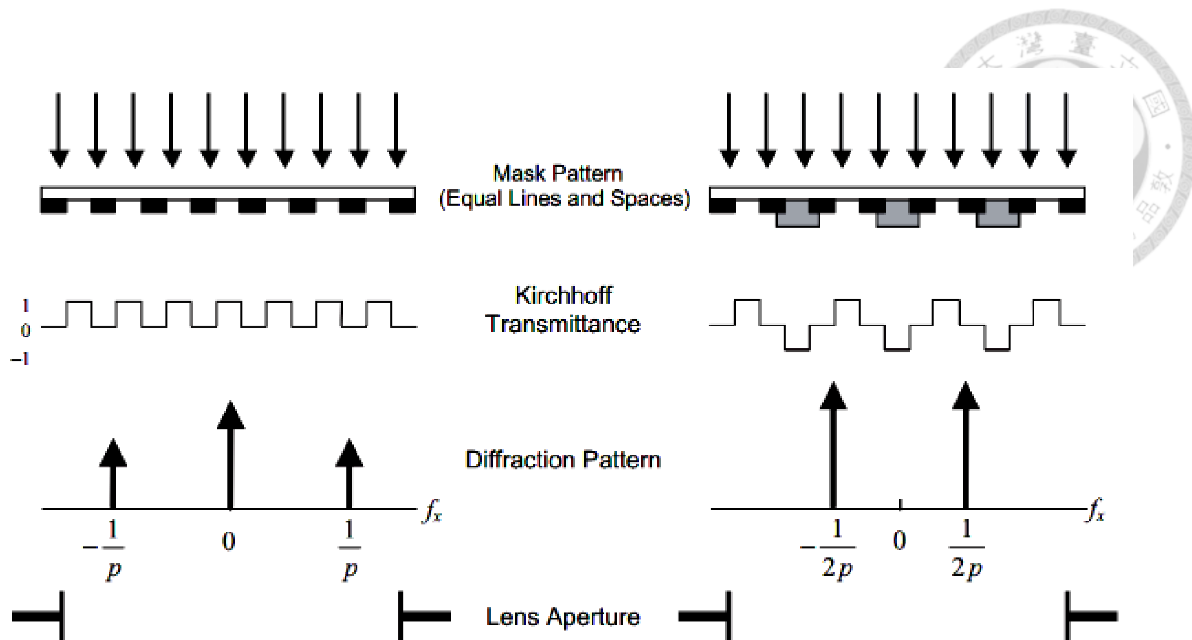

Figure 28: Using a phase shifted mask effectively doubles the periodicity of the mask pattern.

Phase Shifting Mask

Another method to improve the resolution is to use a specialized mask. By covering the mask pattern with small blocks of material in an alternating fashion as portrayed in Figure 28, a phase shift of half the wavelength can be introduced. Doing so doubles the effective periodicity of the mask pattern, and therefore the resolution can be increased to twice as that of an unshifted mask. [27]

One other advantage of using a PSM is that in this configuration, the 0th order diffraction is minimized. Looking at the comparison of the transmittance in Figure 28 reveals that the average of the amplitude function of the transmittance of the unshifted mask is 0.5, which means a significant portion of the total energy is directed to the DC offset (0th order). In the case of the PSM however, the average of the amplitude function of the transmittance is zero, therefore no energy is wasted to the 0th order diffraction. This means that in comparison to a unshifted mask, using the PSM is advantageous in that it doubles the resolution, and at the same time improves the aerial image intensity contrast.

However, one obvious setback of the PSM is that it can be applied to transmission masks only, and that it is difficult to apply to irregular and non-repeating features.

doi:10.6342/NTU201901098

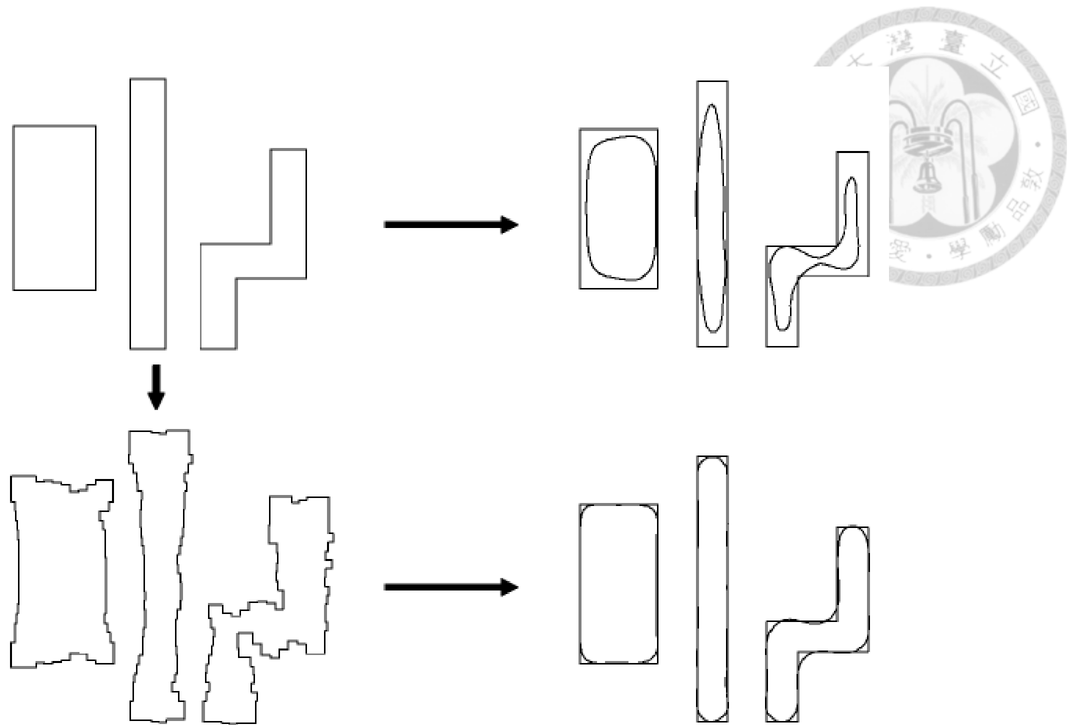

Figure 29: Optical proximity correction makes minor adjustments to the mask such that the imaged pattern stays the same to the pattern intended as much as possible.

Optical Proximity Correction

Since realistic optical systems are finite in size, the higher frequency information outside of the lens aperture are lost in the imaging process. The most pronounced consequence of the loss of high frequency information is that the blurring of the edge sharpness in the intensity of the imaged pattern, causing an inevitable distortion. OPC attempts to make minor alterations to the mask, in order that the final reconstructed image stay as close to the intended pattern as possible. [28] An example of this is shown in Figure 29.

OPC differs from OAI and PSM in the sense that it does not alter the pitch resolution at all, however it still comes under the RET catagory because it helps to maintain the correctness of the image.

doi:10.6342/NTU201901098

RET Enhanced Resolution

Taking RET into account and partial coherence into account, a more complete description of the resolution are given below [6]

- Coherent Illumination

$$R = k_1 \frac{\lambda}{NA} \tag{17}$$

- Partially Coherent Illumination

$$R = k_1 \frac{\lambda}{NA(1+\sigma)} \tag{18}$$

- Off-Axis Partially Choerent Iluumination

$$R = k_1 \frac{\lambda}{NA + NA\sigma + \sin\theta} \tag{19}$$

Depth of Field and Depth of Focus

The depth of field (DOF) and depth of focus (also DOF) refers to a range of depth in which the mask and wafer can be placed while still maintaining the image quality above a given threshold, and is related to the *NA* of the optical system, given by

$$DOF = k_2 \frac{\lambda}{NA^2} \tag{20}$$

similar to the pitch resolution.

Both the depth of focus and depth of field are abbreviated as DOF, with depth of field on the mask (object) side and depth of focus on the wafer (image) side. Both are related to one another by a factor proportional to the square of the magnification of the optical system, given by

$$DOF_{Focus} = M^2 \cdot DOF_{Field} \tag{21}$$

doi:10.6342/NTU201901098

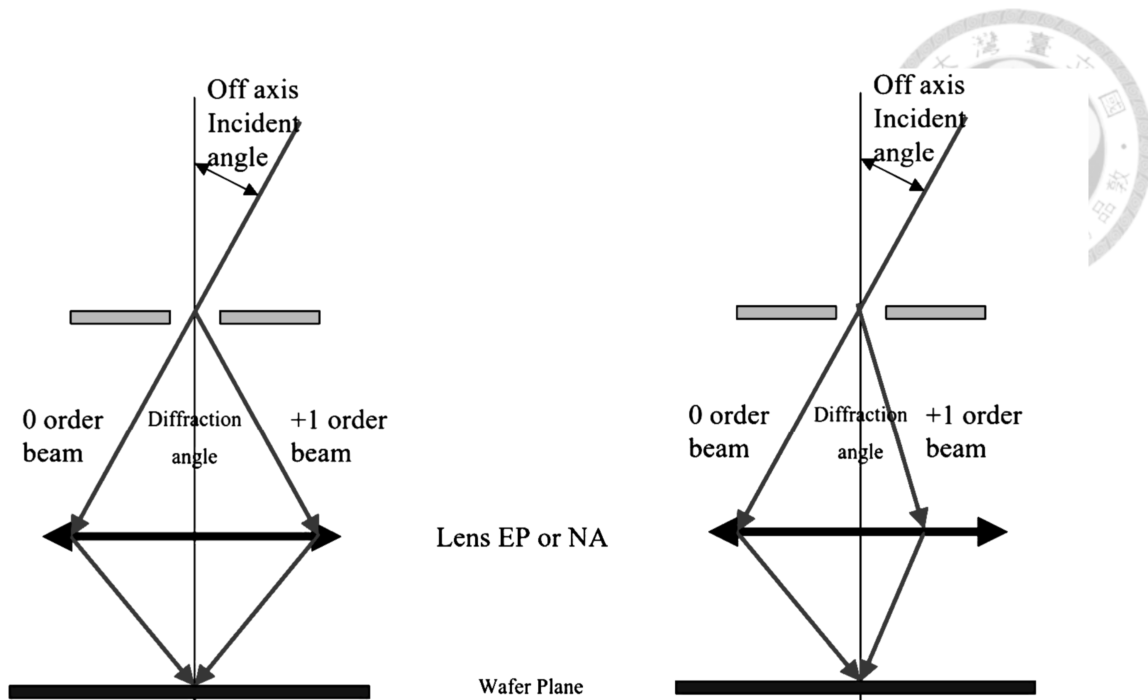

Figure 30: the location of the $\pm 1^{st}$ order diffraction shifts according to the local pitch of the mask pattern illuminated.

Forbidden Pitch

For a lithography tool optimized with OAI, there is a pitch resolution where the projection tool performs exceptionally poor, and is therefore referred to as the forbidden pitch. In designing the mask pattern, lithographers must inform the designer to avoid placing features at the forbidden pitch to ensure optimum result.

When employing OAI optimized for one feature CD, one inevitable consequence is that at larger feature pitch, the location of the 1th order diffraction shifts closer to the 0th order diffraction as depicted in the right part of Figure 30. This induces an optical path difference between the two orders when they recombine at the wafer.

The worst case scenario occurs at the point where the diffraction order shifts to the midpoint between where the two orders were, as shown in Figure 31. As the feature pitch increases to the point where the 1th order diffraction is at the center of the lens *NA*, maximum OPD is reached. At this point, the resultant image quality at the wafer is at its poorest. This pitch is referred to as the Forbidden Pitch, and should be avoided in the mask design where possible.

doi:10.6342/NTU201901098

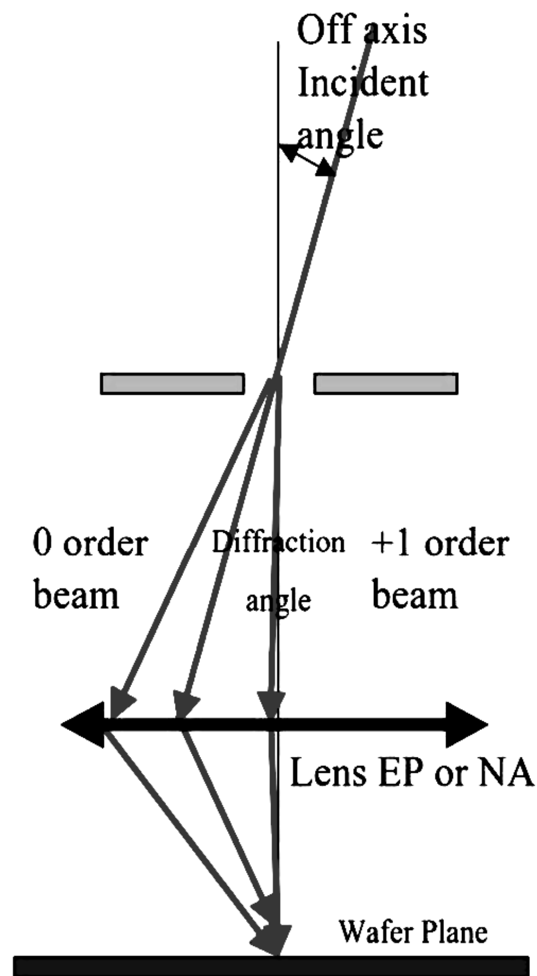

Figure 31: The forbidden pitch, where the 1st order diffraction is at the center of the pupil, with maximum OPD.

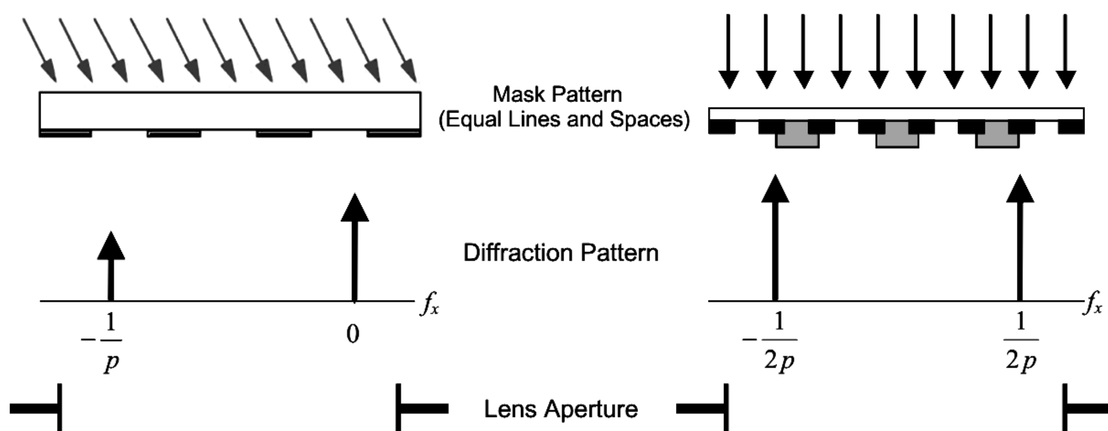

Figure 32: Comparison between off-axis illumination and phase shift mask.

doi:10.6342/NTU201901098

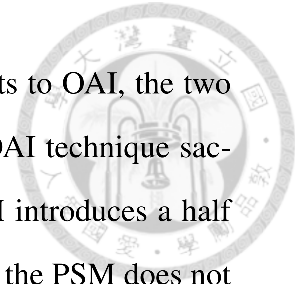

As a side note, although the PSM have similar enhancement effects to OAI, the two rely on different physical mechanisms, as shown in Figure 32. The OAI technique sacrifices one of the $\pm 1^{st}$ order for the gain in resolution, while the PSM introduces a half wavelength phase shift to every second feature in the pattern. As such, the PSM does not suffer from the effect of the forbidden pitch as OAI does.

doi:10.6342/NTU201901098

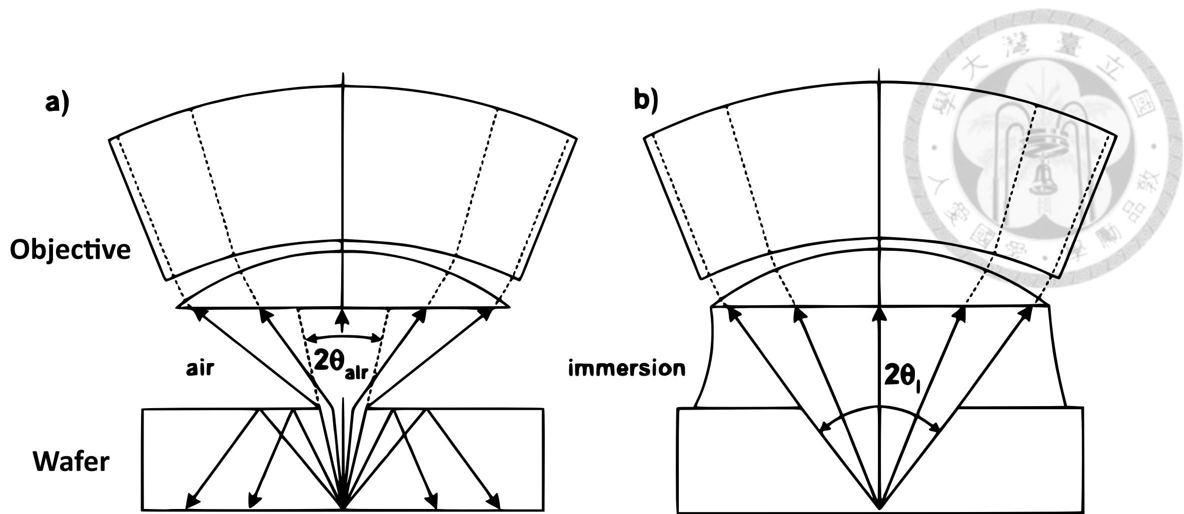

Figure 33: If the imaging target is immersed, the effective NA in air is enhancd by a factor almost equal to the refractive index of the the immersion medium/fluid.

1.4 EUV Lithography

As previously mentioned, the resolution of a projection lens is given by

$$R = k_1 \frac{\lambda}{NA} \tag{22}$$

where R is the resolution, k_1 is the process parameter usually ranging from 0.5 to 1.0, λ is the operation wavelength of lithography process, and NA is the numerical aperture of the projectiopn lens. From this relationship, there are two possible methods to decrease the pitch size even further. Either increase the NA of the projection lens, or decrease the operation wavelength.

The NA of an existing optical system can be further enhanced by the method of immersion technique. Figure 33 shows a basic setup of the immersion method [29]. By submerging the imaging target in a medium of high refractive index, the NA of the projection can be increased above what is normally possible in air, by a factor almost equal to the refarctive index of the immersion medium.

doi:10.6342/NTU201901098

1.4.1 Extreme Ultraviolet Source

In lithography, constraints on the projection system comes from the desired requirements on the image (wafer) side. The illumination system then accomodates to the properties of the projection system accordingly, such that the constraints on the projection system can be met. And once the property of the exposure system is determined, the light source in question must then comply with the constraints on the exposure system.

Therefore, some considerations must be given regarding the properties of the source [30], since they will directly influence the quality of the image at the wafer end. Some points to consider are:

- **Operation Wavelength**

  The wavelength of the light source. As previously mentioned, this affects the resolution limit directly.

- **EUV Power**

  The power of the light source. This affects the throughput of the lithography process, as well as the sensitivity of the lithography process to noise.

- **Hot Spot (Source) Size**

  The size of the source, together with the illuminator optics, influences the degree of coherence of the illumination.

- **Collection Angle**

  The larger the collection angle, the more light from the source is collected and used.

- **Pulse-to-Pulse Repeatability** (Consistency)

  The fluctuation of the source output power.

- **Debris Induced Component Lifetime** (Damage and Contamination)

  Longer lifetime means less downtime, and less cost spent on maintainance.

doi:10.6342/NTU201901098

Influences on Lithography Operation

These properties of the lithography process influence the lithography operation in different ways.

- **Process Throughput**

  Operation Wavelength, EUV power, Source Size, Collection Angle, Pulse-to-Pulse Repeatability

- **CD (Imaging) Control**

  Pulse-to-Pulse Repeatability

- **Cost of Operation**

  Debris Induced Component Lifetime

Laser Produced Plasma

The schematic illustrated in Figure 34 shows the basic generation of EUV light [31]. First, stream of liquid xenon is injected from the top of the chamber. A high powered laser then heats the xenon to plasma state, which then emits EUV radiation. The stream of xenon stream is then collected and recirculates back to be reused.

Fast-Ion Mitigation

As a byproduct of LPP, the Xe ions from Xe^{1+} up to Xe^{6+} has been observed in the EUV generation process. Due to the high energy nature of the laser bombardment, these ions

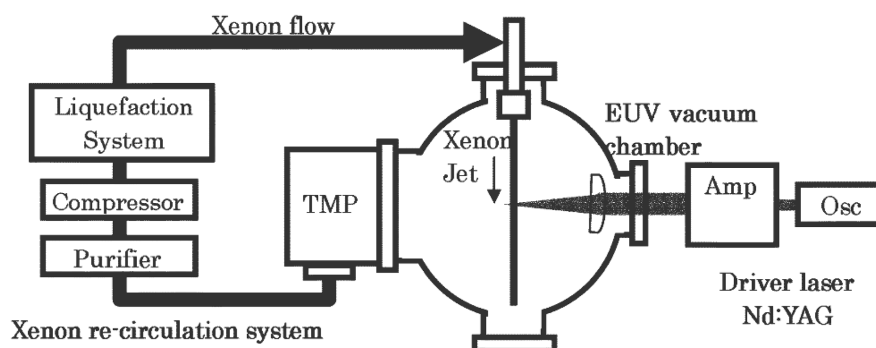

Figure 34: Basic schematic of EUV generation.

doi:10.6342/NTU201901098

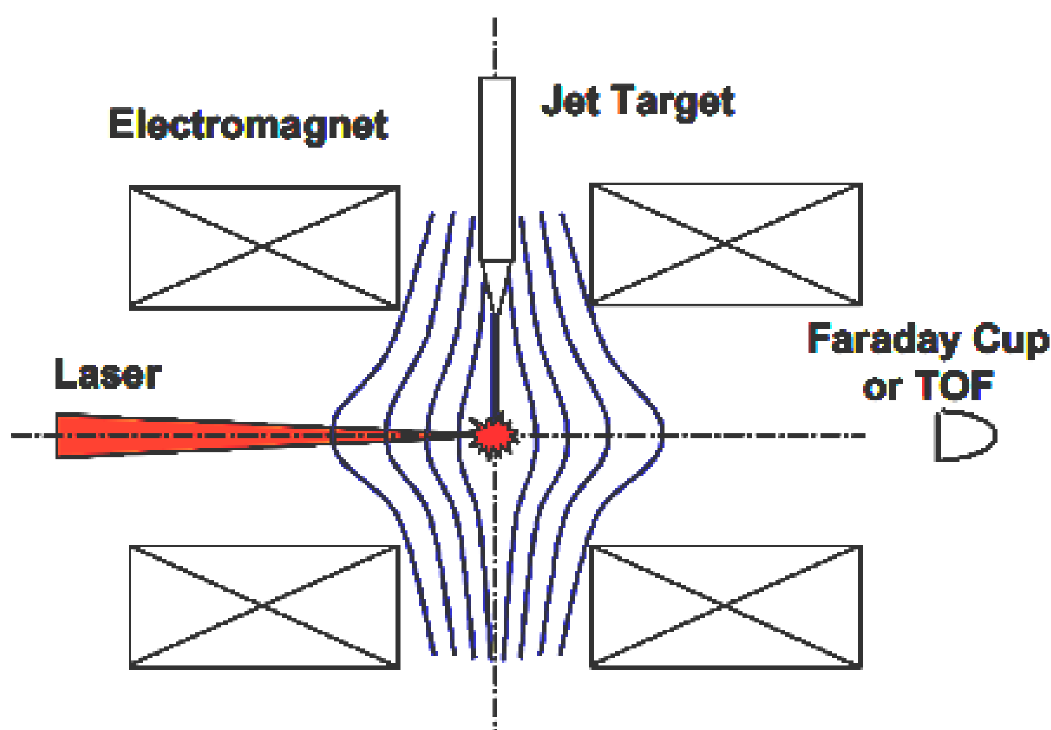

Figure 35: A mechanism to prevent (or reduce the amount of) byproducts of the EUV source from entering and contaminating the lithographic optical system. [3]

possess high kinetic energy, which cause contamination and damage to the multilayer coating when striking the collector mirror, and to the subsequent optical elements.

As such, preventive measures are necessary to eliminate or reduce the damage. Figure 35 demonstrates an example of mechanism using a strong magnetic field to deflect the ions into a collector cup to prevent damage to the reflective mirror [3].

1.4.2 Mirror Optics

At the EUV wavelengths, absorption in almost all media (air included) is high. This leads to a drastic change in the lithography tool, in that conventional refractive optics must be abandoned for reflective systems made entirely of mirrors. Aside from that, some other consequences of EUV are that:

- The entire process must be performed in vacuum.
- Resolution enhancement techniques requiring transmission (e.g. phase shifting mask) cannot be used.

doi:10.6342/NTU201901098

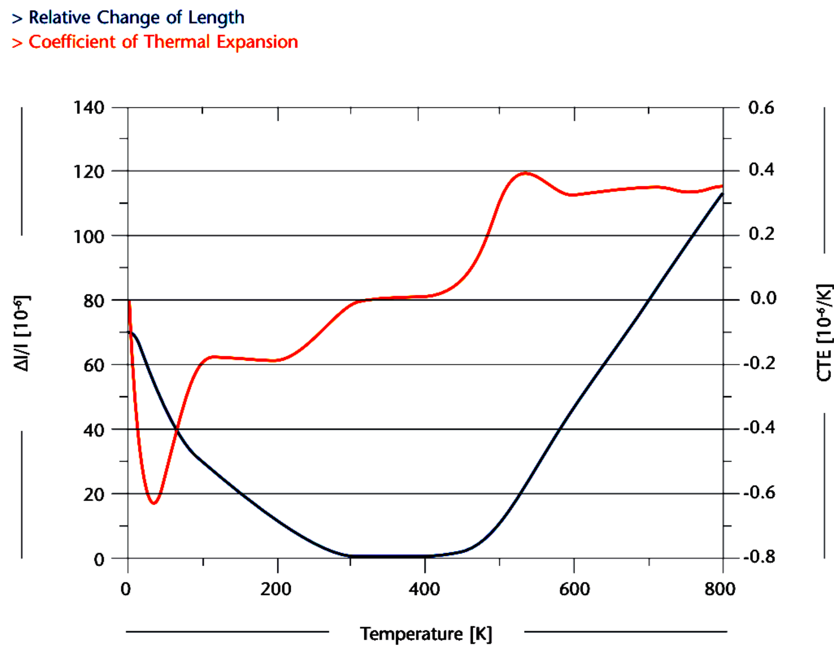

Figure 36: Thermal expansion of Schott's Zerodur.

- Immersion technique cannot be used.

Mirror Substrate

Due to the choice of operation wavelength at EUV, at the production of the mirrors one very important requirement or trait of the mirror substrate material is that the thermal expansion of the material must be small. In EUVL, the mirrors are under constant concentrated illumination from a high energy source. This means that which causes the mirrors to heat up quickly.

Presently, from well known vendors, two such materials are available. ZERODUR® from Schott, and ULE® from Corning. Figures 36 and 37 are thermal expansion curves for Schott's ZERODUR® glass [32] and Corning's ULE® (Ultra Low Expansion) glass [33] respectively.

doi:10.6342/NTU201901098

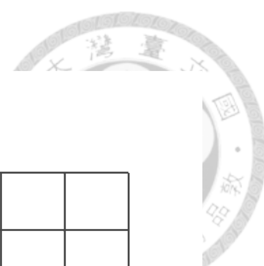

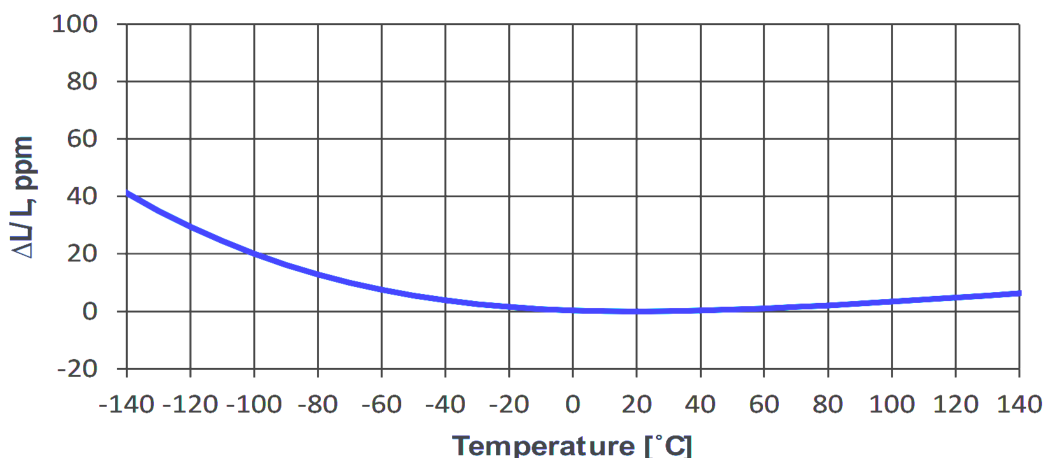

Figure 37: Thermal expansion of Corning's ULE.

Multilayer Coating

In EUVL, the illumination is highly absorbed in all materials, conventional refractive optics cannot be used, and the optical system must consist entirely of reflective optics. Due to the extremely short wavelength, uncoated mirrors still exhibit very poor reflectance. As such, multiple layers of reflection coatings, typicall molybdenum (Mo) and silicon (Si) coating pairs, are employed. The Mo/Si multilayer acts as Bragg reflector, and is designed to operate at the EUV wavelength, at near-normal incidence angles. Figures 38 and 38 shows the reflection spectrum and angular reflection distribution of a designed Mo/Si multilayer coating with 40 layer pairs, at EUV wavelengths. The Mo layer have thickness of 2.76 nm and Si layer of 4.14 nm. [4]

Reflection Depth Offset

There is, however, the issue of where the reflection occurs exactly. In many cases with optical coatings, the difference is minute due to the coating thickness being very small. With the multilayer in EUVL however, where the the multilayer number easily exceeds "a few", the multilayer thickness becomes a serious concern. The 40 layer pairs of Mo/Si are of 2.76 and 4.14 nm thickness respectively, and totals up to 276 nm for the entire stack, more than 20 times longer than the wavelength of EUV. With the multilayers, in

doi:10.6342/NTU201901098

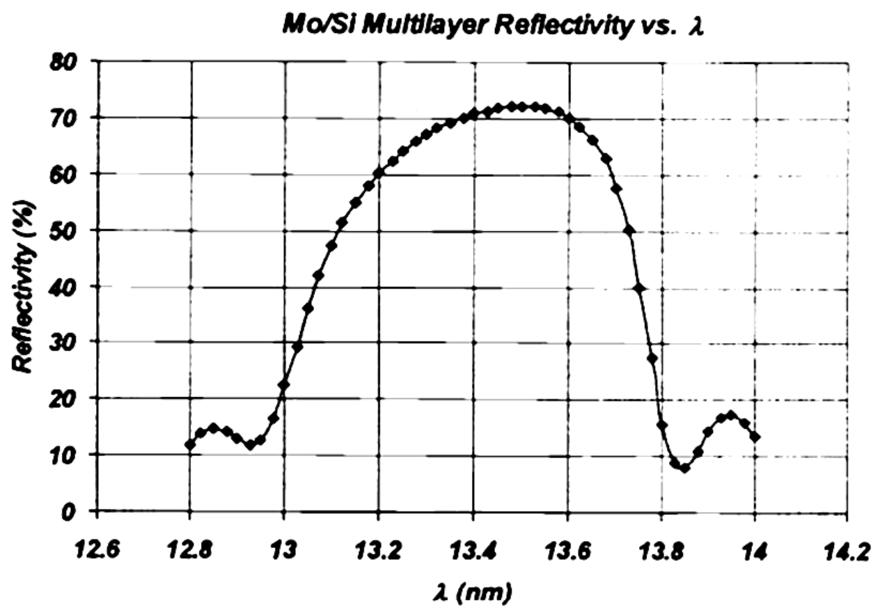

Figure 38: Reflection spectrum of the 40 Mo/Si multilayer coating. [4]

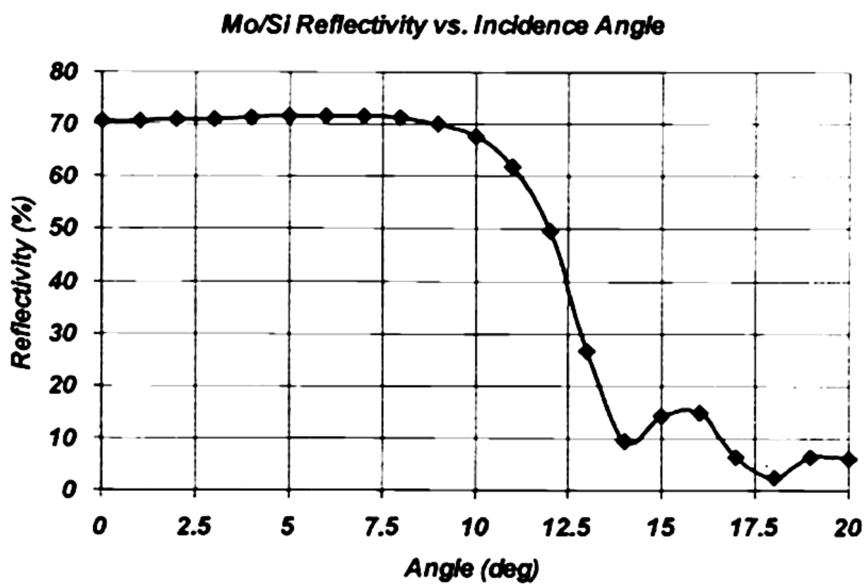

Figure 39: Anuglar reflection distribution of the 40 Mo/Si multilayer coating. [4]

doi:10.6342/NTU201901098

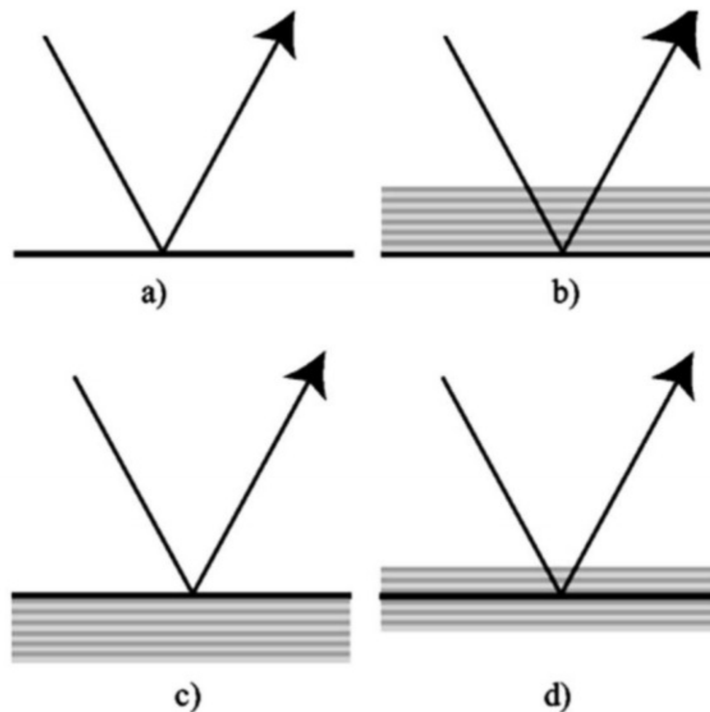

Figure 40: Candidates of the reflection depth offset. **(a)** Without the multilayers, the reflection occurs at the surface interface. **(b)** At the bottom of the multilayers. **(c)** At the top of the multilayers. **(d)** Somewhere inside the multilayers.

actuallity, reflection occurs at every multilayer interfaces, tapering off to zero as the light propagates further into the multilayers. This ambiguity is not useful for optical designers, there are simply not enough resources to allow the inter-mirror distances to split over a range values each time a mirror is encountered. There must be one reference point to say that this is where the reflection occured. Figure 40 shows some possible candidates of positions to define where the reflection occured.

Figure 40(a) shows the situation where the multilayers are not present, in which case the reflection can be defined to be at the air-mirror interface. In Figure 40(b), in the presence of the multilayer stack, it seem illogical to use the multilayer-mirror interface at the bottom as the reference plane of reflection, that the reflection occurs only after propagation through the entire multilayer stack. In fact, at the bottom of the stack there are hardly any EUV radiations left to reflect. Likewise, in Figure 40(c) the air-multilayer boundary is also illogical. Since the reflections occur over a range of depths, the first interface is unlikely to be representative of where the reflection occurs. Therefore, lastly in Figure 40(d), the most appropriate representation seems to be somewhere between the

doi:10.6342/NTU201901098

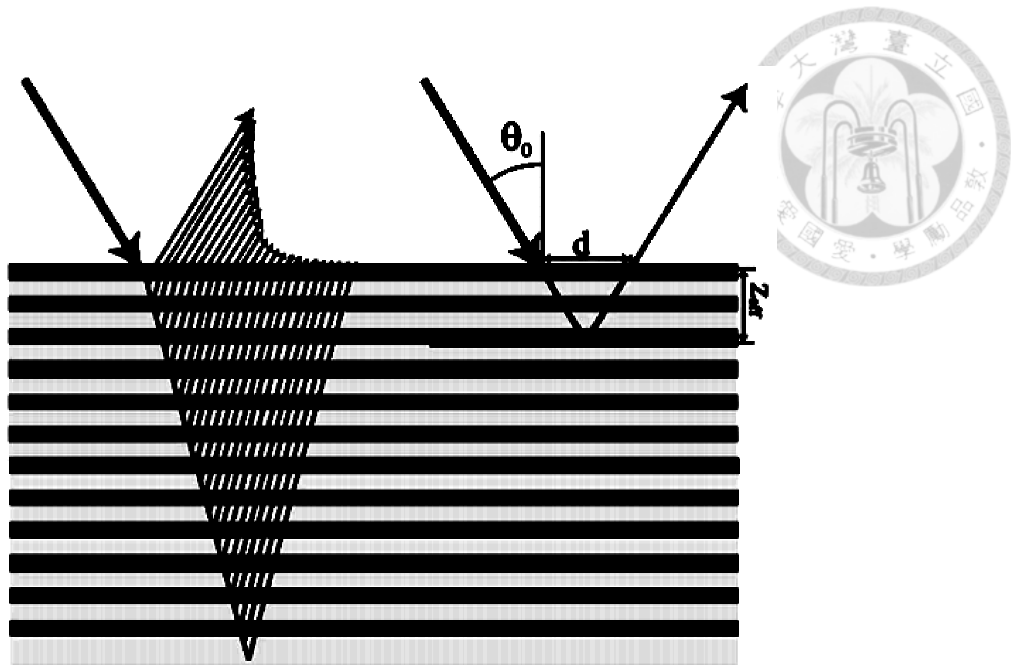

Figure 41: The reflections of the EUV light over a multilayer stack. The center of the reflection lies inside the stack towards the air-multilayer interface.

top and bottom of the stack.

As each coating layer contributes to the total reflection, where the actual reflection occurs is ambiguous. In this situation, an effective reflection depth z_{eff} can be best used to approximate the depth where the reflection occurs [34].

Multilayer Imperfections

In theoretical calculation, the Bragg reflector configuration of the Mo/Si multilayer coating has a theoretical limit of reflectivity of 75.5%, at the EUV spectrum [4]. However due to the multilayer imperfections, the measured reflectivity of the manufactured coating do not exceed 69%. Some of the imperfections are associated with the manufacturing, while some are inevitable physical phenomenons.

- **Interdiffusion**

  This imperfection comes from a third intermixing zone formed at the interface between the Mo and Si layers due to interdiffusion. Insertion of thin barrier layer of B_4C or C can allow consistent production of multilayer coating of reflectivity of 70%.

doi:10.6342/NTU201901098

- **Mirror Substrate Roughness**

  Manufacturing errors on the mirror profile leads to errors in the multilayer coating profile, and hence further impacts the total reflectivity.

Aside from optical coating, another affecting factor that impacts the mirror reflectivity in EUV lithography is the mirror roughness itself.

Marechal's Criterion

Typical definition of diffraction limited optical system requires that the peak wavefront error OPD_{peak} be smaller than

$$OPD_{Peak} < \frac{1}{4}\lambda, \tag{23}$$

this is known as Rayleigh's criterion.

For EUV lithography, the requirement for precision is so high that Rayleigh's criterion is not enough warrant performance. Another more useful difinition is Marechal's criterion, which states that the RMS wavefront error OPD_{rms} must be contrained under

$$OPD_{rms} < \frac{1}{14}\lambda. \tag{24}$$

As an optical designer, it is easy to be tempted into thinking that more optical elements leads to better optical performance. However a consequence of Marechal's criterion is that, since the total wavefront error is spread across the entire optical system, the allowable error on one particular element in a system with N elements is

$$OPD_{individual} < \frac{OPD_{rms}}{N}. \tag{25}$$

As an example, for a 6 mirror EUVL projection system operating at 13.4 nm, the maximum allowable RMS error on the surface figure of each element is approximately 0.2 nm. Increasing the number of elements means to further reduce the allowable RMS error on the mirror surface.

doi:10.6342/NTU201901098

Power Spectrum Density Analysis

The impacts of mirror surface roughness can be seen clearly in the spatial frequency domain, by taking a Fourier transform of the roughness profile. In general, the magnitude of the roughness at different frequencies affects the result in different ways.

- **Low Spatial Frequency Roughness**
  LSFR impacts the overall shape of the mirror surface profile, and hence reduces the aerial image sharpness and worsens the resolution.

- **Mid Spatial Frequency Roughness**
  Overall shape of the mirror is unaffected, but the MSFR causes increased scattering at the mirror surface, which results in flares in the optical system.

- **High Spatial Frequency Roughness**
  HSFR at the scale of the illumination wavelength disrupts the constructive interference mechanism that the multilayer coating relies on, and reduces the resultant reflectivity.

doi:10.6342/NTU201901098

1.5 EUV Lithographic Tool Design

1.5.1 Projector Design

As previouly mentioned, the optical lithography process encompasses many stages. During the exposure stage, a mask of the desired pattern to be transferred is first illuminated by a light source, then a projector system picks up light from the mask, and images the pattern onto the photoresist coated on the wafer. This projection system is the heart of optical lithography, and is conventionally composed of many lenses, spanning well over a meter in length. The design and manufacturing of this projection system will largely determine the quality and performance of the lithography process, and its attainable resolution.

The designing of a lithography tool, portrayed in many textbooks as the pinnacle of imaging optical system design, the sheer number of optical elements required, coupled with the stringentness of the required imaging quality, all contributes to the overall design difficulty. Currently, many publications detailing such a design tend to focus mainly on the result of the design rather than the process of the design. While the design result of the lithography tool and its performance are undeniably important, the other equally important question is how to reach that design form in the first place, in keeping with a given set of optical constraints and requirements.

Unlike optical lithography tools in the previous deep ultraviolet (DUV) generation, the shorter wavelength of extreme ultra violet (EUV) exhibits high absorption in almost all propagation mediums. This absorption forces optical projection systems consisting mainly of lenses to be abandoned in favor of the reflective projection systems consisting entirely of mirrors. [35] As such, the optics undergoes a paradigm shift from mainly refractive systems to entirely reflective systems, and designers are forced outside the past comfort of the familiar refractive lens design. To address this, the hope of this study therefore, is to propose a method to analyze and design a completely reflective EUV lithography (EUVL) tool, using the mathematics of the Generalized Gaussian Constants (GGC) [36], based on the Gaussian Bracket [37].

In principle, reflective optics is similar to refractive optics in that the only difference

doi:10.6342/NTU201901098

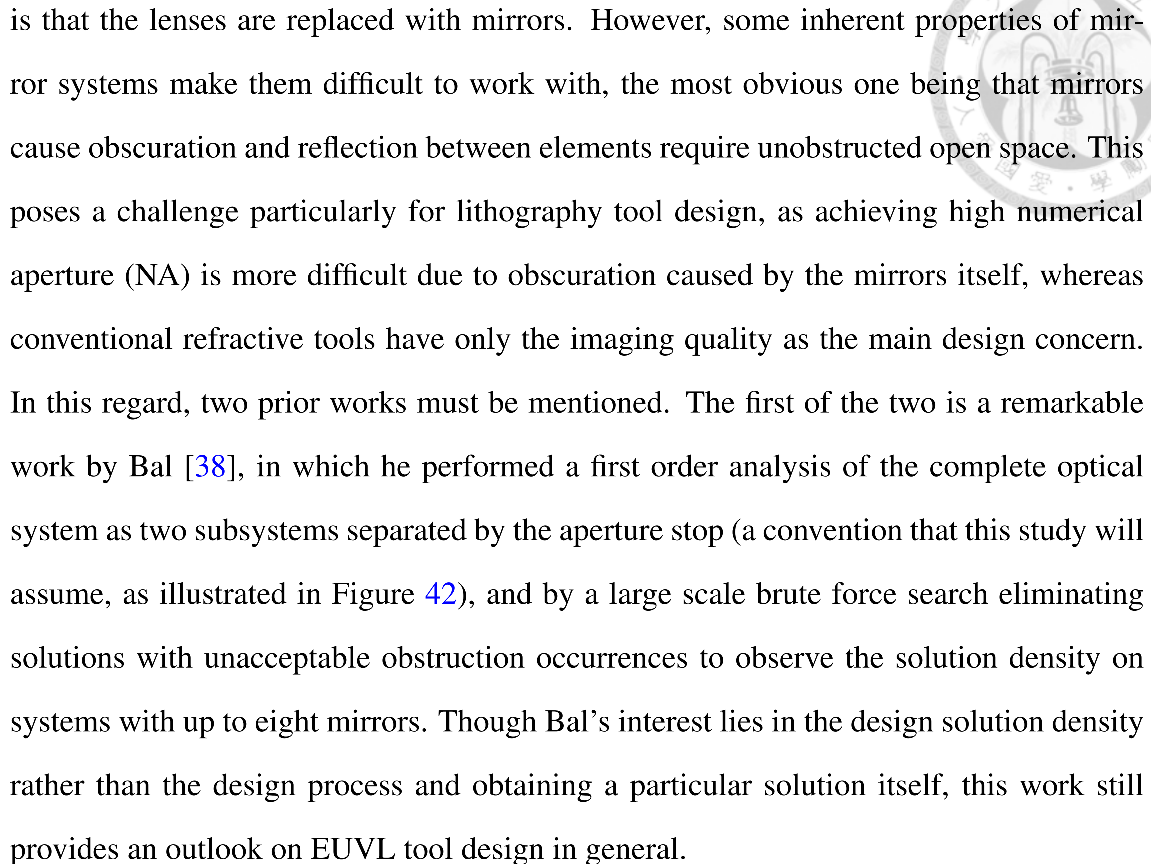

is that the lenses are replaced with mirrors. However, some inherent properties of mirror systems make them difficult to work with, the most obvious one being that mirrors cause obscuration and reflection between elements require unobstructed open space. This poses a challenge particularly for lithography tool design, as achieving high numerical aperture (NA) is more difficult due to obscuration caused by the mirrors itself, whereas conventional refractive tools have only the imaging quality as the main design concern. In this regard, two prior works must be mentioned. The first of the two is a remarkable work by Bal [38], in which he performed a first order analysis of the complete optical system as two subsystems separated by the aperture stop (a convention that this study will assume, as illustrated in Figure 42), and by a large scale brute force search eliminating solutions with unacceptable obstruction occurrences to observe the solution density on systems with up to eight mirrors. Though Bal's interest lies in the design solution density rather than the design process and obtaining a particular solution itself, this work still provides an outlook on EUVL tool design in general.

Following, a later development by Liu [39] introduces the concept of systematic design approach. The system is first split into three parts, front, rear, and middle group. Liu made the assumption that the aperture stop is located on the second mirror of the front group, and an exact solution is calculated for the front group under the condition of zero obstruction. Likewise for the rear group, an exact solution can be calculated, under the condition of wafer side telecentricity and zero obstruction. After evaluating the first order properties of the front and rear groups, the middle group connects the two groups together through pupil matching and paraxial imaging theory, forming the complete system. The significance of this approach is that telecentricity and unobstructed front and rear group is prioritized. Unfortunately the design uncertainty remained in the middle bridging group, however this already significantly simplified the design task.

This study aims to develop a systematic design procedure for EUVL tools, by taking elements from and improving upon the two works above. By adopting the pre-stop post-stop description (Figure 42), the loss of generality in the aperture stop location can be averted. Each subsystem have its own first order properties EF (Effective Focal Length)

doi:10.6342/NTU201901098

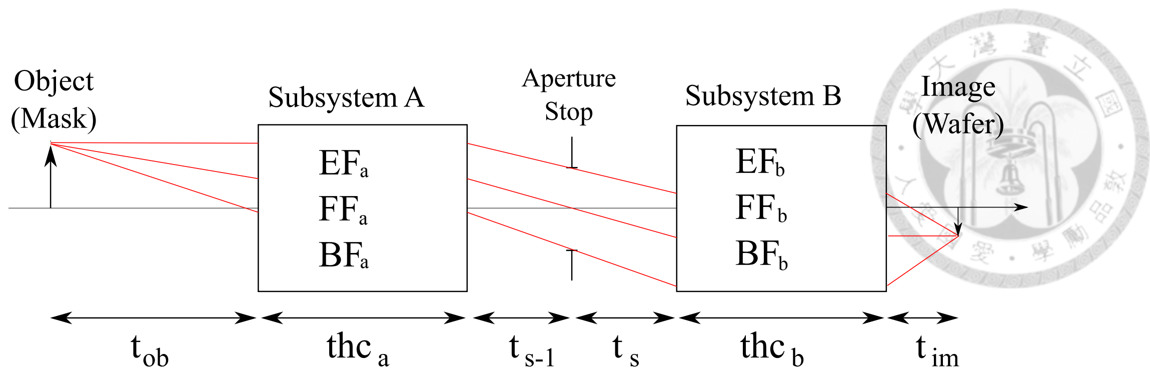

Figure 42: Basic configuration of the lithographic projection system, consisting of two subsystems separated by an aperture stop. The quantities EF, FF, BF, and thc are the effective focal length, front focal length, back focal length, and thickness of the two subsystems respectively.

FF (Front Focal Length) and BF (Back Focal Length), and through GGC analysis, the relationship between each of the properties can be obtained. The obtained relations can then be incorporated into existing commercial optical design software giving rise to a novel design method ensuring that optical system properties required for EUVL tools are upheld during the design process.

1.5.2 Illuminator Design

During the exposure stage of extreme ultraviolet lithography (EUVL), light from an EUV source ($\lambda = 13.4$ nm) is directed by the illuminator to strikes a mask of the desired pattern to be transferred, which is picked up and imaged onto the wafer by the projection tool. For such a projection tool, one might be tempted to assume that light from a point on the mask simply travels through the tool and to the photoresist coated wafer, and indeed this would be true if the majority of the incident light striking the mask is scattered uniformly in all directions, however the specularly reflective nature of the EUV optics complicates this matter.

Since wavelengths in the EUV region is highly absorptive in almost all mediums, EUV optical elements are forced to be coated with reflective multilayers coating pairs to ensure that at least some degree of reflectivity is retained. [35] [4] It is for this reason that a complete paradigm shift from refractive lens optics to reflective mirror optics occurred when going from the deep ultraviolet ($\lambda = 193$ nm) to the current stage of optical lithography with EUV.

doi:10.6342/NTU201901098

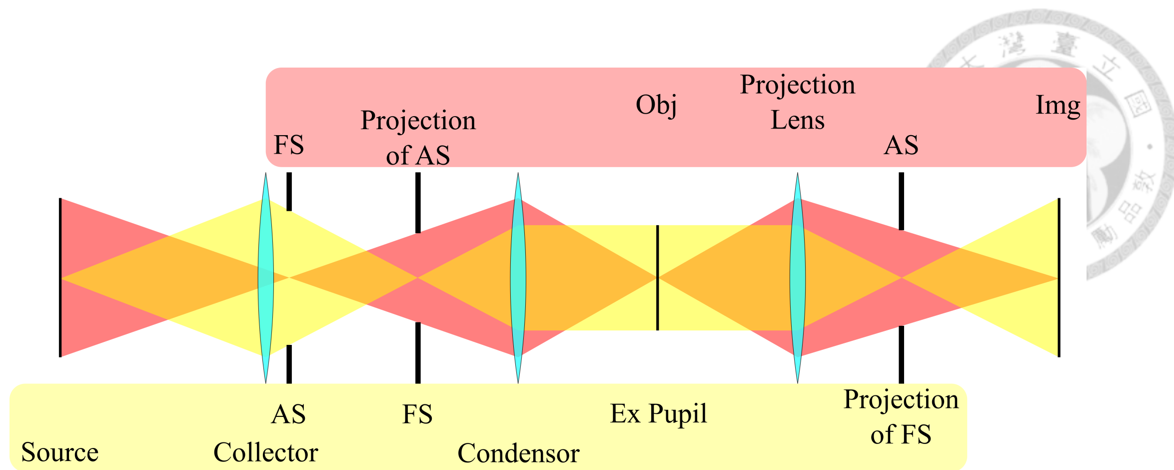

Figure 43: A diagram of an illuminator in Kohler illumination configuration with a matching imaging optical system.

In principle, the illuminator have but one seemingly simple task, provide illumination to the mask such that the intensity of the imaged pattern at the wafer end is uniform. As it is specularly reflective, the direction of the light reflecting off the mask must depend on the direction of the illumination incident. Therefore, if an arbitrary point on the mask is expected to give off a cone of light in a solid angle determined by the size and location of the entrance pupil of the projection tool, then the light incident provided by the illuminator must be designed to satisfy this expectation. Mismatched illuminator and tool can lead undesired consequences, such as the waste of the EUV source power and compromised aerial image uniformity at the wafer.

Kohler Illumination

In providing illumination for the mask, commonly employed methods include critical illumination, and Kohler illumination. For critical illumination, the light source is imaged directly onto the mask. It is the simplest method, however requires a uniform surface source in the shape of the target illuminated. Kohler illumination on the other hand is more complex, however no longer requires source uniformity, or for the source to be of a specific shape. Figure 43, is a diagram of an illuminator in Kohler illumination configuration, coupled with a matching imaging system. In the figure, *AS* refers to the aperture stop, *FS* is the field stop, *Obj* is the illuminated object, and *Img* is the image of the object through the imaging system.

doi:10.6342/NTU201901098

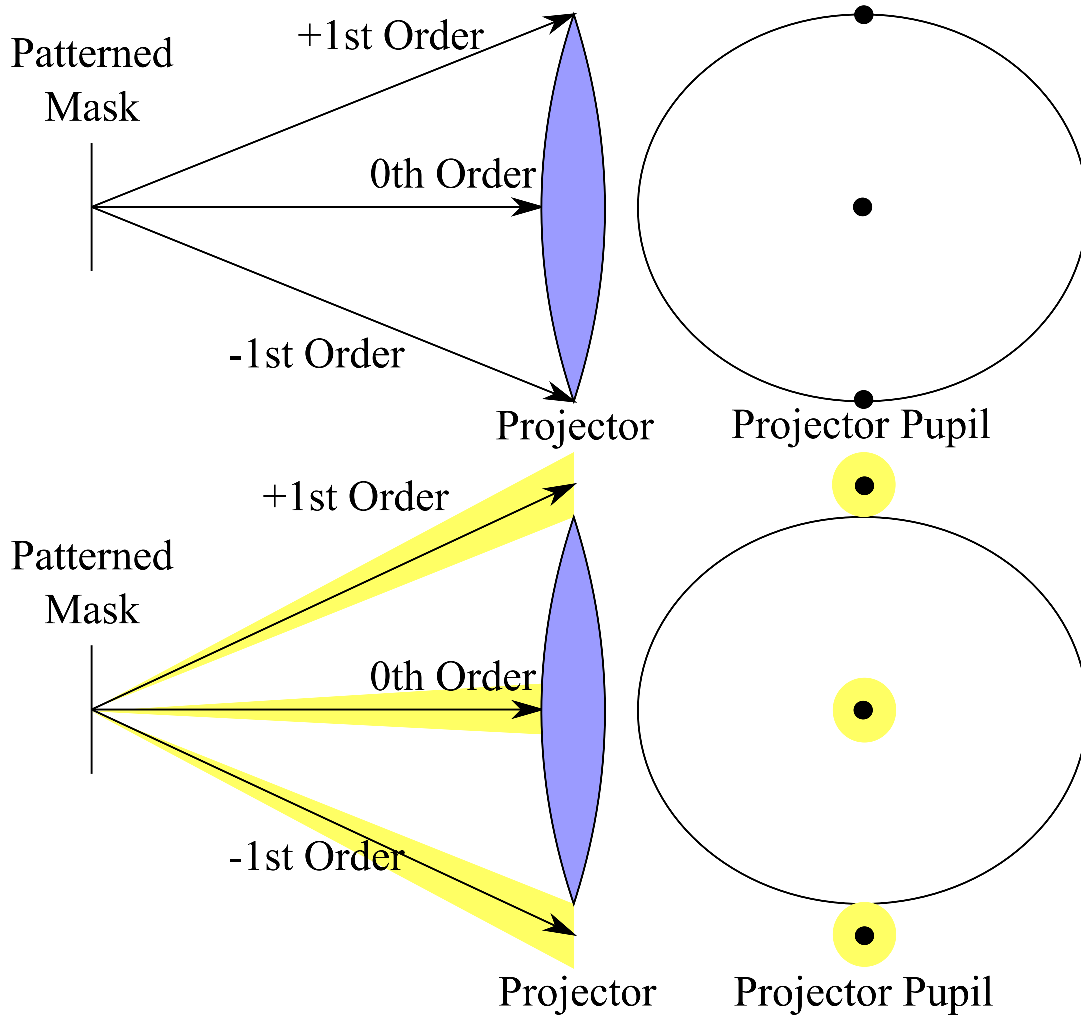

Figure 44: Effect of the partial coherence RET. **Top:** Coherent illumination. **Bottom:** Partially coherent illumination. Broadened diffraction spot allows the limit of the ± 1 order to be collected at a larger angle (i.e. higher resolution).

doi:10.6342/NTU201901098

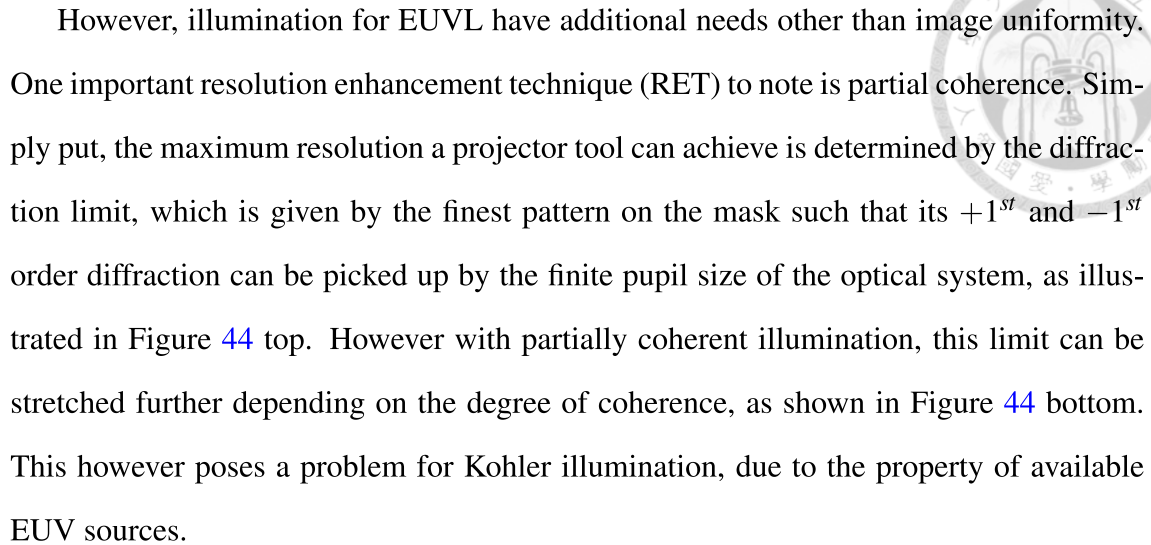

However, illumination for EUVL have additional needs other than image uniformity. One important resolution enhancement technique (RET) to note is partial coherence. Simply put, the maximum resolution a projector tool can achieve is determined by the diffraction limit, which is given by the finest pattern on the mask such that its $+1^{st}$ and -1st order diffraction can be picked up by the finite pupil size of the optical system, as illustrated in Figure 44 top. However with partially coherent illumination, this limit can be stretched further depending on the degree of coherence, as shown in Figure 44 bottom. This however poses a problem for Kohler illumination, due to the property of available EUV sources.

Kohler Integrator

Currently, a common way to produce an EUV source is through a method known as laser produced plasma (LPP), which involves focusing a high powered laser onto a thin stream of dye. This process gives the dye enough energy to turn into its plasma state, which then emits its characteristic 13.4 nm EUV. EUV produced in this fashion behaves as if it originates from a single point, and when used as the light source in Kohler illumination arrangement, will produced a single point on the pupil plane of the projector tool (illustrated by the yellow path in Figure 43), whereas partial coherence RET requires a spot of a certain size on the pupil plane. Therefore, a slight modification to the Kohler illumination arrangement was made, into what is now known as the Kohler integrator. [40] Figure 45 is a diagram of the illuminator configuration. In the figure, ϕ_P, ϕ_F, ϕ_{L1}, and ϕ_{L2} are the optical power of the pupil array (PA), field array (FA), and field lenses 1 and 2 (FL1 and FL2) respectively; and t_F, t_L, t_{L1}, and t_{L2} denote the inter-element spacings. The final distance parameter t_{En} differs from the rest in the sense that it is not a parameter of the illuminator, but is instead the distance from the mask to the entrance pupil (EnP) of the projection tool.

The Kohler integrator added a pair of lens arrays, or mirror arrays (e.g. Figure 46) for the case of EUVL, to the configuration. The first mirror array forms a grid sources (GS) from a collimated LPP source, and the second array placed after the grid source adjusts

doi:10.6342/NTU201901098

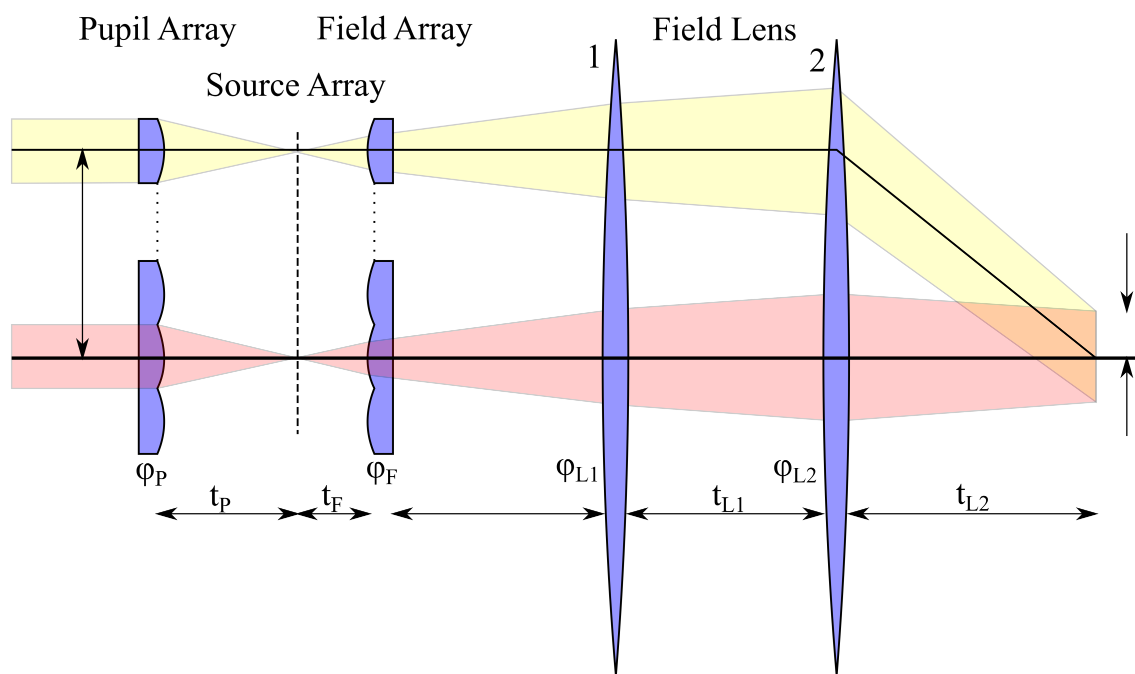

Figure 45: A diagram of the Kohler integrator configuration.

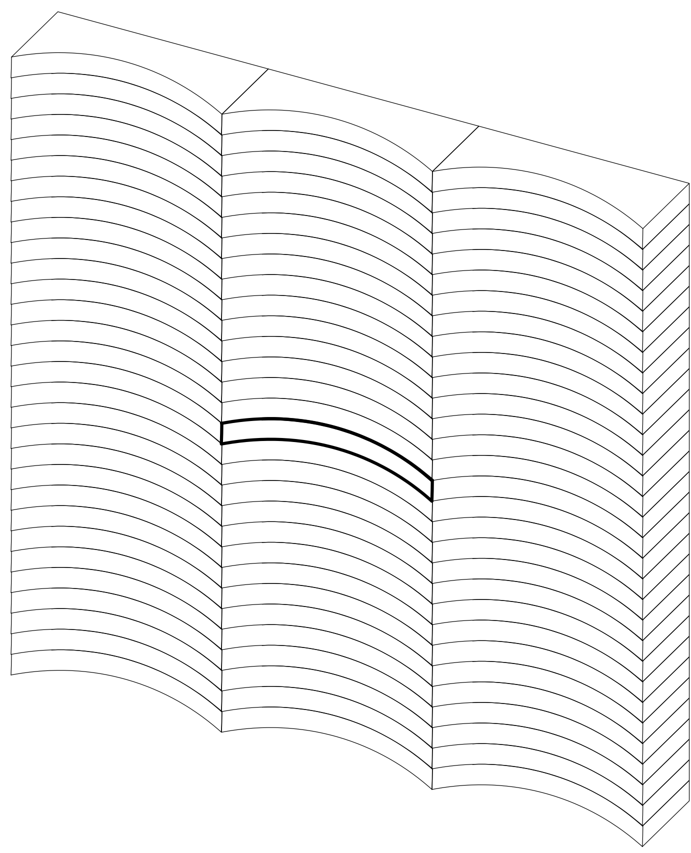

Figure 46: A diagram of the ringfield mirror array, or fly eye reflector.

doi:10.6342/NTU201901098

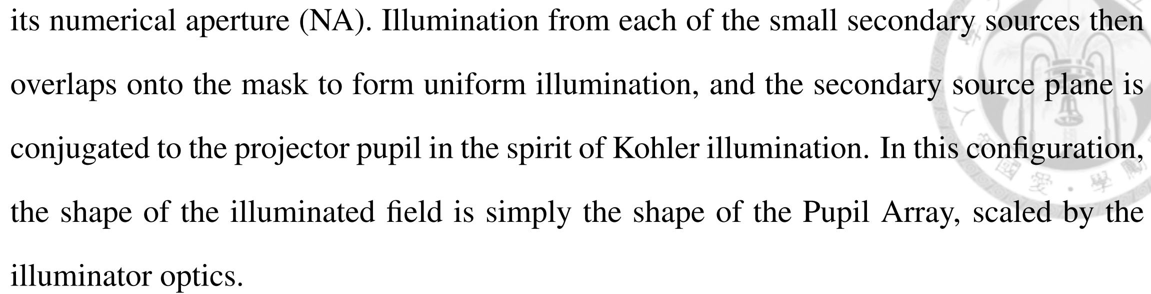

its numerical aperture (NA). Illumination from each of the small secondary sources then overlaps onto the mask to form uniform illumination, and the secondary source plane is conjugated to the projector pupil in the spirit of Kohler illumination. In this configuration, the shape of the illuminated field is simply the shape of the Pupil Array, scaled by the illuminator optics.

This crucial feature, coupled with the possibility for partial coherence RET, makes the Kohler integrator a suitable choice for EUVL illuminator. As explained by Antoni [41], since an EUVL projection tool need to be arranged such a way that the mirrors do not obstruct the light paths, for projection tools designed in primarily coaxial arrangement (e.g. [39]) the object and image field must result in the shape of a ringfield. Numerous methods exist capable of producing ringfield illuminations, however the Kohler integrator is often chosen for its illumination shape flexibility, as well as its illumination uniformity.

The aim of this work therefore, is to establish a systematic design method of a Kohler integrator illuminator for EUVL through the mathematics of the Generalized Gaussian Constants (GGC). [36] The GGC is a method of representing first order properties of an optical system similar to the ABCD matrix, however with a noted difference in that the GGC is capable of handling complex optical systems with ease, whereas expansion of the ABCD matrix quickly becomes overly tedious with increasing number of optical elements. For this reason, the GGC is a suitable analysis method to accommodate the multitude of optical requirements necessary to formulate the Kohler integrator. As a test design example, in this work the illuminator will be designed to match the specifications of an existing projection tool design, taken from the author's previous work. [5]

doi:10.6342/NTU201901098

2 Mathematical Methods

2.1 Gaussian Bracket

The Generalized Gaussian Constants (GGC) is first developed by Tanaka [36] in his analysis of paraxial theories in optical design, and is itself built upon of an even earlier work by Herzberger [37], on the Gaussian Bracket. It is closely related to the ABCD matrix method, however over and above, GGC is also useful in analyzing the whole system as a combination of smaller subsystems, which can then again be broken down into even smaller subsystems to any degree desired. This abstraction of raw lens data into optical properties of the sub-systems at arbitrary level of abstraction is a great help in analyzing the inter-subsystem relations, which are easily lost in the raw expansion of the ABCD matrix of even a slightly larger optical system. In fact, the development of GGC was initially intended for purpose of zoom lens design and analysis [42], where inside the complex optical system the optical elements are constantly moving in relation to one another. This analytic power lends itself well to optics design of other applications, such as this case of EUVL projection systems.

2.1.1 Definition

The basic definitions of the Gaussian bracket are as follows.

doi:10.6342/NTU201901098

First, an empty Gaussian bracket has unitary value.

$$[\ \ ] \equiv 1 \tag{26}$$

Second, the Gaussian bracket of a single value is the value itself.

$$[a_1] \equiv a_1 \tag{27}$$

Third, the Gaussian bracket of a serie of values can be decomposed by

$$[a_1\ a_2\ \dots\ a_n] \equiv [a_1\ a_2\ \dots\ a_{n-1}]a_n + [a_1\ a_2\ \dots\ a_{n-2}] \tag{28}$$

Together, these three basic definitions form the basis of the mathematics of the Gaussian bracket.

2.1.2 Identities

Stemming from the basic definitions, after some derivations useful results can be obtained.

Linear Combination - Final Element

First, from its definition itself 28

$$[a_1, \dots a_n] = [a_1, \dots a_{n-1}]a_n + [a_1, \dots a_{n-2}], \tag{29}$$

a Gaussian bracket can be decomposed to into a linear function of its final element.

Symmetry

The Gaussian bracket is symmetric.

$$[a_1\ \dots\ a_n] = [a_n\ \dots\ a_1] \tag{30}$$

doi:10.6342/NTU201901098

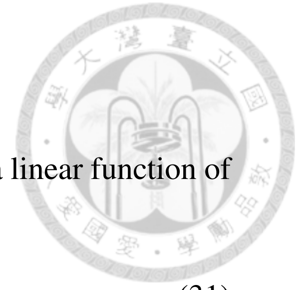

Linear Combination - First Element

By combining 28 and 30, a Gaussian bracket can be decomposed into a linear function of its first element.

$$[a_1 \dots a_n] = a_1[a_2 \dots a_n] + [a_3 \dots a_n] \tag{31}$$

Linear Combination - Any Element

A Gaussian is can be decomposed into a linear function of any one of its elements

$$[a_1 \dots a_n] = Ca_x + D \tag{32}$$

where

$$\begin{aligned} C &= [a_1 \dots a_{x-1}][a_{x+1} \dots a_n] \\ D &= [a_1, \dots a_{x-2}, a_{x-1} + a_{x+1}, ax+2, \dots a_n] \end{aligned}$$

Derivative

From 32, the derivative of a Gaussian bracket by one of its element can be given by

$$\frac{d}{d\, a_x}[a_1 \dots a_n] = [a_1 \dots a_{x-1}][a_{x+1} \dots a_n]. \tag{33}$$

Linear Combination - Gaussian Brackets

A Gaussian bracket can be decomposed into linear combinations of smaller Gaussian brackets

$$[a_1 \dots a_n] = [a_1 \dots a_x][a_{x+1} \dots a_n] + [a_1 \dots a_{x-1}][a_{x+2} \dots a_n]. \tag{34}$$

doi:10.6342/NTU201901098

2.2 Generalized Gaussian Constants

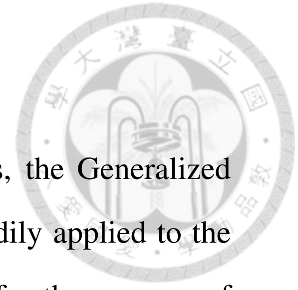

Whereas the Gaussian bracket is simply a set of mathematical rules, the Generalized Gaussian Constants (GGC) is where the Gaussian bracket can be readily applied to the geometric analysis of optical systems. The GGC is a powerful tool for the purpose of performing analysis on optical systems, and have the advantage of notational clearity and simplicity (relatively speaking) when dealing with systems with extensive complexity.

2.2.1 Definition

Consider an optical system consisting of many elements (with respective powers ϕ_1, ϕ_2, $...\phi_n$), separated by inter-element distances ($t_1, t_2, ...t_{n-1}$), the four GGC terms are defined as follows

$$
\begin{aligned}
{}^iA_j &= [\phi_i, -t_i, \phi_{i+1}, -t_{i+1} ... - t_{j-1}] && (35) \\
{}^iB_j &= [-t_i, \phi_{i+1}, -t_{i+1} ... - t_{j-1}] && (36) \\
{}^iC_j &= [\phi_i, -t_i, \phi_{i+1}, -t_{i+1} ... - t_{j-1}, \phi_j] && (37) \\
{}^iD_j &= [-t_i, \phi_{i+1}, -t_{i+1} ... - t_{j-1}, \phi_j] && (38)
\end{aligned}
$$

A simple way to remember is that C is the complete bracket, A is without the tail, D is without the head, and B have neither.

2.2.2 Relationship to the Matrix Method

In the matrix method of optical system analysis, the refraction through an optical surface of power ϕ is

$$R = \begin{bmatrix} 1 & 0 \\ -\phi & 1 \end{bmatrix}, \quad (39)$$

and the transfer in space by distance t is

$$T = \begin{bmatrix} 1 & t \\ 0 & 1 \end{bmatrix}. \quad (40)$$

doi:10.6342/NTU201901098

As such, an optical system consisting of n lenses can be described by the ABCD matrix, given by

$$\begin{bmatrix} A & B \\ C & D \end{bmatrix} = R_n T_{n-1} R_{n-1} T_{n-2} \ldots T_1 R_1$$
$$= \begin{bmatrix} 1 & 0 \\ -\phi_n & 1 \end{bmatrix} \begin{bmatrix} 1 & t_{n-1} \\ 0 & 1 \end{bmatrix} \begin{bmatrix} 1 & 0 \\ -\phi_{n-1} & 1 \end{bmatrix} \begin{bmatrix} 1 & t_{n-2} \\ 0 & 1 \end{bmatrix} \ldots \begin{bmatrix} 1 & t_1 \\ 0 & 1 \end{bmatrix} \begin{bmatrix} 1 & 0 \\ -\phi_1 & 1 \end{bmatrix} \tag{41}$$

Incidentally, the elements A, B, C, and D obtained by performing series of matrix multiplication, is the same as the result obtained by calculating the four GGC terms ${}^1A_n$, ${}^1B_n$, ${}^1C_n$, and ${}^1D_n$, with some corrections to the inconsistencies resulting from the difference in the sign convention used by Herzberger.

2.2.3 GGC and Optical System Properties

Here, some useful corollaries follows, as given in Tanaka's work, [36] for an optical system consisting of n number of elements.

Effective Focal Length

The effective focal length of a system consisting of n elements can be expressed as

$$\text{EF} = \frac{1}{\Phi} = \frac{1}{C_{(1,n)}}. \tag{42}$$

The effective focal length is the focal length of the combined optical system. It is the distance required for the optical system to focus incoming parallel rays of light into a point as if it is one optical element. Figure 47 is a diagram shown an optical system focusing parallel light, coming from both the front and back of the optical system.

doi:10.6342/NTU201901098

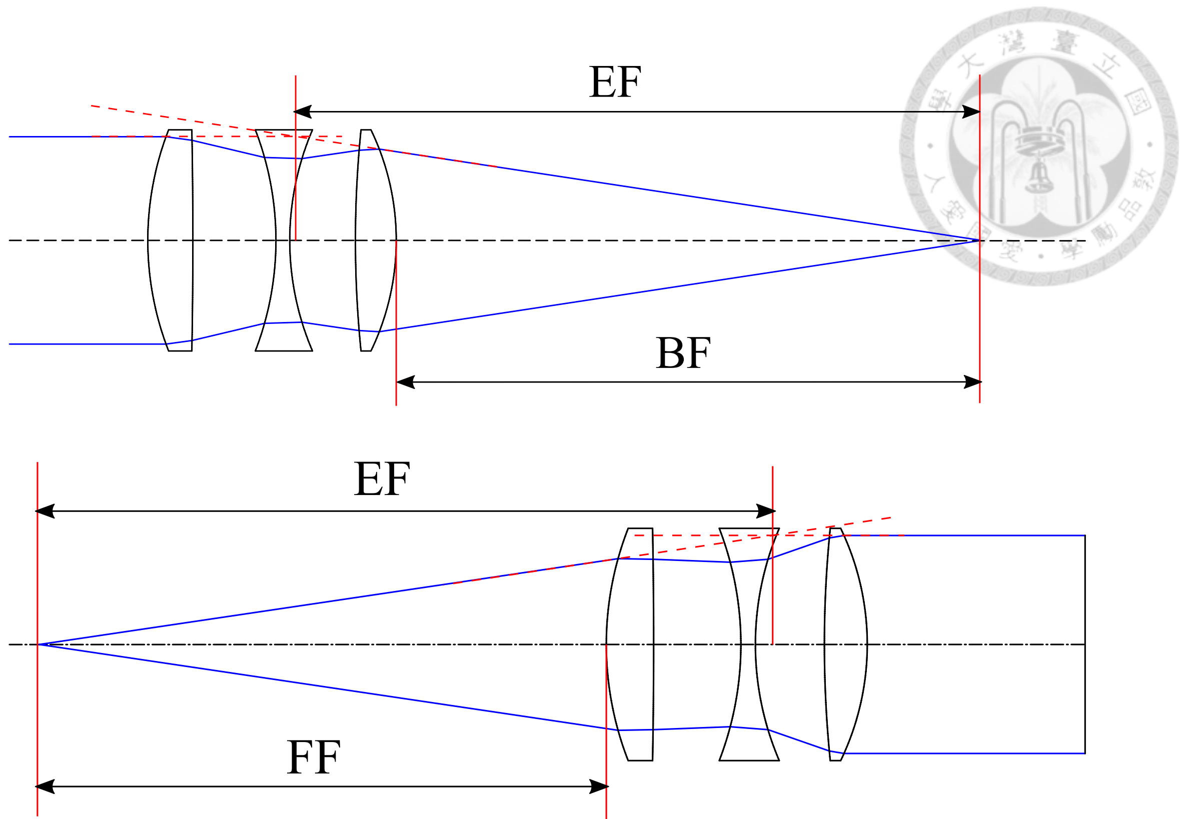

Figure 47: The effective focal length, back focal length, and front focal length of an optical system.

Back Focal Length

The back focal length of a system of n elements is

$$\mathrm{BF} = \frac{A_{(1,n)}}{C_{(1,n)}} = \mathrm{EF} \cdot A_{(1,n)}. \tag{43}$$

The back focal length is the distance from the final optical to the back focal point of the optical system, shown in the upper part of Figure 47.

Front Focal Length

The front focal length is given by

$$\mathrm{FF} = -\frac{D_{(1,n)}}{C_{(1,n)}} = -\mathrm{EF} \cdot D_{(1,n)}. \tag{44}$$

Likewise, also shown in Figure 47, the front focal length is the distance from the first optical element to the front focal point. In general, the front focal length and the back

doi:10.6342/NTU201901098

focal length do not have to be the same, except for some rare special cases.

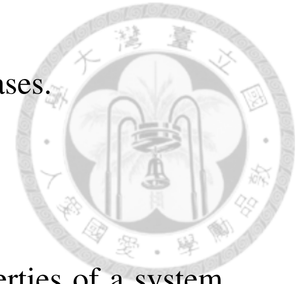

The GGC Term B

The $B_{(1,n)}$ GGC term has no obvious relationship to the optical properties of a system, however by taking into account of the property of an ABCD matrix representing an optical system that its determinant gives

$$\begin{vmatrix} A & B \\ C & D \end{vmatrix} = A \cdot D - B \cdot C = 1. \tag{45}$$

Arranging for the B term gives

$$B = \frac{A \cdot D - 1}{C} = \frac{\frac{A \cdot D}{C^2} - \frac{1}{C^2}}{\frac{1}{C}}, \tag{46}$$

which when combined with Equations 42 to 44 gives the following condition that

$$B_{(1,n)} = -\frac{\mathrm{EF}^2 + \mathrm{FF} \cdot \mathrm{BF}}{\mathrm{EF}}. \tag{47}$$

Object-Image Conjugation

With the addition of an object, the formation of the image of the object through the optical system, is given in the following object-image conjugate relationship

$$B_{(0,n+1)} = 0. \tag{48}$$

In Figure 48, this is represented by the ray trace of the blue lines, an object at distance t_0 to the optical system is imaged by the optical system to form an image at distance t_n away from the optical system.

doi:10.6342/NTU201901098

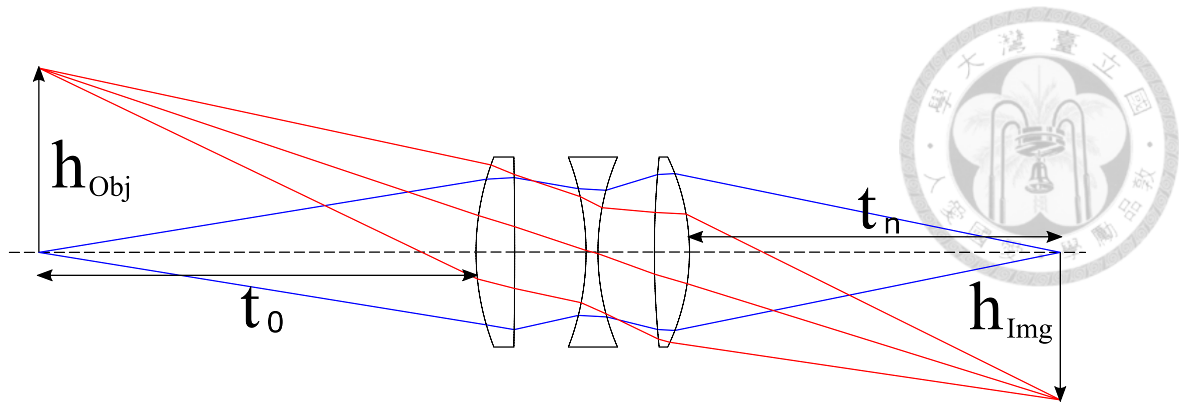

Figure 48: Illustration of a finite conjugate optical system.

Lateral Magnification

The lateral magnification (often referred to simply as the magnification) of the image through the optical system is

$$M = \frac{1}{D_{(0,n)}} = A_{(1,n+1)}. \tag{49}$$

In an optical system, the magnification of the optical system is the ratio of the size of the image against the size of the original object. The ray trace of an off-axis object point (the red lines) in Figure 48 gives the object height h_{Obj} and the image height h_{Img}, and the magnification is given by

$$M = \frac{h_{Img}}{h_{Obj}} \tag{50}$$

Other Identities

Some other commonly used identities for GGC regarding an optical system are as listed below.

- **Object-Image Conjugate Relationship** (Infinite Conjugate)

$$^{1}A_{n+1} = 0 \tag{51}$$

- **Angular Magnification**

$$M_A = \frac{1}{^{0}A_n} = {^{0}D_n} \tag{52}$$

doi:10.6342/NTU201901098

- **Front Principal Plane Location** (w.r.t. Element 1)

$$s_P = \frac{1 - {}^1D_n}{{}^1C_n} \tag{53}$$

- **Rear Principal Plane Location** (w.r.t. Element n)

$$s'_P = \frac{{}^1A_n - 1}{{}^1C_n} \tag{54}$$

- **GGC Decomposition**

  The GGC of a group of optical elements can be broken down into a linear combination of GGC of two smaller groups. Assuming a system of n elements formed by two subsystems consting of the first to the kth element, and the $k+1^{th}$ to the nth element, with

$$1 < k < n, \tag{55}$$

  separated by a distance t_k, the following expansions can be obtained by applying the the Gaussian bracket property in Equation 34.

$$A_{(1,n)} = A_{(1,k)}A_{(k+1,n)} + C_{(1,k)}(B_{(k+1,n)} - t_k A_{(k+1,n)}) \tag{56}$$

$$B_{(1,n)} = B_{(1,k)}A_{(k+1,n)} + D_{(1,k)}(B_{(k+1,n)} - t_k A_{(k+1,n)}) \tag{57}$$

$$C_{(1,n)} = A_{(1,k)}C_{(k+1,n)} + C_{(1,k)}(D_{(k+1,n)} - t_k C_{(k+1,n)}) \tag{58}$$

$$D_{(1,n)} = B_{(1,k)}C_{(k+1,n)} + D_{(1,k)}(D_{(k+1,n)} - t_k C_{(k+1,n)}) \tag{59}$$

doi:10.6342/NTU201901098

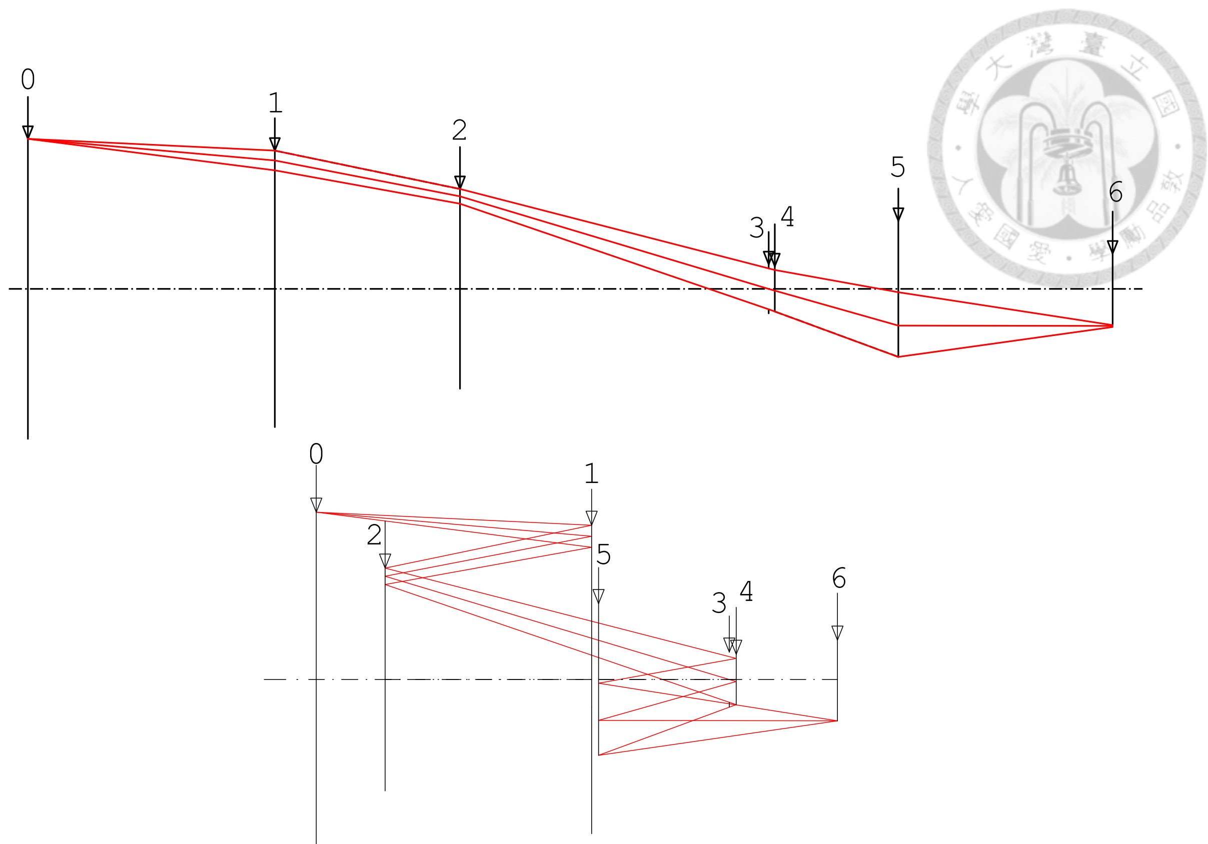

Figure 49: **Upper**: The paraxial representation of an optical system formulated with GGC. **Lower**: The exact same optical system represented using reflective elements.

2.2.4 GGC in Mirror Systems for EUV

The GGC makes no specific distinctions when treating reflective optical systems involving mirrors to conventional refractive lens systems. However, caution must be exercised when applying the results obtained through GGC to be implemented in mirrors systems, in particularily with the sign conventions. Unlike conventional refractive systems, with reflective systems the light bounces back and forth between elements, resulting in the constant plus-minus-plus-minus... switch in the progation distance when expressed in commercial optical design software. Figure 49 shows two layouts of an optical system formulated with GGC. The upper layout is represented using paraxial thin lens elements, while the lower is represented using reflective mirror elements.

doi:10.6342/NTU201901098

2.3 Numerical Optimization

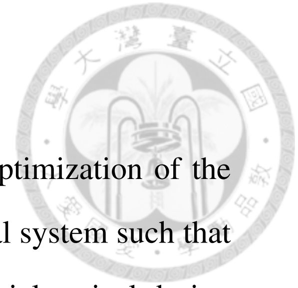

In optical design, a significant portion of effort is dedicated to the optimization of the design, in an attempt to find the optimal parameter values of the optical system such that the aberration of the image is minimized. For this reason, a commercial optical design software (e.g. Code V, Zemax) is desirable when performing optical system design, as each comes with its own set of optimization tools.

2.3.1 Commercial Opical Design Software

The exact process involved in design optimization using each commercial optical design software differs from program to program. [43] [44] However, the fundamental principle is very similar across all design software.

Defining Error Function

First, a set of error functions (some referred to as the merit function) are defined. These functions dictates the quantities to be minimized during optimization, and does not necessarily have to be related to specific optical system properties in general. For example, if for some odd reason that an occasion should arise that for a system consisting of two lenses, the lens diameter of the second lens (D_2) is required to be twice as large as the diameter of the first lens (D_1), then that particular error function can simply be expressed as the quantity

$$\varepsilon = D_2 - 2D_1 \tag{60}$$

to serve as the criterion of the optimization.

Commercial design software usually have a set of default merit functions dedicated to improve the image quality by reducing the aberration of the optical system. This allows optical designers to dedicate their efforts in defining the set of error functions to target specific goals that they might want to achieve in the design, while the formulation of the general image aberration error functions can be handled by the software. The total error

doi:10.6342/NTU201901098

is then a weighted square sum of each of the individually defined errors

$$\varepsilon_{total} = \sum_n \varepsilon_n{}^2 \tag{61}$$

Defining Variable Parameters

After the error functions are defined, before optimization can commence the variable parameters must be defined. Parameters that defines an optical system are parameters such as

- **Surface Profile Parameters**

  The surface profile parameters of the optical elements. Surface radius of curvature, conic constant, and aspheric polynomial coefficients.

- **Element Thickness and Spacings**

  The thickness of the optical elements, and the spacing between each of them.

- **Material Properties**

  Refraction indices and dispersion coefficients of the material of the optical elements.

- **Optical System Properties** Effective focal length, field of view, NA, F-Number, entrance pupil and exit pupil location and diameter.

Optical Design Optimization

The act of optical design optimization is an attempt to find the optimal combination of optical system parameters such that the total error defined is minimized. Mathematically, if the number of variable parameters are few, this can be as simple as taking a derivative of the error function and finding where it goes to zero

$$\frac{d}{d\rho} \sum_n \left[\varepsilon_n(\rho)^2\right] = 0. \tag{62}$$

doi:10.6342/NTU201901098

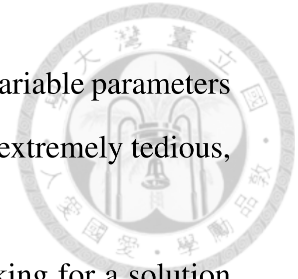

However this is also apparent that when either (or both) the number of variable parameters or the number of defined error functions is large, this process becomes extremely tedious, or practically impossible to perform.

How the optimization algorithm tackles this task is by simply seeking for a solution that is better than the current solution. By tuning the variable parameters, the optimization algorithm checks if the total error is decreased each time when the parameters are varied. If so, the result is accepted, saved, and the optimizer moves on to find the next better solution; or else if the error function did not decrease, the result is discarded and again the optimizer moves on to find the next better solution. This way, if one continues to find solutions that are better than the current solution, then hopefully, given enough time, the optimal solution can be reached eventually. Up to this day, many optimization methods exist. A typical method of optimization employed by optical design software is the damped least square method. [45]

The Problem

By defining a set of error functions as the optimization criterion and allowing some parameters of the optical system to be variable, the optical design software can optimize the design to the error functions given, by varying the available parameters. However, one glaring issue is that not all error functions are equal in importance or priority. For example, in the case of a lithographic projector, the property of telecentricity against a desired mask-wafer magnification. To the optimizer, some degree of loss in the telecentricity will have the same measure of "badness" as some degree of change in the system magnification, depending on the relative weightings given to the error functions associated. However in terms of lithographic projectors, some level of difference between the desired magnification and the actual magnification is not a problem as long as the actual magnification can be known and measured, the loss of telecentricity on the other hand is a very serious offense leading to a multitude of undesired imaging quality deterioration.

As such, optics designers faces these questions constantly:

- How much weighting should be assigned to each error function?

doi:10.6342/NTU201901098

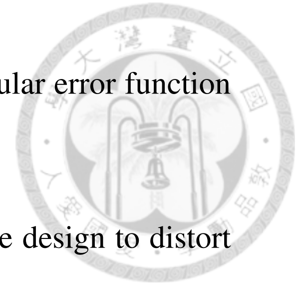

- How large does the weighting has to be to ensure that the particular error function maintained unvioleted throughout the optimization?
- Is the assigned weighting too large (or too small) as to cause the design to distort beyond intended?
- What should the weighting balance be between the error functions associated with the desired optical properties, and the error functions associated with the image aberration in general?

These question have no simple straightford answers, and is likely to haunt the designers throughout the entire design process.

The optical design software Code V attemps to address this issue of unequalness of the importance of the error functions by separating them into two "tiers" of error functions. The lower tier error functions are weighted, and the higher tier error functions are hard solved by sacrificing one available variable as the compensator to guarantee its maintainance. In the case that the option to hard solve the solution is not possible, either due to the error function being overly complex or convoluted to calculate, or the number of defined error functions exceed the number of available variables, they will be given a considerably larger weighting to be optimized along with the lower tier error function.

In practice, except for extremly limited and simple cases, the number of defined error functions will always exceed the number available variable parameters. Also, the notion of setting one variable parameter aside purely as a compensator parameter to fulfill one particular error function, aside from being a luxurious choice that most designs could not afford, is also quite dangerous. First, there is the risk of the calculated value of the compensator parameter being unrealistic or impossible is also present, such as having negative propagation distances (e.g. point of convergence for a diverging optical system) and a lens with radial thickness larger than the surface radius of curvature of the lens. Second, if during the optimizing process that error function was somehow violated, the large weighting assigned to it would cause the optimization algorithm to focus all optimizing efforts on it until it was remedied, most of the time in complete disregard to all other error functions

doi:10.6342/NTU201901098

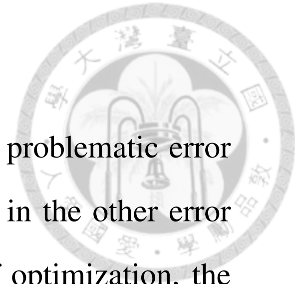

and likely rending the design irrecoverable beyond recognition.

One possible roundabout to deal with this is to first deal with the problematic error functions first in the initial stage of the optimizations, before adding in the other error functions that are less likely to cause trouble. After a few rounds of optimization, the design should be at a point where the problematic error function are mostly satisfied, and only then start adding in other error functions while keeping the weighting on the problematic error functions large and hope that the large weighting would deter the optimization algorithm from steering the solutions away from them. Of course, from this other problem arises. For example, there is no way of knowing which defined error functions in the set are more problematic or sensitive prior to performing the optimization. And even then, since the addition of other error functions changes the solution space, problematic error functions in the previous case might not be in the new solution space, and vice versa error functions that did not cause problems may become problematic in the new solution space.

It is in this situation that GGC can be proven useful.

2.3.2 GGC Integrated Optimization

The convenience of GGC lies in that it provides a clean and consise notation for representing optical properties. Using GGC, a system of equations describing the relationship between a desired optical property and the various parameters of the optical system can be derived. This system of equations can then be solved to obtain one governing equation that satisfies all of the desired optical properties. This governing equation can then be integrated into the optimization algorithm as the kernel, such that the output of the algorithm are always bound by the governing equation.

The idea is that, instead of listing deviation from the desired optical properties as error functions to be optimized along with the imaging aberrations of the optical system, let the optimizer search for solutions on the premise that the desired optical properties are met in the first place. This way, the optimizer of the optical design software can focus its resources on doing what it does best, what it was designed to do, which is reduce

doi:10.6342/NTU201901098

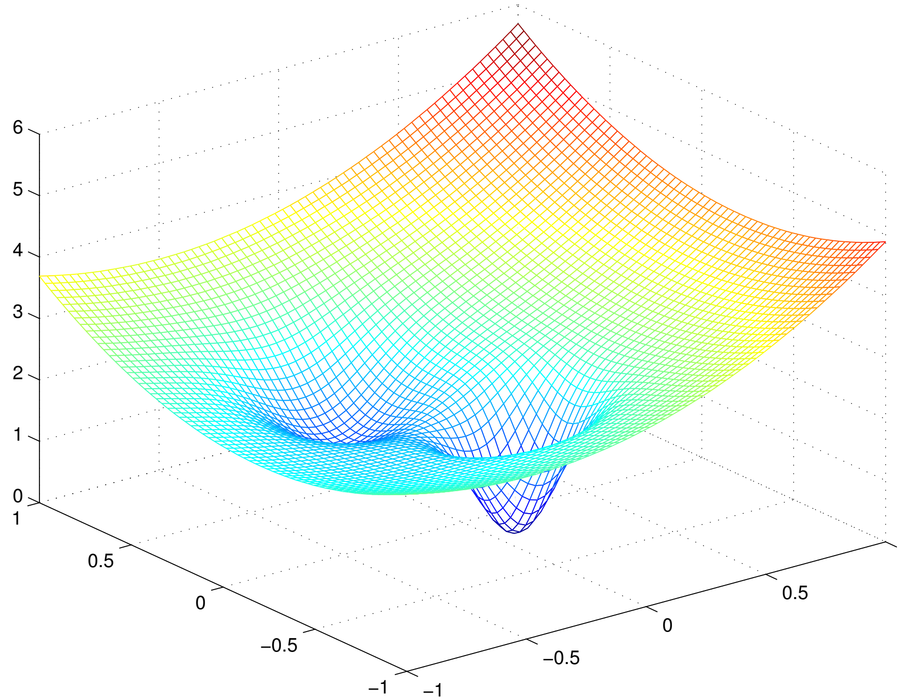

Figure 50: Example of a solution space with two local minima.

aberration and improve imaging quality.

With that said, the optimizer algorithm and procedure is a critical part of commercial optical design software, and is in most cases beyond reach for end users to view, let alone modify. Nevertheless, the incorporation of the governing equation derived with GGC is still possible, however the exact procedure to do so will depend on the software.

Although the optimizer of commercial design software cannot be modified, they can be called upon as the core of a customized optimization program in the form of a subroutine inside a programmable macro (*.seq* and *.zpl* files for Code V and Zemax respectively). In this research, a simple Monte Carlo random walk algorithm is used as the base of the customized optimizer, for its simplicity and robustness. The damped least square method often utilized by commercial design software, mentioned previously in Section 2.3.1, does an excellent job for finding the local minima, however has a limited capability of escaping it.

A local minima can be visualized as a "dip" in the solution space of the error functions, a point in which the error function is the smallest relative to other points in the neighborhood. Figure 50 shows an example of the solution space with two minima in

doi:10.6342/NTU201901098

close proximity. The optimizer have but one simple job, and that is to find the point in the error function solution space such that the error function is the smallest.

In general, there are two types of search over the variable parameters, global and local. What a designer hopes to achieve using the design software is to find the globa minimum, however most of the time what the optimizer is feasible of is only finding a local minimum in the neighborhood of the state prior to the optimization. This has to do with the nature of the variable parameters of the optical system. A global search on a parameter is possible only if the range of which the parameter is able (or allowed) to vary over are known explicitly. This is, unfortunately, not true in general for optical design optimization. For example, the range of values for the surface radius of curvature can vary from negative to positive infinity, and the inter-surface thicknesses from zero to positive infinity. As such, the optimizer can only sample over these parameters locally. In terms of the solution space in Figure 50, this means that if the algorithm chances upon the left minimum first, subsequent iterations would have trouble excaping it and finding the other lower minimum to the right.

Note that, this is not necessarily a bad thing. In fact, the ability to find the local minima is by definition what an optimizer should do in the first place. If the optimization algorithm repetitively tries to find a point in the solution space that yields a smaller error than the current system, it will eventually reach a local minimum. What the design software, or designers ourselves, should consider is how to find the next one with even smaller error.

Again, commercial design software each deals with this issue differently (*Global Synthesis* option in Code V, *Global Search* in Zemax), to various degree of effectiveness. The direction this research takes is to take advantage of the ability to find and homes in to the local minima using the optimizer algorithm of a commercial optical design software, and incorporating the ability to escape the local minimum to form a customized optimizer algorithm. The reason for this desicion is that, since commercial design software do not allow end users to inspect or modify the optimizer, there is little choice but to simply accept it as a blackbox that finds the local minima, and that although the optimizer algorithm

doi:10.6342/NTU201901098

cannot be modified, calling on it to act as part of a larger customized optimizer algorithm is completely fine.

Monte Carlo Random Walk Algorithm

The Monte Carlo random walk is an effective and simple method to construct an optimization algorithm. Displayed in Figure 51 is a diagram of the algorithm. The basic steps of this Monte Carlo algorithm are as follows.

- **Step 1** Begin with an initial state.
- **Step 2** Calculate $err_{current}$, the current error.
- **Step 3** Propose a new state.
- **Step 4** Calculate err_{new}, the new error.
- **Step 5** Compare err_{new} with $err_{current}$.
  - **Step 5A** $err_{new} < err_{current}$
    Accept the new state as the current state in the next iteration.
  - **Step 5B** $err_{new} > err_{current}$
    Reject or accept the new state with probability.
- **Go back to Step 3**

The robustness of the Monte Carlo algorithms lies in its random probabilistic nature (Step 5B). Allowing the algorithm to sometimes accept a "bad call" with a small probability leads to two important results. First, each iteration of the algorithm now have a small non-zero chance of escaping the current local minimum; and second, since the probability to accept a worse state is small, this is unlikely to cause a significant hinderance to the ability of the optimizer algorithm to find the current local minimum. When the number of iteration is large, this leads to:

doi:10.6342/NTU201901098

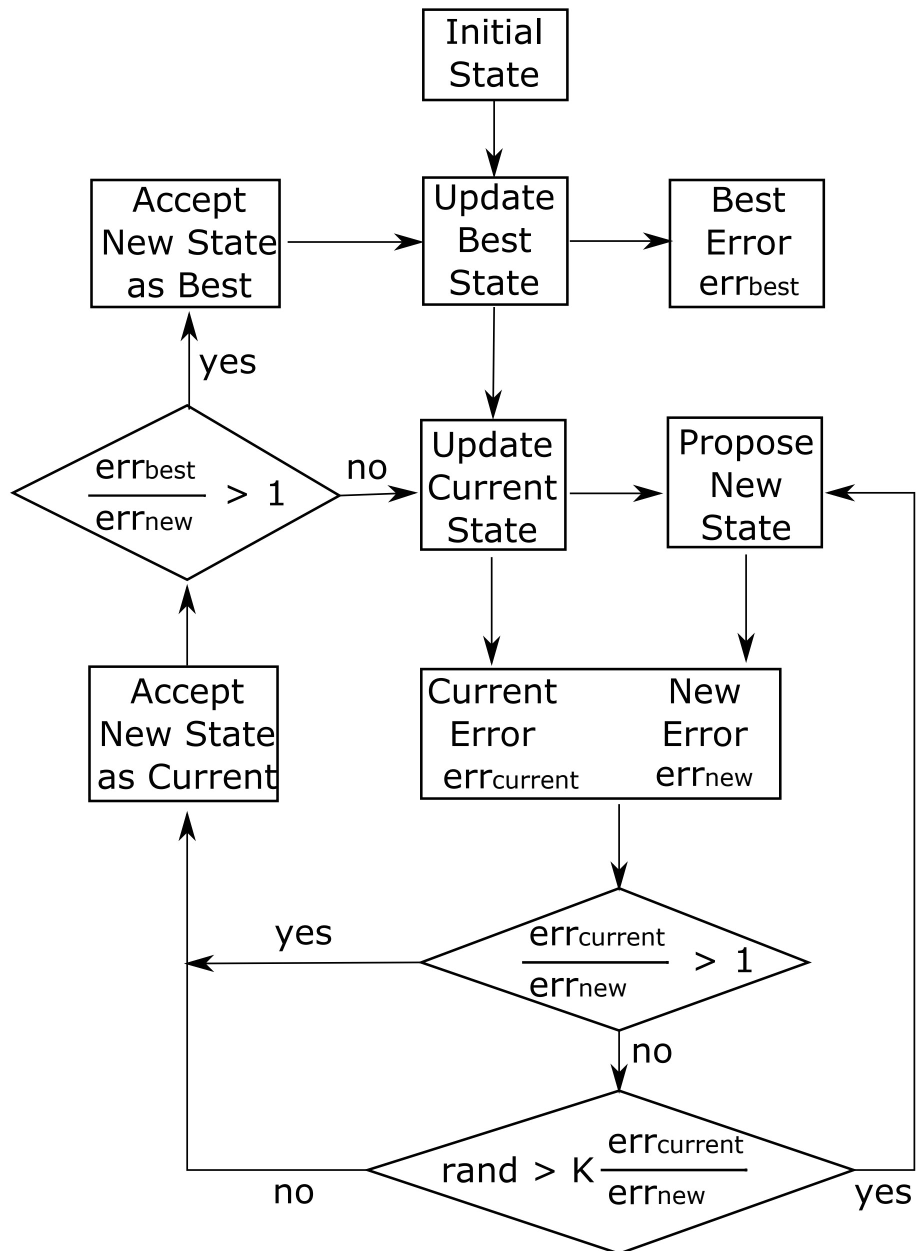

Figure 51: Flow diagram of the Monte Carlo random walk algorithm.

doi:10.6342/NTU201901098

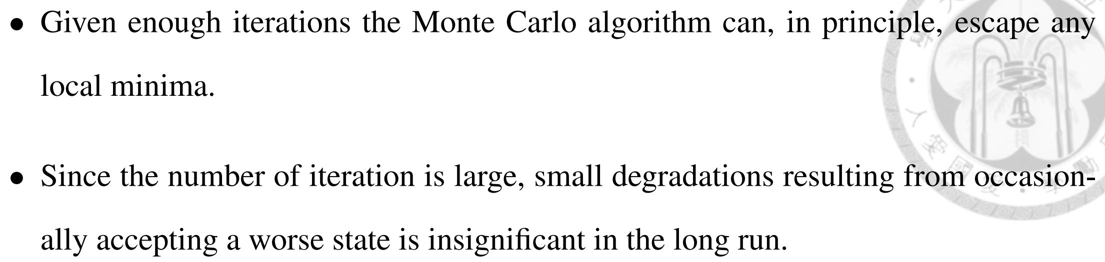

- Given enough iterations the Monte Carlo algorithm can, in principle, escape any local minima.
- Since the number of iteration is large, small degradations resulting from occasionally accepting a worse state is insignificant in the long run.

These two proerties form the fundamental principle behind this Monte Carlo algorithm.

doi:10.6342/NTU201901098

3 Projection Tool Design

3.1 Optical System Properties

3.1.1 Telecentricity

Telecentricity (wafer side) is one of the most crucial condition in lithographic projection systems. In principle, during the exposure process the photoresist (PR) coated wafer should be placed exactly on the image plane of the projection, which is not easily accomplished. In practice, even if alignment precision allows exact placement, the finite thickness of the PR layer warrants that some degree of defocus will always be present and must be tolerated. For non-telecentric systems, where defocus is present, both image blurring and image shift occur. If however the system is telecentric, the image shift is eliminated and only blurring remains, as illustrated in Figure 52.

In optics terms, telecentricity is when all chief rays emerges at the image parallel to the optical axis. Since all chief rays pass through the center of the aperture stop, telecentricity therefore occurs when the aperture stop lies exactly on the front focal plane of the post-stop group. For a system with n number of elements, this can be derived to be

$$D_b = D_{(s,n)} = 0 \tag{63}$$

where s is the stop surface number, by Equation 48 with the aperture stop as the object and setting the image distance at infinity. Expansion of the Gaussian bracket through

doi:10.6342/NTU201901098

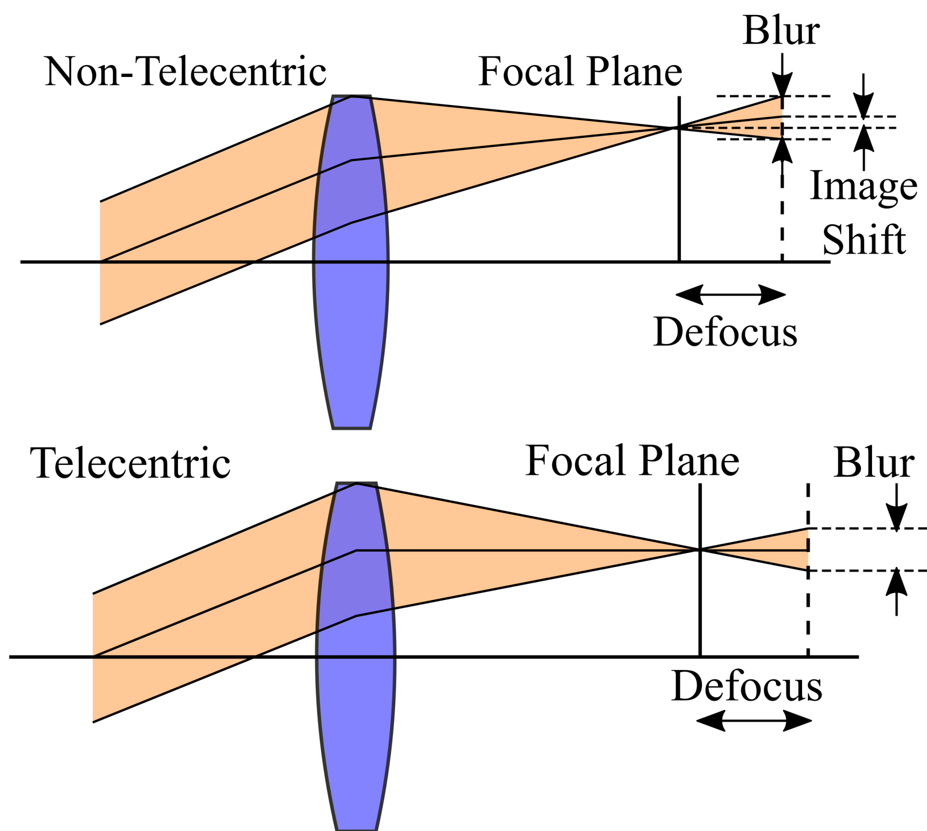

Figure 52: Defocus on a non-telecentric system causes blurring and image shift, while on a telecentric system only blurring occurs.

doi:10.6342/NTU201901098

Equation 31 then gives

$$\begin{aligned} D_{(s,n)} &= [-t_s, \phi_{s+1}, -t_{s+1} \ldots -t_{n-1}, \phi_n] \\ &= -t_s[\phi_{s+1} \ldots \phi_n] + [-t_{s+1} \ldots \phi_n] \\ &= -t_s C_{(s+1,n)} + D_{(s+1,n)} \\ &= -t_s C_B + D_B \ , \end{aligned} \tag{64}$$

and combined with Equation 63 the condition for telecentricity on the wafer side can be obtained

$$t_s = \frac{D_B}{C_B} = -FF_B \ . \tag{65}$$

Similar treatment can reveal, should the necessity arise, that the condition for mask side telecentricity is

$$t_{s-1} = \frac{A_B}{C_B} = BF_A. \tag{66}$$

3.1.2 Magnification

The magnification, or reduction ratio by some, of the EUVL tool determines the ratio between the feature size designed on the mask to the imaged feature size on the wafer. From Equation 49, Gaussian bracket expansion of the $A_{(1,n+1)}$ term for the pre-stop post-stop configuration gives

$$\begin{aligned} M &= [\phi_1, -t_1 \ldots \phi_n, -t_n] \\ &= [\phi_1 \ldots -t_{s-1}]\phi_s[-t_s \ldots -t_n] \\ &\quad +[\phi_1 \ldots -t_{s-1}][\phi_{s+1} \ldots -t_n] + [\phi_1 \ldots \phi_{s-1}][-t_s \ldots -t_n] \\ &= A_{(1,s)}A_{(s+1,n+1)} + C_{(1,s-1)}B_{(s,n+1)} \\ &= (A^1_{s-1} - t_{s-1}C^1_{s-1})(A^{s+1}_n - t_n C^{s+1}_n) \\ &\quad +C^1_{s-1}(B^{s+1}_n + t_s t_n C^{s+1}_n - t_s A^{s+1}_n - t_n D^{s+1}_n) \\ &= (A_A - t_{s-1}C_A)(A_B - t_n C_B) \\ &\quad +C_A(B_B + t_s t_{im} C_B - t_s A_B - t_n D_B) \ . \end{aligned} \tag{67}$$

doi:10.6342/NTU201901098

Substituting of the GGC in terms of the optical properties (42 to 47) then gives

$$M = \frac{-\mathrm{EF}_B{}^2 + (\mathrm{BF}_B - t_{im})(\mathrm{BF}_A - \mathrm{FF}_B - t_s - t_{s-1})}{\mathrm{EF}_A \mathrm{EF}_B} \quad , \tag{68}$$

or treatment for $D_{(0,n)}$ gives another expression for the magnification

$$\frac{1}{M} = \frac{-\mathrm{EF}_A{}^2 + (\mathrm{FF}_A + t_{ob})(\mathrm{BF}_A - \mathrm{FF}_B - t_s - t_{s-1})}{\mathrm{EF}_A \mathrm{EF}_B} \quad . \tag{69}$$

Then with the telecentricity condition (Equation 65), the expression for magnification can be rearranged into an expression for the object distance t_{ob} and the image distance t_{im} under the condition of image side telecentricity

$$t_{im} = -\mathrm{FF}_A + \frac{\mathrm{EF}_A \mathrm{EF}_B + M \cdot \mathrm{EF}_A{}^2}{M(\mathrm{BF}_A - t_{s-1})} \tag{70}$$

and

$$t_{ob} = \mathrm{BF}_B - \frac{M \cdot \mathrm{EF}_A \mathrm{EF}_B + \mathrm{EF}_B{}^2}{\mathrm{BF}_A - t_{s-1}} \quad . \tag{71}$$

For most current tools, the magnification lies between 0.2 to 0.25.

3.1.3 Mask-Wafer Conjugate

Again, Gaussian bracket expansion of the $B_{(0,s+1)}$ term in Equation 49 gives

$$\begin{aligned}
& B_{(0,s+1)} \\
= \; & [-t_0, \phi_1 \ldots \phi_n, -t_n] \\
= \; & [-t_0 \ldots - t_{s-1}] \phi_s [-t_s \ldots - t_n] \\
& + [-t_0 \ldots - t_{s-1}][\phi_{s+1} \ldots - t_n] + [-t_0 \ldots \phi_{s-1}][-t_s \ldots - t_n] \\
= \; & (B_A + t_{ob} t_{s-1} C_A - t_{ob} A_A - t_{s-1} D_A)(A_B - t_{im} C_B) \\
& + (B_B + t_s t_{im} C_B - t_s A_B - t_{im} D_B)(D_A - t_{ob} C_A) \quad .
\end{aligned} \tag{72}$$

doi:10.6342/NTU201901098

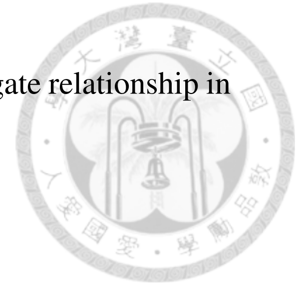

then substitution of Equations 42 to 47 to obtain the mask-wafer conjugate relationship in terms of the subsystem optical properties

$$0 = \frac{\mathrm{EF}_B}{\mathrm{EF}_A}(\mathrm{FF}_A + t_{ob}) - \frac{\mathrm{EF}_A}{\mathrm{EF}_B}(\mathrm{BF}_B + t_{im}) - \frac{(\mathrm{FF}_A + t_{ob})(\mathrm{BF}_B + t_{im})(\mathrm{BF}_A - \mathrm{FF}_B - t_s - t_{s-1})}{\mathrm{EF}_A \mathrm{EF}_B} \quad . \tag{73}$$

3.1.4 Total Tract Length

The total tract length (TTL) refers to the length spanning the entirety of the optical system. In the case of infinite conjugate, the TTL is often measured from the first element to the image. In the case of finite conjugate, as with lithography, TTL begins with the mask (object) and ends at the wafer (image), as illustrated in Figure 42. That is,

$$\mathrm{TTL} = t_{ob} + sep_a + t_{s-1} + t_s + sep_b + t_{im} \quad . \tag{74}$$

Though not immediately obvious, the choice of TTL is not arbitrary. In many cases, some maximum length constraints are placed on the TTL by form factor and manufacturability considerations.

3.2 Number of Mirrors

Up to this point, all derived conditions are general and independent of the number of optical elements. For EUVL tools, the choice of the number of mirrors in the design is a compromization between many factors, most notably between the power output and imaging quality. Regarding the power output, even with a perfectly manufactured mirror and coated with over 40 layer pairs of optical coating optimized for EUV, the reflection is only at maximum 70%, for normal incidence and decreases as the angle of incidence increases. [4] Assuming a six-mirror system, at the wafer side only 11.7% of the power from the mask remains, or 4.0% of the power from the EUV source assuming a simple three mirror illumination optics. Therefore considering the throughput efficiency, the

doi:10.6342/NTU201901098

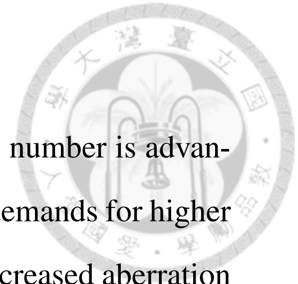

number of mirrors should be as few as possible.

On the other hand, regarding the EUVL tool design, increasing the number is advantageous for the purpose of aberration correction. With ever increasing demands for higher NA, the EUVL tool design will be unable to sufficiently mitigate the increased aberration associated with higher NA, if not given the necessary number of mirrors to design with. As such, for most designs in the past decade, the compromization between power output and imaging quality are met at either four, six, or eight mirrors depending on the intended NA.

As for the even number of mirrors, this decision originates from a simple notion regarding high volume manufacturability. Even number of reflection ensures that the mask (object) and the wafer (image) are positioned at the two opposing sides of the tool, allowing ample working space for the machineries at both the mask side and the wafer side.

3.2.1 Notes on the Aperture Stop Position

For an EUVL tool, the position of the aperture stop is often bound to a particular surface, and in many cases the second mirror is often chosen as the aperture stop, as in the case of Liu's design. [39] While in general there are no laws or guidelines dictating that this must be so, optimizations with respect to the physical obstruction of the mirrors will most undoubtedly arrive at this result. For reflective optical systems, space is a precious and scarce resource since the mirrors will cause obstruction in the image if the mirror is placed in the path of the light, and care must be taken during the design to ensure that obstruction do not occur. If the aperture stop is located on a mirror surface, there will be one less element of uncertainty to consider for.

3.2.2 Mirror Pair Concept

Therefore, an EUVL tool can be decomposed into units of mirror pairs. As such, when simulating a mirror pair using the lens module, the optical properties must specified in accordance to what is possible for a mirror pair to produce.

doi:10.6342/NTU201901098

For a mirror pair, its the effective optical power Φ is given by

$$\Phi = \phi_1 + \phi_2 - \phi_1 \phi_2 sep = C_{(1,2)} \tag{75}$$

where ϕ_1 and ϕ_2 are the power of the first and second mirror respectively, and sep is the separation between the mirrors. In terms of GGC and its Gaussian bracket expansion, its back focal length is given by

$$\mathrm{BF} = \frac{A_{(1,2)}}{C_{(1,2)}} = \frac{1 - sep\phi_1}{\Phi} \ , \tag{76}$$

and likewise for the front focal length

$$\mathrm{FF} = -\frac{D_{(1,2)}}{C_{(1,2)}} = -\frac{1 - sep\phi_2}{\Phi} \ . \tag{77}$$

Substitution of Equations 76 and 77 into 75 then gives the required mirror separation for the mirror pair

$$sep = \mathrm{EF} + \frac{\mathrm{BF} \cdot \mathrm{FF}}{\mathrm{EF}} \ . \tag{78}$$

Note that, this separation must be a positive length, otherwise ray tracing using this lens module would show that light is not reflected but instead travels through the mirror surfaces instead.

3.2.3 Multiple mirror pair expansion

At this point, the number of mirrors in each subsystems must be decided before further derivation can continue. For the sake of simplicity, the simplest system configuration of one mirror pair on either side of the aperture stop forming a four-mirror system, is chosen for further derivations. However, the subsystem can also be expanded into multiple mirrors pairs.

Here, expansion of a subsystem into two and three mirror pairs, as shown in Figure 53, are demonstrated. For expansion of the subsystem into two mirror pairs, simply substitute

doi:10.6342/NTU201901098

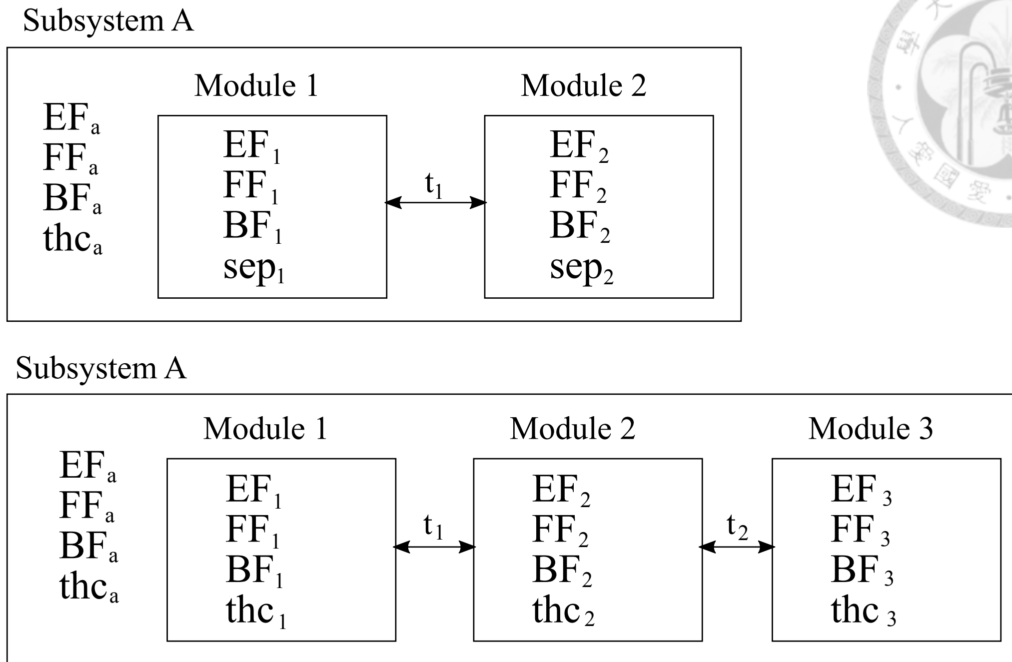

Figure 53: A subsystem can be further expanded into multiple mirror pairs, represented by the individual lens modules. **Upper**: Expansion into two mirror pairs. **Lower**: Three mirror pair expansion.

the following properties into the derivations for the subsystem

$$\Phi_{sub2} = \frac{t_1 - \mathrm{BF}_1 + \mathrm{FF}_2}{\mathrm{EF}_1\mathrm{EF}_2} \tag{79}$$

$$\mathrm{BF}_{sub2} = \mathrm{BF}_2 + \frac{\mathrm{EF}_2{}^2}{t_1 - \mathrm{BF}_1 + \mathrm{FF}_2} \tag{80}$$

$$\mathrm{FF}_{sub2} = \mathrm{FF}_1 - \frac{\mathrm{EF}_1{}^2}{t_1 - \mathrm{BF}_1 + \mathrm{FF}_2} \quad . \tag{81}$$

For expansion into three mirror pairs, the substitutions are

$$\Phi_{sub3} = \frac{(\mathrm{BF}_1 - \mathrm{FF}_2 - t_1)(\mathrm{BF}_2 - \mathrm{FF}_3 - t_2) - \mathrm{EF}_2{}^2}{\mathrm{EF}_1\mathrm{EF}_2\mathrm{EF}_3} \tag{82}$$

$$\mathrm{BF}_{sub3} = \mathrm{BF}_3 + \frac{\mathrm{EF}_3{}^2(t_1 - \mathrm{BF}_1 + \mathrm{FF}_2)}{(\mathrm{BF}_1 - \mathrm{FF}_2 - t_1)(\mathrm{BF}_2 - \mathrm{FF}_3 - t_2) - \mathrm{EF}_2{}^2} \tag{83}$$

doi:10.6342/NTU201901098

$$\mathrm{FF}_{sub3} = \mathrm{FF}_1 - \frac{\mathrm{EF}_1{}^2(t_1 - \mathrm{BF}_1 + \mathrm{FF}_2)}{(\mathrm{BF}_1 - \mathrm{FF}_2 - t_1)(\mathrm{BF}_2 - \mathrm{FF}_3 - t_2) - \mathrm{EF}_2{}^2} \ . \tag{84}$$

3.2.4 Mask and Wafer Side Working Distance

The mask side working distance is the clearance between the mask and the closest element of the tool to the mask, and likewise for the wafer side. This allows space for other procedures and operations, such as transporting the post-exposure wafer onward to the next stage of lithography, and bringing in new unexposed wafer for exposure.

Therefore for a four mirror tool, the mask side working distance

$$\mathrm{WD}_{ob} = t_{im} + thc_A \tag{85}$$

must be kept at a reasonable distance away, and similar is true for the wafer side

$$\mathrm{WD}_{im} = t_{ob} + thc_B \ . \tag{86}$$

3.2.5 Subsystem Magnifications

As the t_{ob} is bound in a relationship to WD_m and thc_A, consequently so is the magnification of the subsystem, given by

$$\begin{aligned} \frac{1}{M_a} &= D_{(0,2)} \\ &= -t_0 C_{(1,2)} + D_{(1,2)} \ , \end{aligned} \tag{87}$$

and after substitution with Equation 85 gives

$$\mathrm{WD}_{ob} + sep_A = -\mathrm{FF}_A - \frac{\mathrm{EF}_A}{M_A} \ . \tag{88}$$

Again, similar treatment of the wafer side gives

$$\mathrm{WD}_{im} + sep_B = \mathrm{BF}_B - M_B \cdot \mathrm{EF}_B \ . \tag{89}$$

doi:10.6342/NTU201901098

3.3 Monte Carlo Random Walk Kernel

Combining the various derived relations (Equations 65, 70, 71, 73, 78, 88, and 89), this relationship is obtained

$$
\begin{aligned}
& \frac{M}{\mathrm{EF}_A}(sep_A+\mathrm{WD}_{ob})\big(\ M_2\Delta(sep_B+\mathrm{WD}_{im}) \\
& \qquad +\mathrm{EF}_B(sep_B+M_Bsep_B+{M_B}^2\Delta+\mathrm{WD}_{im})\ \big) \\
& \qquad + \ (sep_B+\mathrm{WD}_{im})\big(\ MM_Bsep_A \\
& \qquad\qquad +{M_B}^2\Delta+M^2(sep_A+\mathrm{WD}_{ob})\ \big) \\
& + \ \mathrm{EF}_BM_B\big(\ MM_Bsep_A+sep_B+M_B(sep_B+M_B\Delta) \\
& \qquad\qquad +\mathrm{WD}_{im}+M^2(sep_A+\mathrm{WD}_{ob})\ \big) \ = \ 0,
\end{aligned}
\tag{90}
$$

with

$$\Delta = \mathrm{TTL} - \mathrm{WD}_{ob} - \mathrm{WD}_{im}. \tag{91}$$

Initial evaluation of Equation 90 given an arbitrary initial state will likely result in an oddly obstructed system, despite fulfilling all of the aforementioned optical properties. To resolve the obstructions, a simple Monte Carlo random walk algorithm is devised to reduce and eventually eliminate the obstructions from the system. A diagram of the algorithm is shown in Figure 54, which is described in more details in a previous work. [46]

The algorithm uses Equation 90 as the kernel of the random walk, with the parameters acting as free running optimization variables. For a single instance between a mirror and a neighbouring ray bundle, the obstruction is defined as the angle of the obstructed region as illustrated in Figure 55. The error function of the random walk is then defined as the total amount of obstruction

$$\varepsilon_{ObsTotal} = \sum_{n=1}^{N} \varepsilon_{Obs,n-} + \varepsilon_{Obs,n+} \tag{92}$$

present in the system, where $\varepsilon_{Obs,n-}$ and $\varepsilon_{Obs,n+}$ denotes the obstruction of the nth mirror

doi:10.6342/NTU201901098

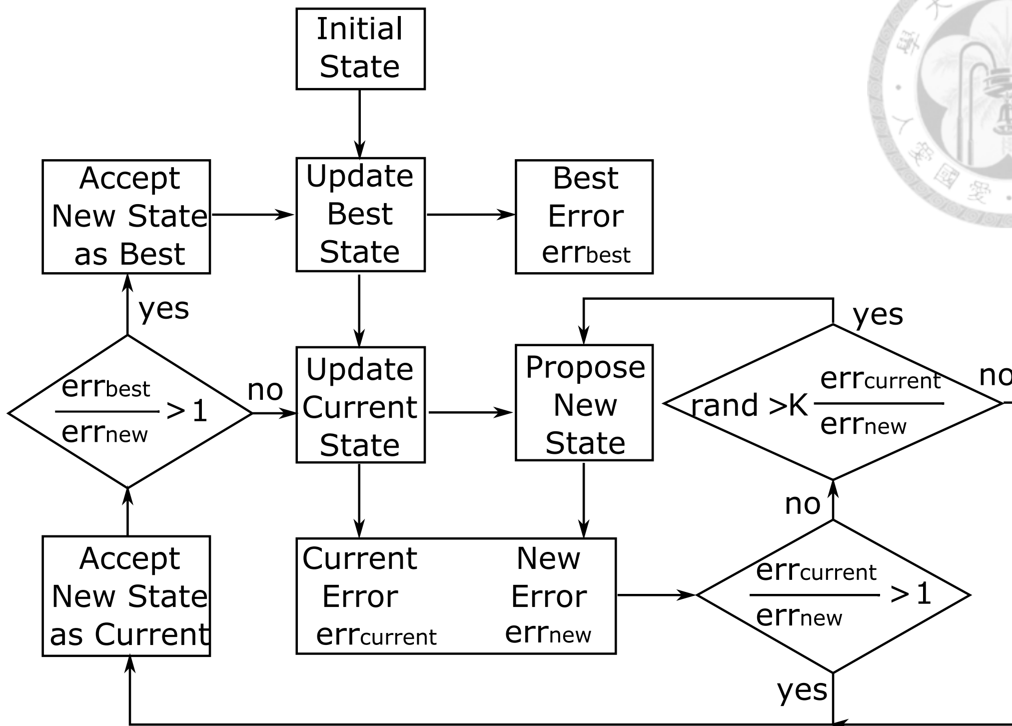

Figure 54: A flow diagram of the Monte Carlo random walk algorithm.

on the neighbouring ray bundle before it and after it, respectively. One other important relation to add to the random walk error function is the Petzval sum, given by

$$\varepsilon_{Petz} = \sum_{n=1}^{N} C_n = \sum_{n=1}^{N} \Phi_n \tag{93}$$

where C_n and Φ_n are the GGC term and optical power of the nth surface, respectively. Upon each iteration of the random walk, the error function is re-evaluated to determine whether the current iteration improves or worsens the total obstruction, and whether to accept or discard the current iteration as the basis of the next iteration.

Taking advantage of Code V lens module functions, this random walk algorithm is written into Code V as a set of instructions in the form of an SEQ (Code V Sequence) file. Other commercial optics design software differs in how this implementation can be achieved, for example in Zemax this is done through the ZPL (Zemax Programming Language) environment instead.

doi:10.6342/NTU201901098

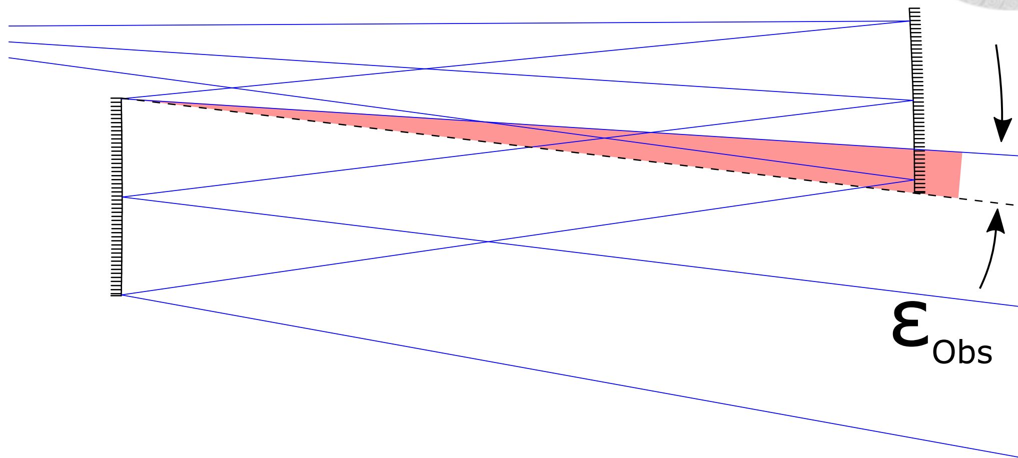

Figure 55: The amount of obstruction between a ray bundle and mirror is defined as the angle of the overlapping region.

Table 3: Specification of a EUVL tool design trial run.

Specifications	
Magnification	0.25
Numerical Aperture	0.2
Chief Ray Angle (Mask)	4°
Chief Ray Angle (Wafer)	0°
Total Tract Length	1000 mm
Working Distance (Mask)	200 mm
Working Distance (Wafer)	100 mm
Minimum Obstruction Clearance	10 mm

doi:10.6342/NTU201901098

Table 4: Initial lens module parameters of the optimization run. The four free variables are marked with an asterisk (*), the remaining parameters are dependent.

Module		Thickness	
*EF_a	800 mm	t_{ob}	600 mm
FF_a	1320 mm	*thc_a	-400 mm
BF_a	-242.4 mm	t_{s-1}	395.8 mm
EF_b	-182.8 mm	t_s	304.2 mm
FF_b	-304.2 mm	*thc_b	-300 mm
BF_b	290.2 mm	t_{im}	400 mm
M_a	-0.146		
*M_b	0.6		

3.3.1 Demonstration: Four-Mirror System

For the following four-mirror system design, some mock specifications are given, listed in Table 3, including the system magnification, system NA, and mask side and wafer side chief ray angle (CRA). Other packaging constraints includes the TTL, mask side and wafer side working distance, and obstruction clearance.

Out of the nine quantities present in Equation 90, four of which (M, TTL, WD_{ob}, and WD_{im}) are predetermined as design constraints, listed in Table 3. As one parameter must be dependent as to satisfy the relationship as the other four quantities are varied, four parameters remains free and can be used as optimizing parameters. The priority of dependency can be chosen freely. Table 4 lists a set of initial values, chosen at random, for the four-mirror system. Here, The four active variables are marked with an asterisk, and the rest are calculated from the derived relations (Equations 65, 70, 71, 73, 78, 88, 89, and 90).

The resultant optical system calculated from the four initial variable values are displayed in Figure 56, and large amount of obstructions can be observed on almost every ray paths. After application of the random walk, the algorithm quickly converges to a solution. The stop condition of the random walk is adjustable to suit the situation, and in this example a combination of a maximum cycle number of one thousand iterations and zero total obstruction is used. Under these stop conditions the walk will terminate either when one thousand steps are reached, or when the total obstruction reaches zero. At termination of the walk the best solution discovered during the course of the walk is recalled, and can

doi:10.6342/NTU201901098

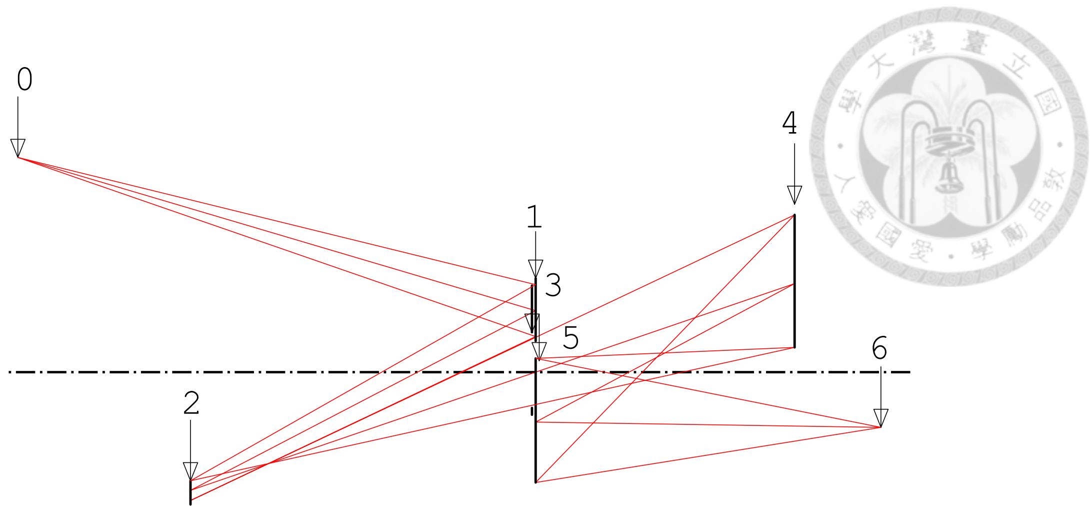

Figure 56: The initial state of the four mirror trial run.

Table 5: Random walk result of the four-mirror system. Left: Lens module properties. Right: Conversion to raw lens data.

Properties	(mm)	Surface	R (mm)	T (mm)
EF$_a$	1038.80	Object	-	531.76
FF$_a$	-781.14	1	-6994.42	-331.76
BF$_a$	940.25	2	2675.11	698.77
EF$_b$	245.21	Stop	-	1.23
FF$_b$	-1.23	4	1428.16	-243.56
BF$_b$	328.84	5	489.57	343.56

be used as the initial state for subsequent application of the walk to refine the solution.

Figure 57 shows an obstruction resolved solution of the four-mirror system, and its direct conversion to spherical mirrors with equivalent optical properties. The module properties and lens data listed in Table 5. This particular solution is obtained after seven applications of the random walk. At this point, with the obstruction resolved and general form stabilized, the design is now a suitable candidate for further optimization.

3.3.2 Brief Note on Solution Convergence and Computation Time

The duration of one application of the random walk (one thousand iterations) of this Four-Mirror setup takes roughly 10 seconds on an average personal computer running Code V, and varies according to number of mirrors present and the complexity of the defined error function. Although, convergence onto an acceptable solution cannot be guaranteed for all initial states all the times, however for most runs conducted an obstruction resolved solution can be obtained after seven to ten applications of the random walk. In comparison

doi:10.6342/NTU201901098

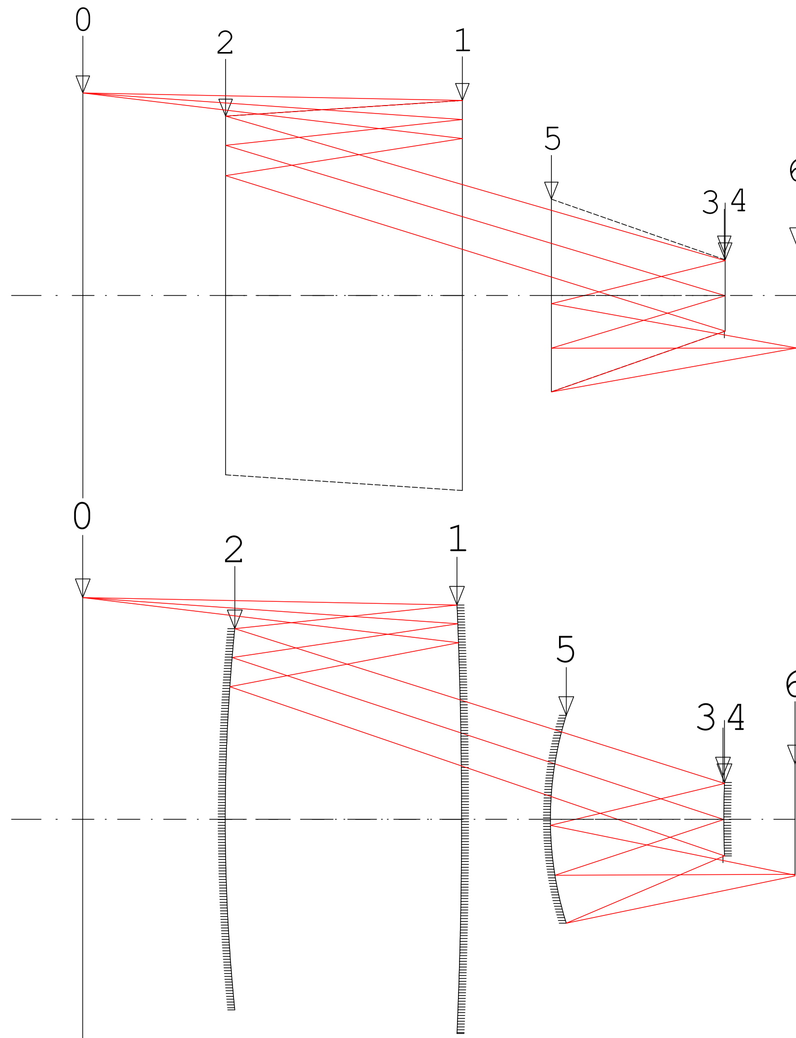

Figure 57: Four-mirror system optimization using Code V. Lens module converted to real mirror surfaces. Lens data and module properties are listed in Table 5.

doi:10.6342/NTU201901098

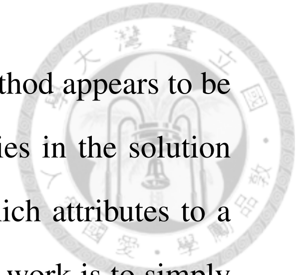

with computation time required in Bal's work [38], admittedly this method appears to be faster, however it should be noted again that in his work the focus lies in the solution density (both unobstructed and obstructed) of all EUVL systems, which attributes to a significant increase in the computation time, whereas the focus of this work is to simply find a particular unobstructed solution, and therefore the shorter computation time.

doi:10.6342/NTU201901098

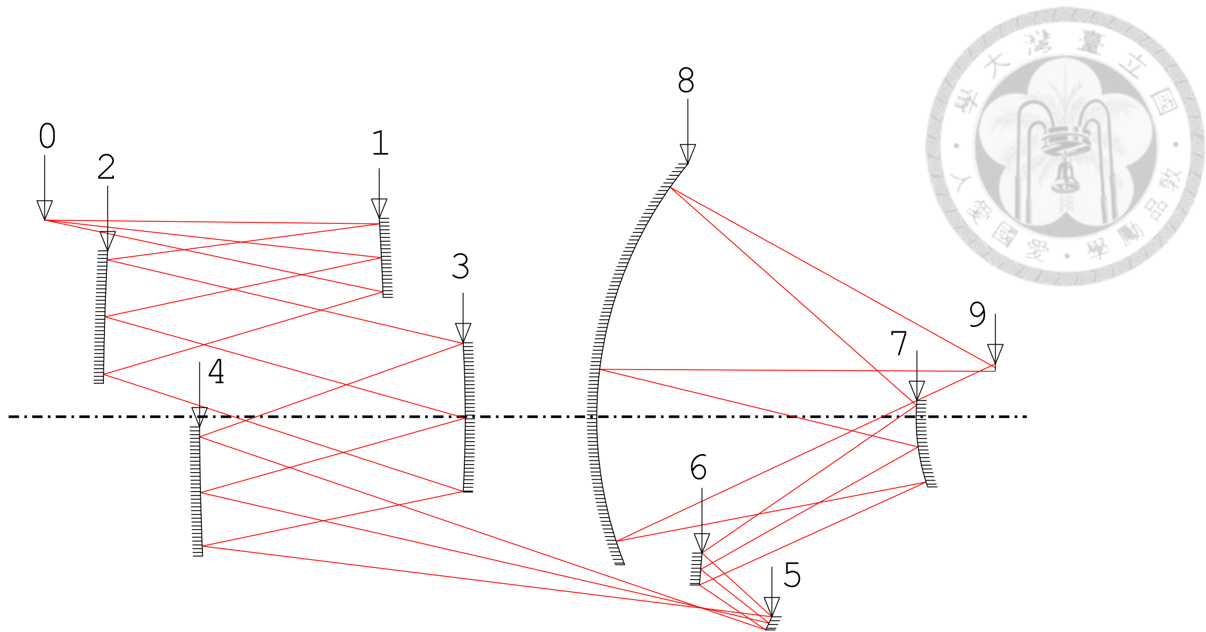

Figure 58: Monte Carlo random walk result of an eight-mirror system.

3.4 Eight-Mirror System

This section details the design of an eight mirror EUVL tool, using the Monte Carlo random walk algorithm in the initial phase of the design. In this case, the mirror pair configuration chosen is one mirror pair for the pre-stop group, and three mirror pairs for the post-stop group. The design specifications are almost the same as the previous four-mirror system, with the exception being the increased 0.4 NA, and tighter working distances. As such, the kernel of the algorithm is obtained using the derived relations 65, 70, 71, 73, 78, 88, 89, and the multiple mirror pair expansions 82 to 84.

The result of the Monte Carlo random walk (after conversion to real mirror curvatures) is shown in Figure 58. From the figure, even more so visible now due to higher NA, is that at the end of the Monte Carlo random walk, the aberration performance at the focus is not very good, however other optical properties such as telecentricity, magnification, and obstruction control are well kept. This is an expected outcome, since the main purpose of the algorithm is to resolve obstruction while keeping the desired properties maintained.

The obstruction resolved solution is then passed on to the optimizer of the optical design software. The derived random walk kernel can be then incorporated into the optimizer to ensure that the desired optical properties are maintained during further optimizations, by setting the deviation to the kernel as part of the optimizer error functions, along

doi:10.6342/NTU201901098

with other aberration related error functions such as the primary Seidel aberrations, spot size, and wavefront errors.

3.4.1 Optical System Optimization

Initial State

Figures 59 shows the initial state of the optical system directly after the Monte Carlo run prior to further optimizations, its optical system layout and spot diagram rescpectly. At this stage, the surface profile of the mirrors are strictly spherical. As can be seen even in the system layout, the focus quality is rather poor, and surely enough this is also reflected in the spot diagram, with RMS spot radius of 3 mm.

An optimized result after optimization runs by allowing surface profiles not limiting to spherical surfaces is shown in Figure 60. Here, the surface profiles is aspherical with various conic constants. As can be seen visually, between Figures 59 and 60, the general form and shape of the projector very much remained unchanged before and after optimization. This is due to the fact that out of all of the parameters that defines an aspheric surface,

$$sag_{asp} = \frac{r^2}{R\left(1+\sqrt{1-(1+\kappa)\frac{r^2}{R^2}}\right)} + A_4 r_4 + A_6 r_6 + A_8 r_8 \ldots + A_n r_n \tag{94}$$

the radius of curvature R usually determines the general shape of the surface, while the conic constant κ and asphere polynomial coefficients A_4, A_6, $A_8 \ldots A_n$ are used for fine tunings. While in general this separation of roles is not necessary, consider that towards the center of the surface where r is small (i.e. when $r << 1$), the sag equation (94) above simplifies to

$$sag \simeq \frac{r^2}{R}, \tag{95}$$

which implies that the paraxial focal strength of an optical element is dependent only on R. Now, as can be seen from the sag equation 94, at larger r the effects κ and A_n ($n \in 4,6,8\ldots$) becomes dominant, and can easily distort the surface if their values are not

doi:10.6342/NTU201901098

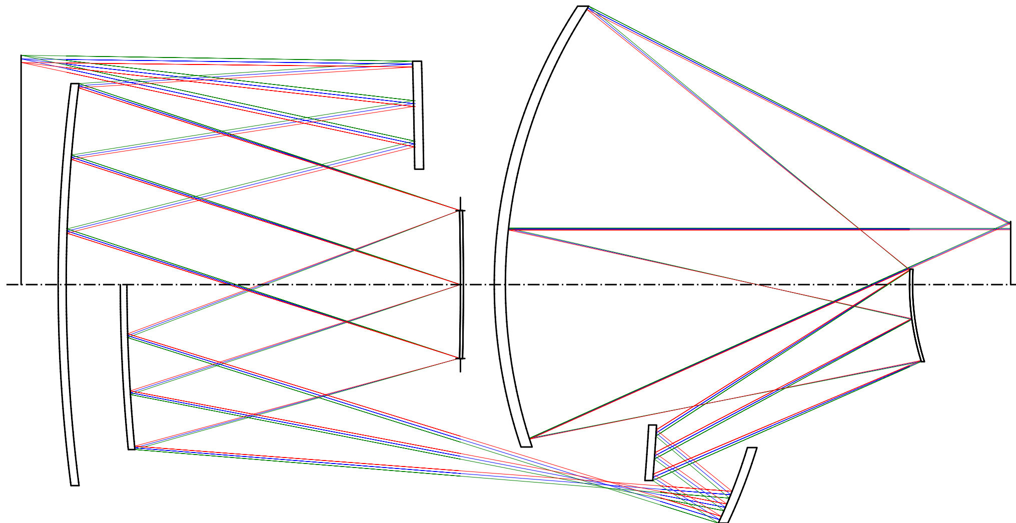

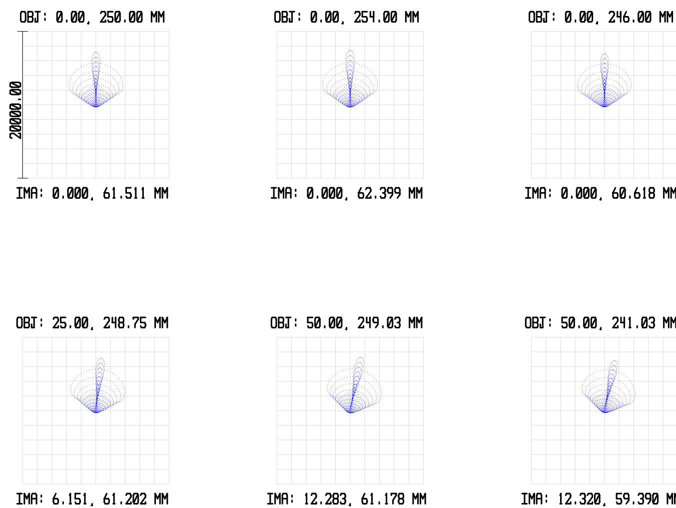

SURFACE IMA: IMG

SPOT DIAGRAM

FRI MAR 1 2019 UNITS ARE µm.

FIELD :	1	2	3	4	5	6
RMS RADIUS :	3022.12	3088.30	2957.16	3022.12	3088.30	2959.76
GEO RADIUS :	7308.79	7535.88	7084.54	7304.23	7535.86	7093.22

SCALE BAR : 2E+004 REFERENCE : CHIEF RAY

SYS13_09_OPT_00_RESTART.ZMX
CONFIGURATION 1 OF 1

Figure 59: Initial state of the 8-mirror system, and its spot diagram. The mirror surface profiles at this point is entirely spherical.

 doi:10.6342/NTU201901098

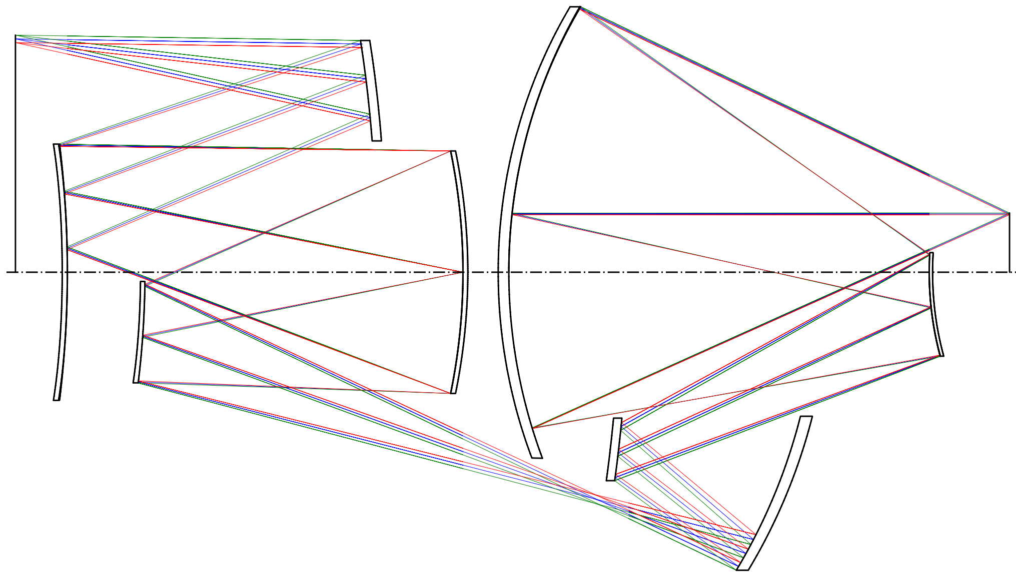

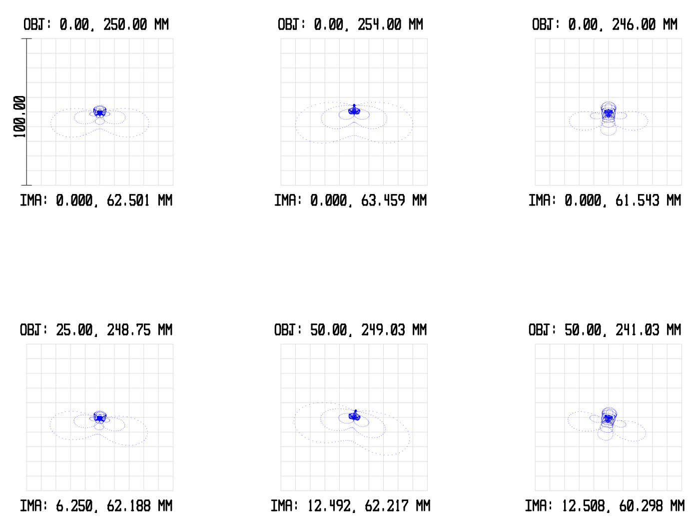

SURFACE IMA: IMG

SPOT DIAGRAM

FRI MAR 1 2019 UNITS ARE µm.

FIELD :	1	2	3	4	5	6
RMS RADIUS :	8.274	10.408	7.138	8.274	10.408	7.162
GEO RADIUS :	34.333	41.060	27.398	34.371	41.062	27.697

SCALE BAR : 100 REFERENCE : CHIEF RAY

SYS13_09_OPT_03_CONIC_04_RESTARTED.ZMX
CONFIGURATION 1 OF 1

Figure 60: The state of the 8-mirror system after optimization runs, after allowing the conic constants of the surface profiles to vary.

doi:10.6342/NTU201901098

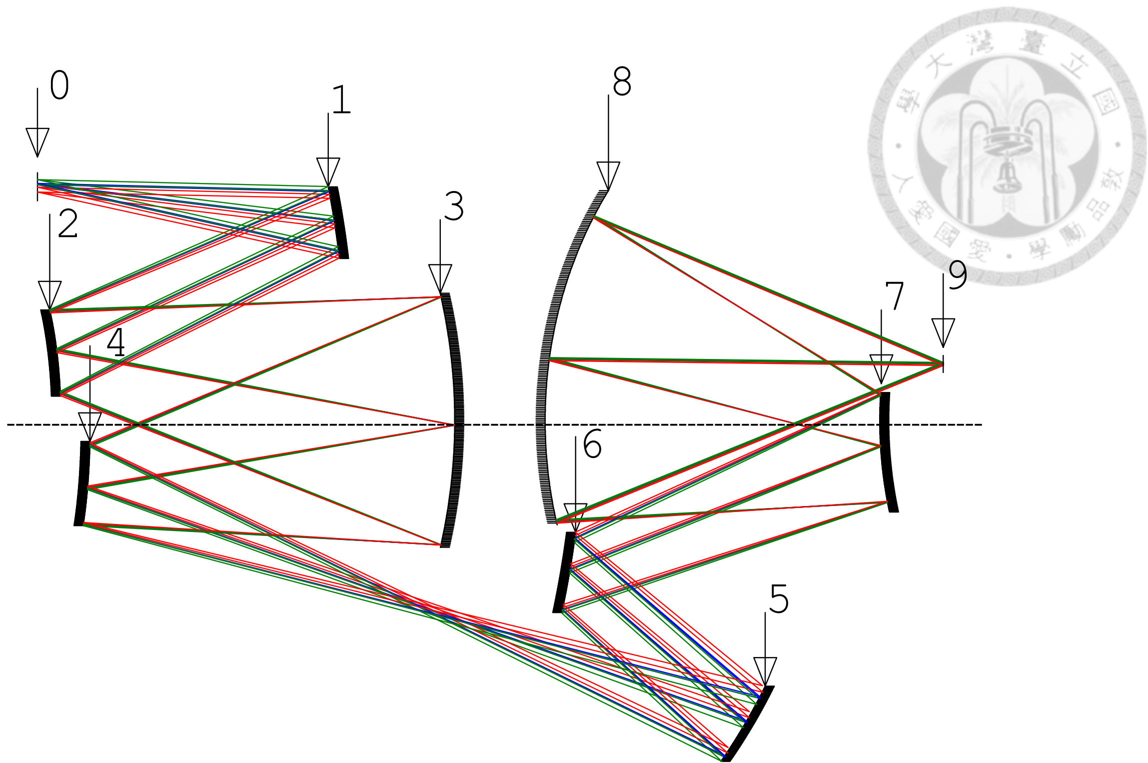

Figure 61: Layout of an eight-mirror EUVL system.

kept small. As such, somewhat ironically, the mark of a good aspheric optical design is that despite being aspheric elements, the surface profile of these elements do not deviate too much from the sphere, measured by a quantity

$$\Delta_{asp} = sag_{asp}(r, \kappa, A_4, A_6, A_8 \ldots) - sag_{sph}(r) \tag{96}$$

referred to as the maximum asphere deviation.

Figure 61 now shows a much more optimized design result after many optimization runs, lens data listed in Table 6. From the analysis report in Figure 62 and 63 and Table 7, the design is well within being diffraction limited. Though it should be noted that for the purpose of EUVL, diffraction limit is only but an entrance requirement.

doi:10.6342/NTU201901098

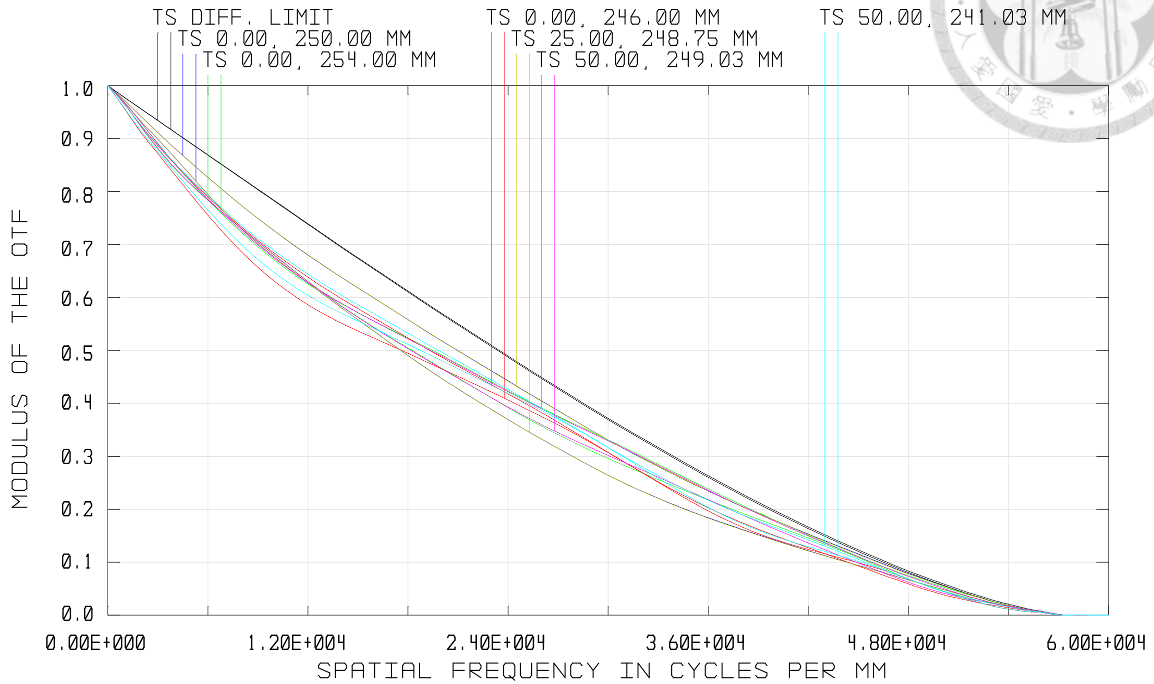

Figure 62: The MTF performance of the eight-mirror EUVL system.

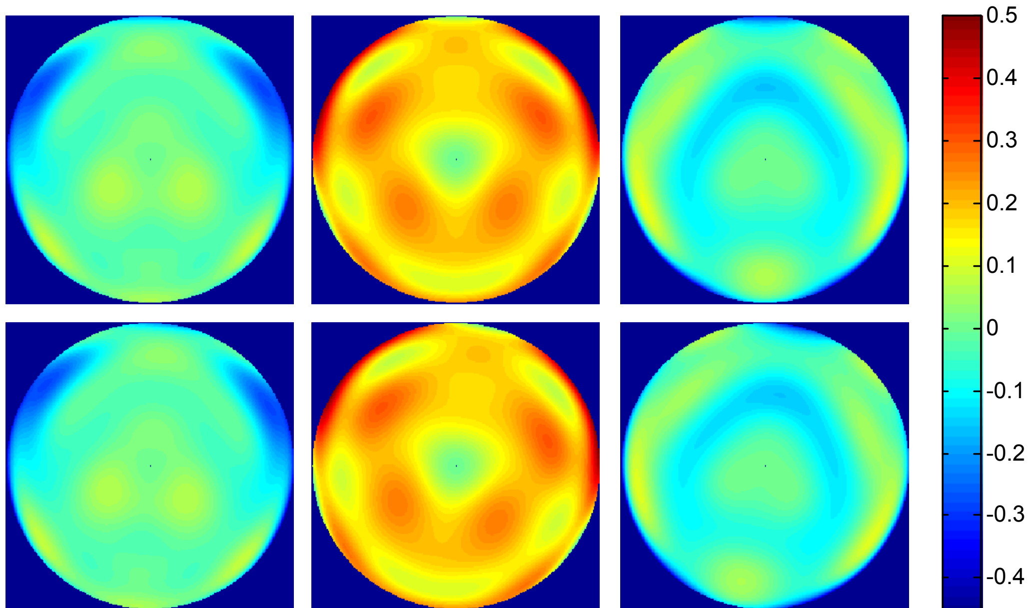

Figure 63: Wavefront aberration of the six defined field positions. **Top Row**: Center, top, and bottom fields on the tangential plane respectively. **Bottom Row**: Center top, and bottom fields at full horizontal mask width.

doi:10.6342/NTU201901098

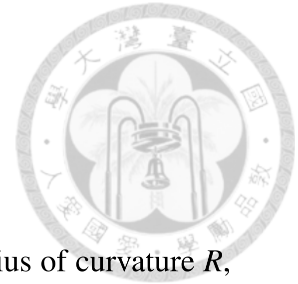

Table 6: Basic lens data of the eight-mirror system, displaying the radius of curvature R, thickness T, conic constant K, and aspheric coefficients from A_4 to A_{12}.

Surf	R (mm)	T (mm)	K	A_4
Obj	-	328.1	-	-
1	-1639.0	-303.4	3.110	-6.3e-10
2	-647.6	415.3	8.503	-1.7e-9
Stop	-579.9	-384.4	-0.483	3.4e-10
4	-942.7	778.0	19.12	-3.2e-9
5	-632.1	-258.3	0.040	2.8e-11
6	-879.9	312.9	-6.818	-3.5e-10
7	459.6	-352.9	1.055	-6.2e-10
8	484.8	419.8	0.371	-5.5e-11
Surf	**A_6**	**A_8**	**A_{10}**	**A_{12}**
1	-4.0e-16	3.4e-21	-6.7e-26	3.9e-31
2	9.1e-16	4.9e-19	-1.8e-23	9.5e-28
Stop	2.8e-15	6.8e-21	-4.3e-25	7.5e-30
4	-1.4e-14	-4.3e-19	1.7e-23	-1.2e-28
5	1.5e-17	8.1e-23	8.5e-28	-5.9e-33
6	-2.5e-16	1.1e-20	-2.7e-25	1.8e-30
7	-6.4e-14	9.6e-19	-1.8e-23	6.6e-27
8	-8.5e-18	2.1e-22	-1.0e-27	-4.0e-32

Table 7: RMS wavefront error and Zernike coefficients (tilt and defocus) in wavelength unit.

Field No.	RMS Error	Z_3	Z_4
1	0.0707	-0.0324	-0.0379
2	0.0666	0.0042	0.0097
3	0.0717	0.0045	0.0188
4	0.0707	-0.0322	-0.0379
5	0.0665	0.0041	0.0097
6	0.0672	0.0001	0.0136

doi:10.6342/NTU201901098

4 Illuminator Design

4.1 Illumination Optics System Properties

4.1.1 Pupil Matching

For the illuminator in Kohler integrator configuration, the pupil matching condition is that the grid source (GS) must be conjugated to the entrance pupil (EnP) of the projection tool. In terms of GGC this yields the following relationship,

$$B(GS, EnP) = 0. \tag{97}$$

GGC expansion of Equation 97 gives

$$\phi_{L2} = \frac{D(GS, FL1)}{t_F + t_L - \phi_F t_F t_L + D(GS, FL1) t_{L1}} + \frac{1}{t_{En} + t_{L2}} \tag{98}$$

with

$$D(GS, FL1) = 1 - \phi_{L1}(t_F + t_L) + \phi_F t_F (\phi_{L1} t_L - 1). \tag{99}$$

4.1.2 Field Lens and Mask Position

For the Kohler integrator, the position of the mask is located at the back focal length (BFL) of the field lens group. This can be verified by consider a ray parallel to the optics

doi:10.6342/NTU201901098

axis entering the field lens group. In terms of the ABCD matrix, this can be expressed by

$$\begin{bmatrix} y' \\ u' \end{bmatrix} = \begin{bmatrix} A & B \\ C & D \end{bmatrix} \begin{bmatrix} y \\ 0 \end{bmatrix} = \begin{bmatrix} Ay \\ Cy + Du \end{bmatrix} \tag{100}$$

where A, B, C, and D makes up the ABCD matrix of the field lens, y' and u' are the exit ray height and angle at the mask, and y is the incident ray height. Here, since the mask is placed at the focal plane of the field lens, rays incident on the field lens parallel to the optical axis by definition must be focused onto the optical axis, therefore

$$y' = Ay = 0, \tag{101}$$

or

$$A = 0 \tag{102}$$

for non-trivial incident ray height. From here, again in terms of the ABCD matrix, for an incident ray of arbitrary angle and height,

$$\begin{aligned} \begin{bmatrix} y' \\ u' \end{bmatrix} &= \begin{bmatrix} A & B \\ C & D \end{bmatrix} \begin{bmatrix} y \\ u \end{bmatrix} \\ &= \begin{bmatrix} 0 & B \\ C & D \end{bmatrix} \begin{bmatrix} y \\ u \end{bmatrix} = \begin{bmatrix} Bu \\ Cy + Du \end{bmatrix}. \end{aligned} \tag{103}$$

This gives the following relationship

$$y' = Bu, \tag{104}$$

which means that at the mask position, the ray height on the mask is dependent only on the ray angle entering the field lens, and is independent of the incident ray height.

doi:10.6342/NTU201901098

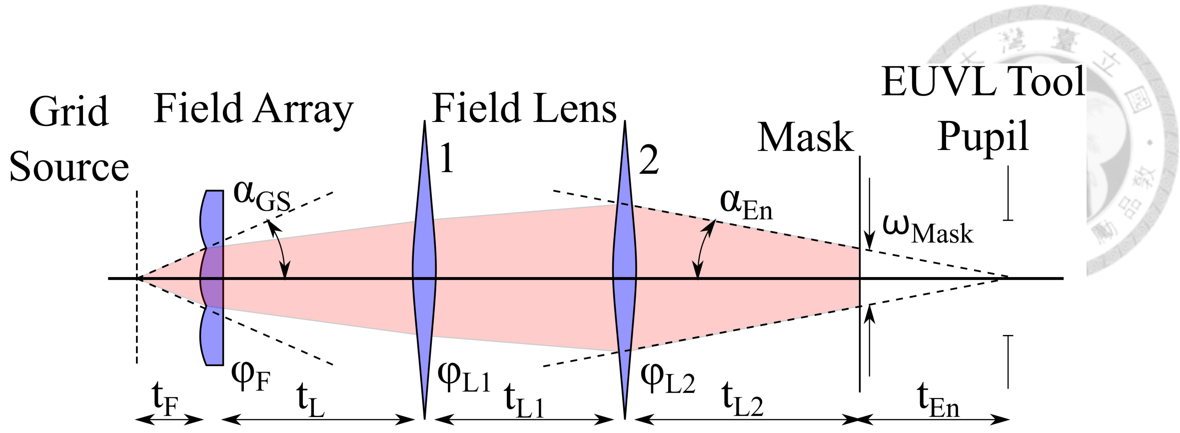

Figure 64: The marginal ray angles at the grid source and at the projection tool entrance pupil is related to the magnification of the finite conjugate system formed by the elements in between.

In terms of GGC, this condition can be expressed by

$$t_{L2} = \frac{A(L1,L2)}{C(L1,L2)}, \tag{105}$$

and GGC expansion gives the following relationship

$$t_{L2} = \frac{1 - \phi_{L1} t_{L1}}{\phi_{L1} + \phi_{L2} - \phi_{L1}\phi_{L2} t_{L1}}. \tag{106}$$

4.1.3 Grid Source NA and Exposure Field Width

Since the grid source and the projector entrance pupil are bound together in a conjugate relationship, the marginal ray angle at the two positions must be bound together by the magnification of the finite conjugate system formed by the elements in between, giving

$$M(GS,EnP) = \frac{\tan(\alpha_{GS})}{\tan(\alpha_{En})} \tag{107}$$

as illustrated in Figure 64. Also can be observed in Figure 64 is that the exposure field width on the mask w_{Mask} can now be expressed as

$$\tan(\alpha_{En}) = \frac{w_{Mask}}{2t_{En}}, \tag{108}$$

doi:10.6342/NTU201901098

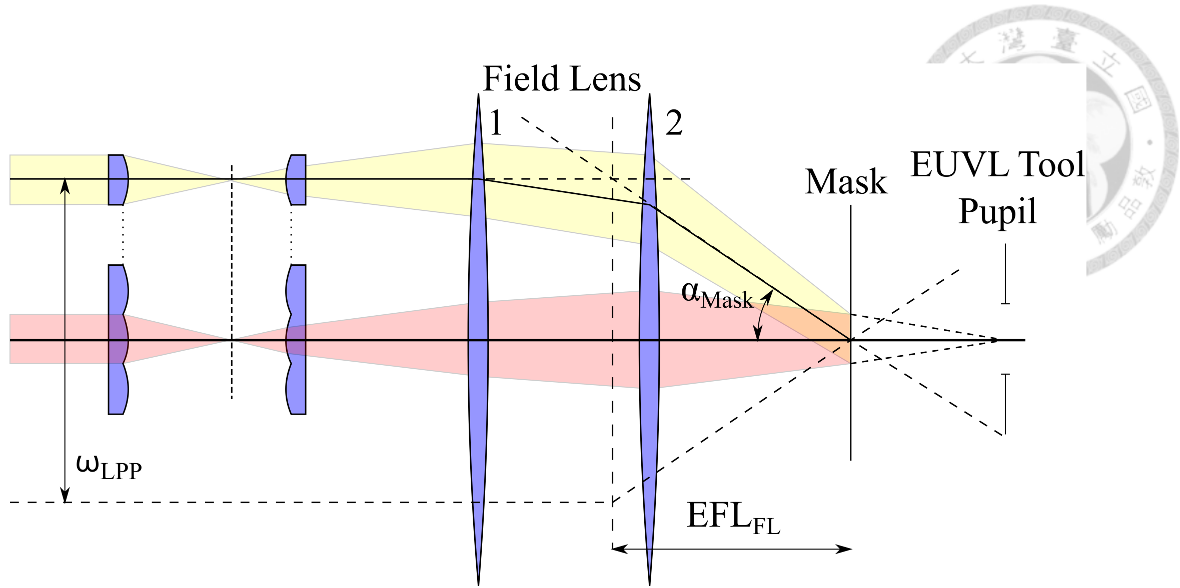

Figure 65: The illumination NA is directly related to the beam size of the collimated LPP source.

and combining the two equations 107 and 108 gives the expression for the exposure width

$$w_{Mask} = \frac{2t_{En}\tan(\alpha_{GS})}{M(GS,En)}. \tag{109}$$

Here, $M(GS,En)$ is the magnification this finite conjugate system, and can be expressed in terms of GGC as

$$M(GS,En) = \frac{1}{D(GS,En)}, \tag{110}$$

which can be expanded to give the following relationship

$$\phi_F = \frac{1-\phi_{L2}(t_F+t_L+t_{L1})-\phi_{L1}(t_F+t_L)(1-\phi_{L2}t_{L1})-\frac{1}{M}}{t_F(1-\phi_{L2}(t_L+t_{L1})-\phi_{L1}t_L(1-\phi_{L2}t_{L1}))} \tag{111}$$

4.1.4 Illumination Optics NA and Collimated Plasma Source Beam Size

As illustrated in Figure 65, the illumination NA is directly related to the beam size of the collimated LPP source and the effective focal length (EFL) of the field lens, through

$$\tan(\alpha_{Mask}) = \frac{w_{LPP}}{2\mathrm{EFL}_{FL}} = \frac{1}{2}w_{LPP}C(L1,L2) \tag{112}$$

doi:10.6342/NTU201901098

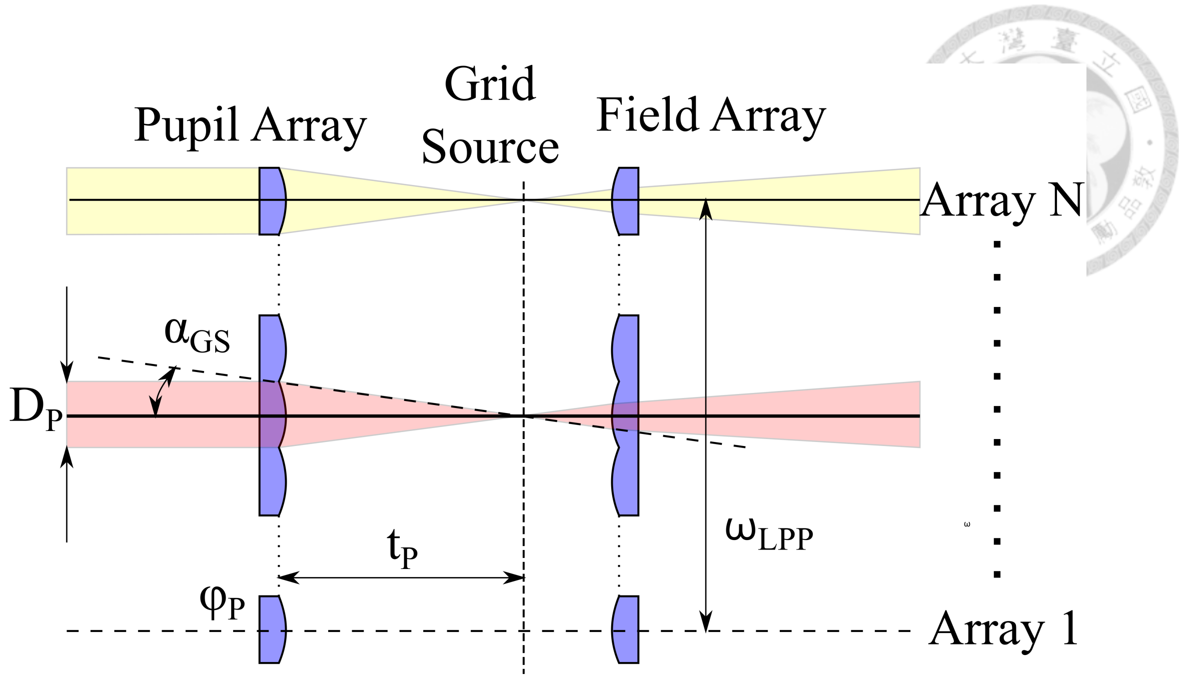

Figure 66: The number of array elements on the pupil array determines the array pitch and the grid source NA.

in terms of GGC, which can be expanded into

$$w_{LPP} = \frac{\tan(\alpha_{Mask})}{\phi_{L1} + \phi_{L2} - \phi_{L1}\phi_{L2}t_{L1}}. \tag{113}$$

4.1.5 Pupil Pitch Size

By simple geometry (Figure 66), the pupil array pitch is related to the NA of the grid source through

$$\tan(\alpha_{GS}) = \frac{D_P}{2t_P}, \tag{114}$$

where

$$\mathrm{NA}_{GS} = \sin(\alpha_{GS}). \tag{115}$$

4.1.6 Number of Array Elements

Likewise, also shown in Figure 66, the number of array elements on the mirror arrays can be determined by

$$N_P = 1 + \frac{2w_{LPP}}{D_P}. \tag{116}$$

doi:10.6342/NTU201901098

4.2 Illumination System Design

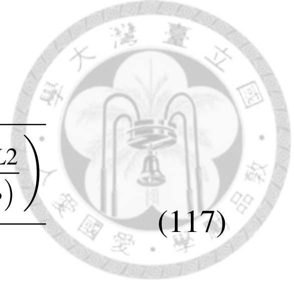

$$w_{LPP} = -\frac{t_{L1} + \sqrt{t_{L1}^2 + 4t_L t_{L2}\left(1 + \frac{t_{L2}}{t_{En}} + \frac{2\tan(\alpha_{Mask})t_F t_{L2}}{t_P w_{Mask}(1-N_P)}\right)}}{\frac{2(t_{En}+t_{L2})}{\tan(\alpha_{Mask})t_{En}} + \frac{4t_F t_{L2}}{t_P w_{Mask}(1-N_P)}} \tag{117}$$

$$\phi_F = \frac{1}{t_F}\left(\frac{w_{LPP}\tan(\alpha_{Mask})t_{En}t_{L1} + w_{LPP}^2(t_{En}+t_{L2}) - \tan^2(\alpha_{Mask})t_{En}(t_F+t_L)t_{L2}}{w_{LPP}\tan(\alpha_{Mask}))t_{En}t_{L1} + w_{LPP}^2(t_{En}+t_{L2}) - \tan^2(\alpha_{Mask})t_{En}t_L t_{L2}}\right) \tag{118}$$

4.2.1 First Order Analysis

Combining the equations derived in the previous section, a set of governing equations 117 to 120 relating the positioning and properties of the mirrors can be obtained.

$$\phi_{L1} = \frac{w_{LPP} + \tan(\alpha_{Mask})t_{L2}}{w_{LPP}t_{L1}} \tag{119}$$

$$\phi_{L2} = \frac{\phi_{L1}}{\phi_{L1}t_{L1} - 1} + \frac{1}{t_{L2}} \tag{120}$$

As can be seen from the derived governing equations, the choice of parameter to be made dependent or independent is rather intentional. Mathematically this choice can be arbitrary in principle, however in practice some parameters are more suited to act as independent variables. For example, parameters that must equate to a specific value (e.g. system specifications), or have a heavy constraint placed upon (e.g. inter-element spacings are positive definite), are better left as independent variables. Keeping these parameters on hand as independent variables allows for much greater control over the validity of the design during the optimization process. Whereas parameters that can roam free without major consequences (e.g. mirror focal lengths) are good candidates for dependent variables.

As a design example, a set of specifications derived from the authors' previous projection tool design [5] are listed in Table 8, along with a set of initial conditions. From the specifications and initial conditions, a complete solution for the illuminator can be

doi:10.6342/NTU201901098

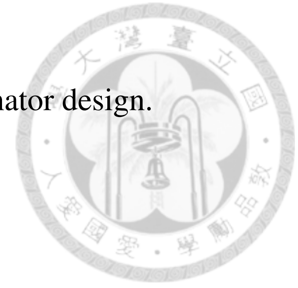

Table 8: A set of specification and initial condition of the illuminator design.

Specifications	
Illumination NA (α_{Mask})	0.1
Mask-Pupil Distance (t_{En})	1518.73 mm
Exposure Width (w_{Mask})	8 mm
Number of Arrays (N_P)	51
Initial Conditions	
t_P	250 mm
t_F	80 mm
t_L	400 mm
t_{L1}	300 mm
t_{L2}	400 mm

Table 9: Initial evaluation of the governing equations using specification and initial conditions provided in Table 8.

	EFL (mm)	Thickness (mm)
Collimated LPP	-	-
Pupil Array	250.0	250
Grid Source	-	80
Field Array	-92.7	400
Field Lens 1	1375.4	300
Field Lens 2	636.9	400

obtained, listed in Table 9.

4.2.2 Resolving Obstructions

A paraxial layout of the optical system described by the initial evaluation is shown in Figure 67, resulting in an obstructed system, as would be expected from an arbitrary initial evaluation.

For a single instance between a mirror and a neighboring ray bundle, the obstruction is defined as the angle of the obstructed region as illustrated in Figure 68. To resolve the obstruction, a random walk optimizing algorithm as devised in a previous work by the

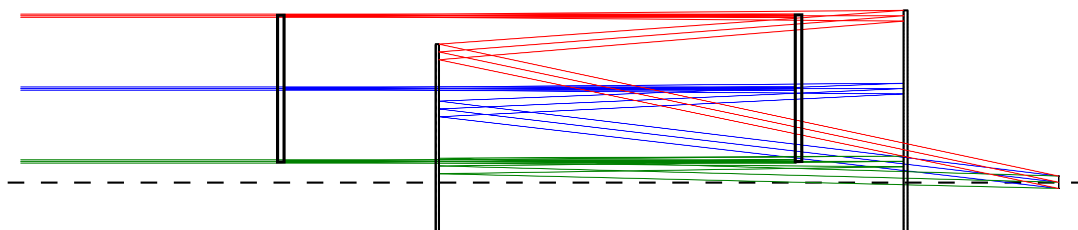

Figure 67: An initial evaluation of the governing equations.

doi:10.6342/NTU201901098

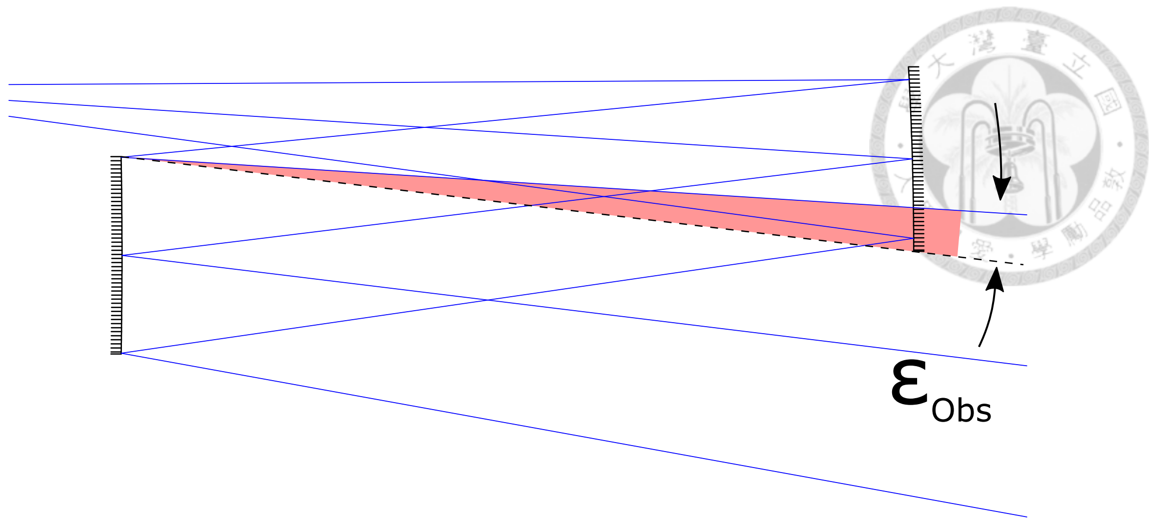

Figure 68: The amount of obstruction between a ray bundle and mirror is defined as the angle of the overlapping region. [5]

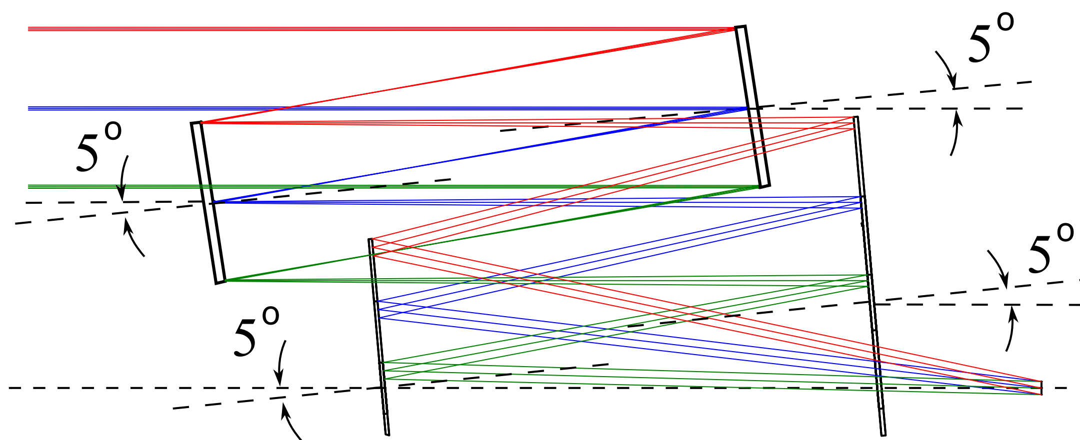

Figure 69: The same initial evaluation with a 5° tilt introduced.

author [46] is used to mitigate the obstructions, using the governing equations 117 to 120 as the kernel and setting the total amount of obstruction present in the system as the error function of the algorithm.

As fewer number of optical elements are desired in the illuminator, simply adjusting the mirror spacings and focal lengths may not be enough to fully resolve the obstructions. As such, element tilts and decenters are introduced to assist in the mitigation of the obstructions. Figure 69 shows the same result from the initial evaluation, however with a 5° tilt applied to each of the mirrors. An obstruction resolved solution of the illuminator is shown in Figure 70, with parameters listed in Table 10.

doi:10.6342/NTU201901098

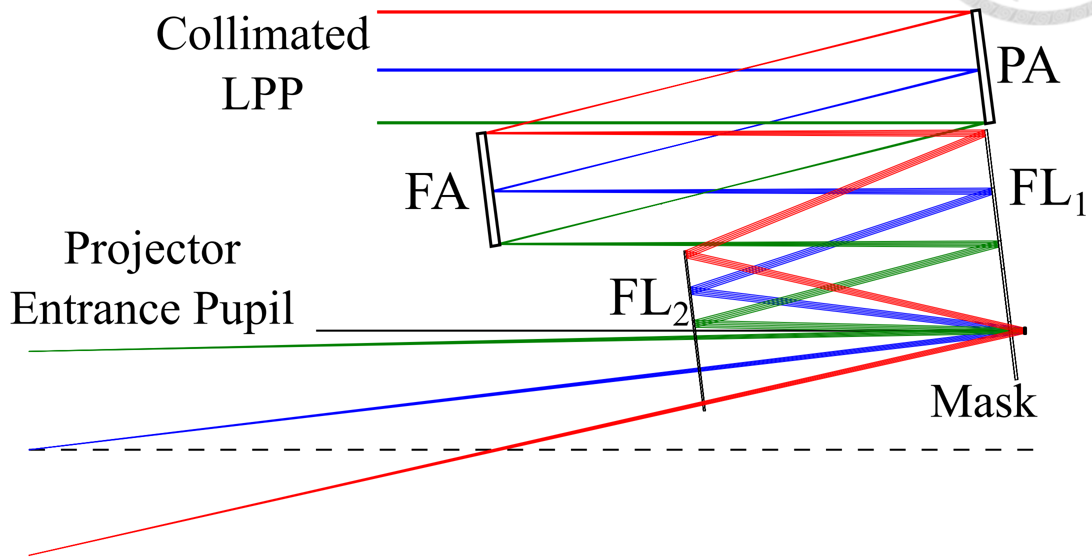

Figure 70: Obstruction resolved paraxial layout. The tilt angle required is $\theta_{tilt} = 6.991°$.

Table 10: Obstruction resolved illuminator parameters.

	EFL (mm)	Thickness (mm)
Collimated LPP	-	-
Pupil Array	506.4	510.2
Grid Source	-	255.1
Field Array	433.6	774.4
Field Lens 1	1274.4	478.5
Field Lens 2	1324.1	502.2
Mask	-	-
Element Tilt Angle	6.991°	

doi:10.6342/NTU201901098

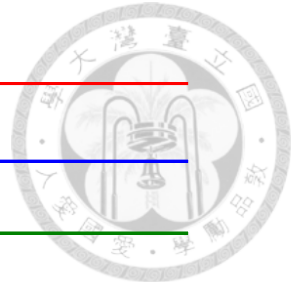

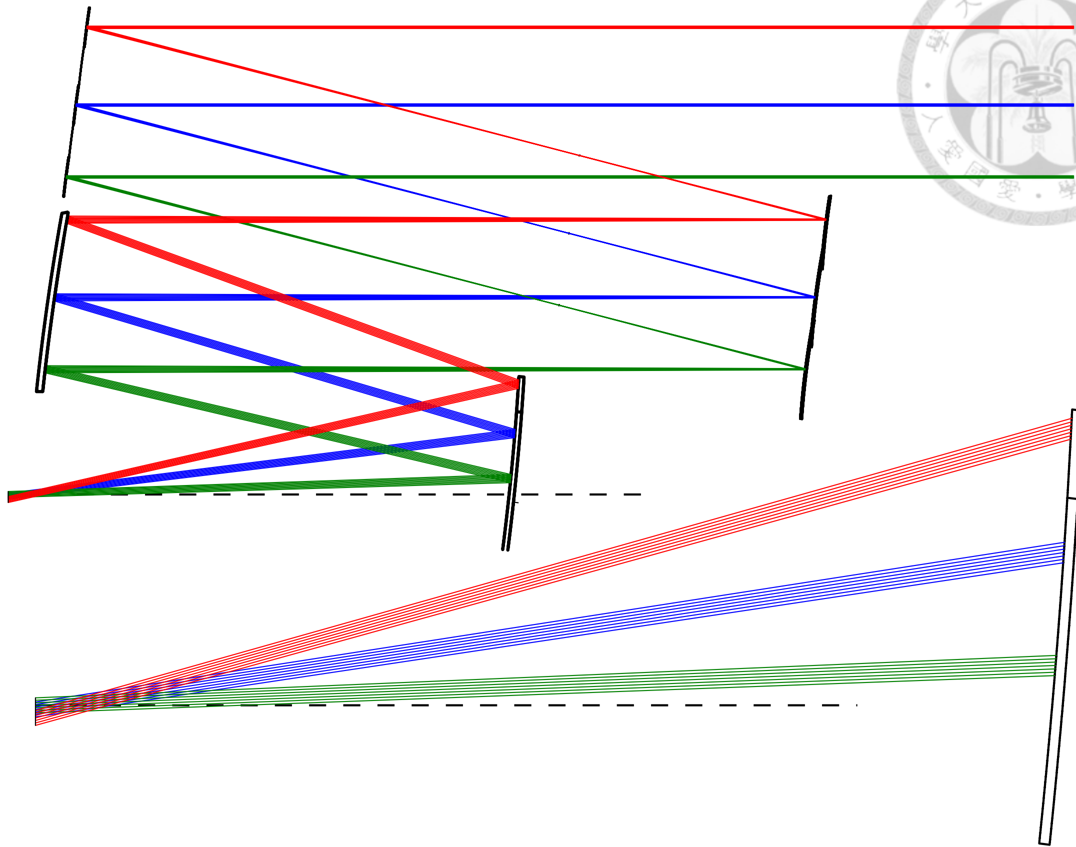

Figure 71: Direct conversion from the paraxial result. The lower zoomed in part shows that aberration resultant from the plain spherical mirror offsets the illumination profile from different array elements.

4.3 Reflective Illuminator System Embodiment

4.3.1 Illuminator Design Result

After resolving the obstructions, the resultant paraxial results can be converted to actual mirror surface geometries (i.e. radius of curvatures) through the relationship

$$R_n = -2 \cdot EFL_n. \tag{121}$$

During the conversion, deviation from paraxial calculations is inevitable, due to the presence of optical aberrations. Figure 71 shows the illuminator design resulting from a direct conversion from the paraxial parameters, and as can be clearly seen in the lower magnified portion of the ray trace diagram, at the mask, the illuminated field from different array elements do not overlap as was predicted by the paraxial system.

To address this issue, a small compensation tilt is introduced to the field array, and

doi:10.6342/NTU201901098

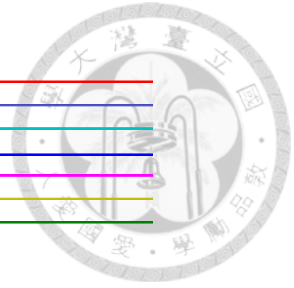

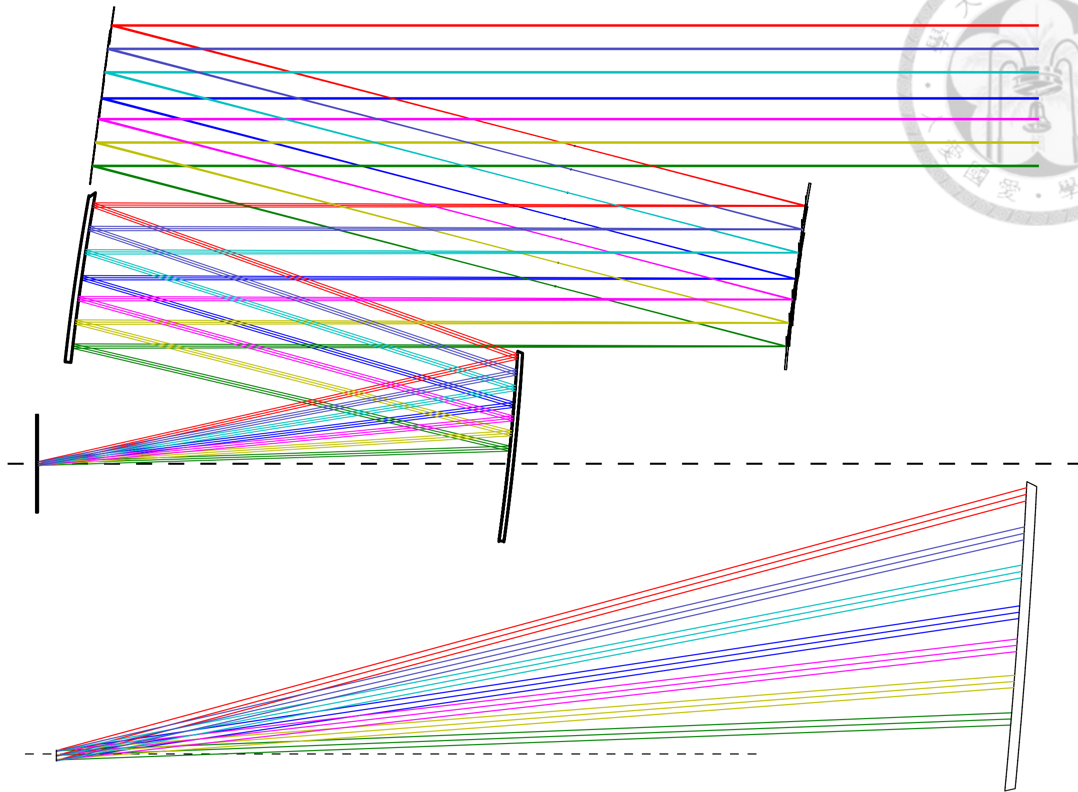

Figure 72: The aberration corrected illuminator.

the mirror surface of the field lens is changed to a more complex conic profile. A quick optimization sun by setting the chief ray deviation on the mask as the error function yields the corrected result, shown in Figure 72. The required compensation parameters are given in Table 11.

Table 11: Obstruction resolved illuminator parameters.

	Radius	Conic Constant
Pupil Array	-1012.7	-
Field Array	-867.1	-
Field Lens 1	-2548.7	-19.314
Field Lens 2	-2648.2	13.124
FA Tilt Adjust	Array Element	Angle
	Uppermost	0.045°
	Middle	0.013°
	Lowermost	0.035°

doi:10.6342/NTU201901098

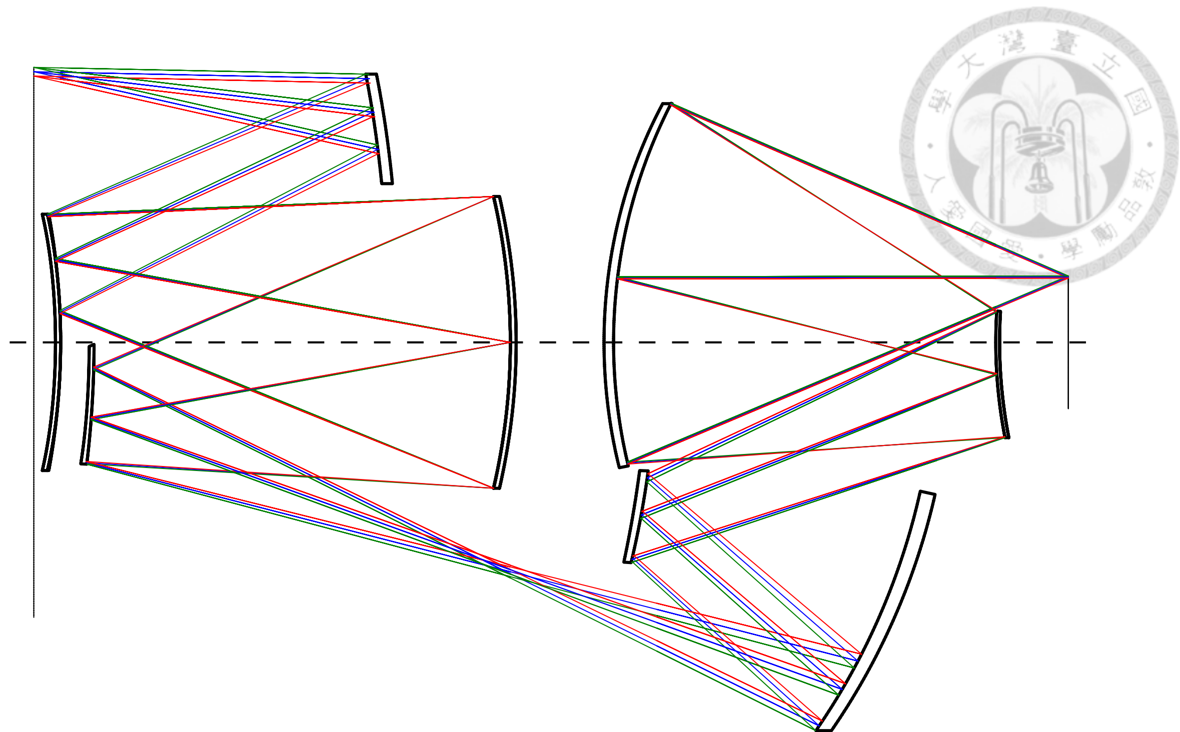

Figure 73: The eight mirror projector design from which the illuminator specifications are derived from.

4.4 Illuminator Projector Integration

At the final step, the illuminated mask is imaged by the projector. Shown in Figure 73 is the lens layout of the projection tool for which the specifications of the illuminator are derived from. The result of the illuminator-projector integration is shown in Figure 74, and Figure 75 is the illumination profile at the mask side and the wafer end respectively. As can be seen in Figure 74, the illuminator matches well with the projector. In this demonstration of the illuminator design, for the explicit purpose of integration with an existing projector design, the lens data of a projector design in a previous work by the authors [5] (Figure 73) is used. As such, important optical properties of the projector (i.e. entrance pupil location and size, and designed mask height) can be known exactly, to ensure that the resultant illuminator designed matches with the projector.

Between projector layout (Figure 73) and the combined layout (Figure 74), one might notice a difference in the color of the rays shown, which is the result of the color code used by the optics software. In the projector layout, different ray colors represents light originating from different points on the mask. In the combined layout, the different ray colors now represent light originating from the light reflecting off different array elements

doi:10.6342/NTU201901098

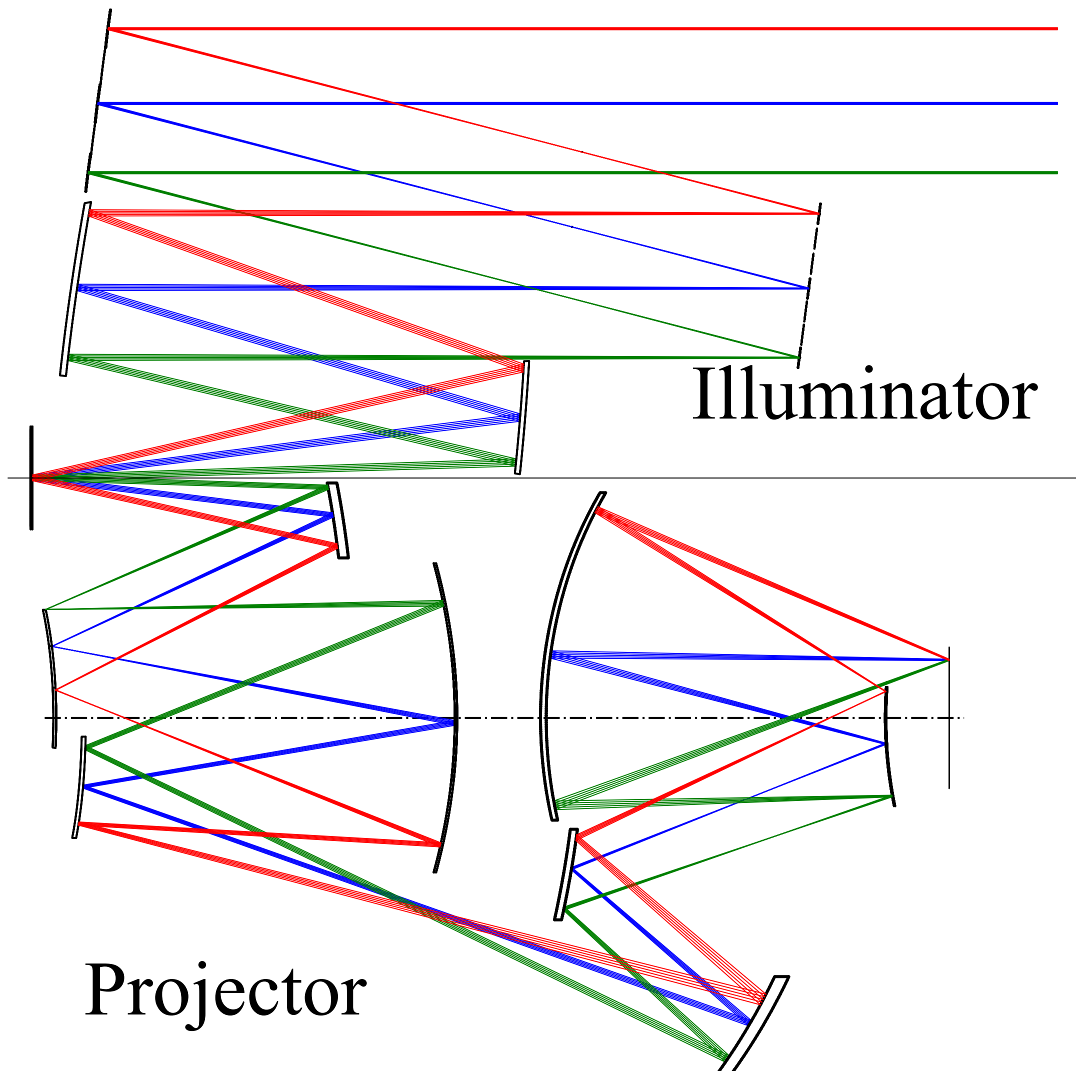

Figure 74: The combined system of the illuminator and the projector.

doi:10.6342/NTU201901098

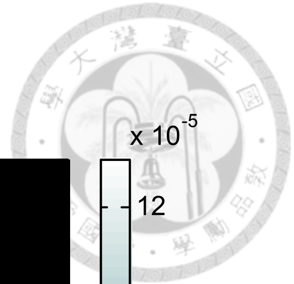

Figure 75: **Upper**: The resultant ringfield illumination profile at the mask side. **Lower**: The illumination profile at the wafer end.

doi:10.6342/NTU201901098

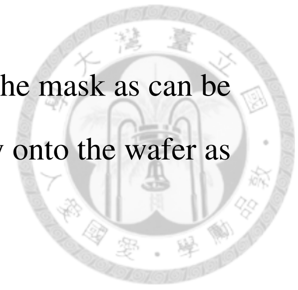

on the pupil array and field array, which is distributed uniformly onto the mask as can be seen in the illuminator layout (Figure 72), and therefore also uniformly onto the wafer as imaged by the projector.

doi:10.6342/NTU201901098

5 Conclusion

A systematic design method for both the EUVL projector and the illuminator has been described. For the projector, an eight mirror design with 0.4 NA has been demonstrated to verify the capability of this design method. This novel application of GGC on EUVL tool design is beneficial in that the relationship between optical properties and requirements can be derived through GGC and implemented into existing optical design software to assist the design process. With GGC, complex optical systems can be analyzed in greater depth, and in relative ease to conventional ABCD matrix.

For the illuminator, using GGC, the optical properties of various parts of the illuminator can be derived, and can be combined to form a general governing equation that, if followed, guarantees the desired optical properties. For simple optical system of few elements, the application of GGC analysis may be overly cumbersome and redundant, however for complex optical systems such as the EUVL illuminator and projector tool, GGC greatly eases the analysis and design difficulty.

Using the obtained governing equations as the kernel, an unobstructed illuminator design can be obtained through application of the Monte Carlo random walk algorithm, and can be implemented into existing optical design software to assist in the optical system optimization.

As a design example, the illuminator specifications are derived from the optical properties of an existing projection tool design (author's previous work [5]). The result of the illuminator design matches well to the projector specs and properties, and is demonstrated to perform well in providing the necessary illumination as required for the projection tool.

 doi:10.6342/NTU201901098

6 References

References

[1] R. Kerth, K. Jain, and M. Latta, "Excimer laser projection lithography on a full-field scanning projection system," *IEEE electron device letters* **7**(5), pp. 299–301, 1986.

[2] D. M. Williamson, "Evolution of ring-field systems in microlithography," in *International Optical Design Conference 1998*, **3482**, pp. 369–377, International Society for Optics and Photonics, 1998.

[3] H. Komori, G. Soumagne, H. Hoshino, T. Abe, T. Suganuma, Y. Imai, A. Endo, and K. Toyoda, "Ion damage analysis on euv collector mirrors," in *Microlithography 2004*, pp. 839–846, International Society for Optics and Photonics, 2004.

[4] S. Braun, T. Foltyn, L. van Loyen, M. Moss, and A. Leson, "Multi component euv multilayer mirrors," in *Proceedings of SPIE*, **5037**, pp. 274–285, 2003.

[5] L.-J. Hsiao and H. Y. Lin, "Reflective euvl tool design with generalized gaussian constant mathematics," *Appl. Opt.* **57**, pp. 5884–5892, Jul 2018.

[6] C. Mack, *Fundamental principles of optical lithography: the science of microfabrication*, John Wiley & Sons, 2008.

[7] A. Tobey, "Wafer stepper steps up yield and resolution in ic lithography," *Electronics* **52**(17), pp. 109–112, 1979.

[8] J. Lyman, "Optical lithography refuses to die," *Electronics* **58**(40), pp. 36–39, 1985.

[9] G. E. Moore *et al.*, "Cramming more components onto integrated circuits," 1965.

[10] G. E. Moore *et al.*, "Progress in digital integrated electronics," in *Electron Devices Meeting*, **21**, pp. 11–13, 1975.

doi:10.6342/NTU201901098

[11] G. E. Moore, "Lithography and the future of moore's law," in *Integrated Circuit Metrology, Inspection, and Process Control IX*, **2439**, pp. 2–18, International Society for Optics and Photonics, 1995.

[12] D. R. Shafer, "Lens usable in the ultraviolet," Sept. 13 1988. US Patent 4,770,477.

[13] J. Braat, "Quality of microlithographic projection lenses," in *Optical Microlithographic Technology for Integrated Circuit Fabrication and Inspection*, **811**, pp. 22–31, International Society for Optics and Photonics, 1987.

[14] H. Matsuzawa, M. Kobayashi, K. Endo, and Y. Suenaga, "Projection optical system and exposure apparatus using the same," Nov. 10 1998. US Patent 5,835,285 A.

[15] Y. Suenaga and K. Yamaguchi, "Projection optical system and method of using such system for manufacturing devices," July 27 1999. US Patent 5,930,049.

[16] D. Shafer and S. Beder, "Projection optical system and method," Nov. 27 2007. US Patent 7,301,707.

[17] W. Ulrich, H.-J. Rostalski, and R. Hudyma, "The development of dioptric projection lenses for deep ultraviolet lithography," *Optical review* **10**(4), pp. 233–240, 2003.

[18] D. Williamson, "Catadioptric microlithographic reduction lenses," *Proc. IODC* **22**, 1994.

[19] S. Hashimoto, Y. Suenaga, and Y. Ichihara, "Catadioptric reduction projection optical system," Dec. 1 1998. US Patent 5,844,728.

[20] J. C. Perrin, A. Epple, and W. Ulrich, "Catadioptric reduction lens," July 20 2004. US Patent 6,765,729.

[21] T. Kato, C. Terasawa, and H. Shinonaga, "Catadioptric projection optical system, exposure apparatus having the same, device fabrication method," Feb. 9 2006. US Patent App. 11/196,378.

doi:10.6342/NTU201901098

[22] D. R. Shafer, H. Beierl, G. Fürter, K.-H. Schuster, and W. Ulrich, "Catadioptric optical system and exposure apparatus having the same," Dec. 17 2002. US Patent 6,496,306.

[23] Y. Omura, H. Ikezawa, and D. M. Williamson, "Projection optical system and method for photolithography and exposure apparatus and method using same," Mar. 04 2004. WO/2004/019128.

[24] D. R. Shafer, A. Epple, A. Dodoc, H. Beierl, and W. Ulrich, "Catadioptric projection objective with geometric beam splitting," Feb. 7 2006. US Patent 6,995,930.

[25] J. W. Goodman, *Introduction to Fourier optics*, Roberts and Company Publishers, 2005.

[26] A. Jain, "Super-resolution imaging system," Aug. 14 1979. US Patent 4,164,788.

[27] H. I. Smith, E. H. Anderson, and M. L. Schattenburg, "Lithography mask with a π-phase shifting attenuator," Dec. 26 1989. US Patent 4,890,309.

[28] Y. Pati and T. Kailath, "Phase-shifting masks for microlithography: automated design and mask requirements," *JOSA A* **11**(9), pp. 2438–2452, 1994.

[29] H. Gross, B. Dörband, and H. Müller, *Handbook of optical systems*, vol. 4, Wiley Online Library, 2005.

[30] V. Banine, J. P. Benschop, M. Leenders, and R. Moors, "Relationship between an euv source and the performance of an euv lithographic system," in *Microlithography 2000*, pp. 126–135, International Society for Optics and Photonics, 2000.

[31] A. Endo, "High-average power euv light source for the next-generation lithography by laser-produced plasma," *Selected Topics in Quantum Electronics, IEEE Journal of* **10**(6), pp. 1298–1306, 2004.

[32] Schott®, "Zerodur® zero expansion glass ceramic." http://www.schott.com / advanced_optics / english / download / schott_zerodur_katalog_july_2011_en.pdf. Accessed: 2016-05-17.

doi:10.6342/NTU201901098

[33] Corning®, "Corning® ule® 7973 low expansion glass." https://www.corning.com / media / worldwide / csm / documents / 7973 Product Brochure 2015_07_21.pdf. Accessed: 2016-05-17.

[34] M. Bal, F. Bociort, and J. J. Braat, "The influence of multilayers on the optical performance of extreme ultraviolet projection systems," in *International Optical Design Conference 2002*, pp. 149–157, International Society for Optics and Photonics, 2002.

[35] H. Gross, W. Singer, and M. Totzeck, *Handbook of optical systems*, vol. 1, Wiley Online Library, 2005.

[36] K. Tanaka, "Ii paraxial theory in optical design in terms of gaussian brackets," *Progress in Optics* **23**, pp. 63–111, 1986.

[37] M. Herzberger, "Gaussian optics and gaussian brackets*†," *JOSA* **33**(12), pp. 651–655, 1943.

[38] M. F. Bal, F. Bociort, and J. J. Braat, "Analysis, search, and classification for reflective ring-field projection systems," *Applied optics* **42**(13), pp. 2301–2311, 2003.

[39] F. Liu and Y. Li, "Grouping design of eight-mirror projection objective for high-numerical aperture euv lithography," *Applied optics* **52**(29), pp. 7137–7144, 2013.

[40] R. Voelkel and K. J. Weible, "Laser beam homogenizing: limitations and constraints," in *Optical Fabrication, Testing, and Metrology III*, **7102**, p. 71020J, International Society for Optics and Photonics, 2008.

[41] M. Antoni, W. Singer, J. Schultz, J. Wangler, I. Escudero-Sanz, and B. Kruizinga, "Illumination optics design for euv lithography," in *Soft X-Ray and EUV Imaging Systems*, **4146**, pp. 25–35, International Society for Optics and Photonics, 2000.

[42] S. C. Park and R. R. Shannon, "Zoom lens design using lens modules," *Optical Engineering* **35**(6), pp. 1668–1676, 1996.

[43] V. CODE, "Reference manuals,(version 10.6)," *Synopsys OSG* , 2014.

doi:10.6342/NTU201901098

[44] R. Zemax, "Zemax user's manual," *July* , 2011.

[45] T. Suzuki and Y. Ichioka, "Automatic lens design," *Applied Physics* **33**(10), pp. 698–706, 1964.

[46] L.-J. Hsiao and H.-Y. Lin, "Extreme ultra violet lithographic optical projection system design method using code v lens module and generalized gaussian constants," in *International Conference on Extreme Ultraviolet Lithography 2017*, **10450**, p. 1045021, International Society for Optics and Photonics, 2017.

doi:10.6342/NTU201901098

7 Appendices

7.1 GGC Implementation into MATLAB

The following is an implementation of the Gaussian bracket in the MATLAB environment, which can be used to assistance with simple analysis of an optical system.

Basic Definition

```
% ===============================================
function out = gb_base(in);
s = size(in);
m = s(2);
if m==0; out = 1; end
if m==1; out = in; end
if m==2; out = in(:,1).*in(:,2)+1; end
if m==3; out = in(:,1) + in(:,3) + in(:,1).*in(:,2).*in(:,3); end
% ===============================================
```

Gaussian Bracket

```
% ===============================================
function out = gbracket(in);
s = size(in);
n = s(2);
if n < 4; out = gb_base(in);
else
    temp = in;
    c1 = temp(:,1);
    c2 = ones(s(1),1);
    temp1 = temp; temp1(:,1)=[];
    temp2 = temp; temp2(:,[1 2])=[];
    stopflag = 0;
    while stopflag == 0;
        c1_ = gb_base(temp1(:,1:2)).*c1 + temp2(:,1).*c2;
        c2_ = temp1(:,1).*c1 + c2;
        c1 = c1_;
        c2 = c2_;
        temp1(:,[1 2])=[];
        temp2(:,[1 2])=[];
        s = size(temp2); n = s(2);
        if n < 3; stopflag = 1; end
    end
    out = c1.*gb_base(temp1) + c2.*gb_base(temp2);
end
% ===============================================
```


doi:10.6342/NTU201901098

7.2 GGC Implementation into Code V

The codes demonstrated in this section is an implementation of the Gaussian bracket and GGC into the commercial optics design software CodeV. This can be used to enhance and finetune its already powerful optical design and analysis capability, allowing for more precise and minute control of a complex optical system, where the optical properties of individual subsystem within the entire system is of importance.

Basic Definition

```
FCT @gb_base(NUM ^gb_base_in(100), NUM ^gb_base_ind)
 IF ^gb_base_ind = 4;
   ^gb_base_out ==
    ^gb_base_in(1)*^gb_base_in(2)*^gb_base_in(3)*^gb_base_in(4)
    + ^gb_base_in(1)*^gb_base_in(4) + ^gb_base_in(3)*^gb_base_in(4)
    + ^gb_base_in(1)*^gb_base_in(2) + 1;
  ELS IF ^gb_base_ind = 3;
   ^gb_base_out == ^gb_base_in(1) + ^gb_base_in(3)
    + ^gb_base_in(1)*^gb_base_in(2)*^gb_base_in(3);
  ELS IF ^gb_base_ind = 2;
   ^gb_base_out == ^gb_base_in(1)*^gb_base_in(2) + 1;
  ELS IF ^gb_base_ind = 1;
   ^gb_base_out == ^gb_base_in(1);
  ELS IF ^gb_base_ind = 0;
   ^gb_base_out == 1;
 END IF
END FCT ^gb_base_out
```

Gaussian Bracket

```
! ============================================== Begin Code
FCT @gbrac(NUM ^gb_in(100), NUM ^gb_ind)
^gb_c1 == ^gb_in(1);
^gb_c2 == 1;
^gb_flag == 0;
^gb_n == 1;
IF ^gb_ind > 4;
  WHI ^gb_flag = 0;
    ^gb_v0(1) == ^gb_in(2*^gb_n);
    ^gb_v0(2) == ^gb_in(2*^gb_n+1);
    ^gb_c1_ == @gb_base(^gb_v0,2)*^gb_c1
              + ^gb_in(2*^gb_n+1)*^gb_c2;
    ^gb_c2_ == ^gb_in(2*^gb_n)*^gb_c1 + ^gb_c2;
    ^gb_c1 == ^gb_c1_;
    ^gb_c2 == ^gb_c2_;
```


doi:10.6342/NTU201901098

```
    ^gb_n == ^gb_n+1;
    IF (^gb_ind-(2*^gb_n)) = 2;
        ^gb_flag == 1;
        ^gb_v1(1) == ^gb_in(2*^gb_n)
        ^gb_v1(2) == ^gb_in(2*^gb_n+1)
        ^gb_v1(3) == ^gb_in(2*^gb_n+2)
        ^gb_v2(1) == ^gb_in(2*^gb_n+1)
        ^gb_v2(2) == ^gb_in(2*^gb_n+2)
        ^gb_out == ^gb_c1*@gb_base(^gb_v1,3)
                    + ^gb_c2*@gb_base(^gb_v2,2);
    END IF
    IF (^gb_ind-(2*^gb_n)) = 1;
        ^gb_flag == 1;
        ^gb_v1(1) == ^gb_in(2*^gb_n)
        ^gb_v1(2) == ^gb_in(2*^gb_n+1)
        ^gb_v2(1) == ^gb_in(2*^gb_n+1)
        ^gb_out == ^gb_c1*@gb_base(^gb_v1,2)
                    + ^gb_c2*@gb_base(^gb_v2,1);
    END IF
  END WHI
ELS
  ^gb_out == @gb_base(^gb_in,^gb_ind)
END IF
END FCT ^gb_out
! =============================================== End Code
```

Generalized Gaussian Constants

```
!! ============================================== Begin Code
FCT @c(NUM ^i, NUM ^j) ! -------------- GGC (C)
FOR ^k ^i (^j-1) 1
  ^c_v(^k*2-1) == ((IND S^k)-(IND S^k-1))/(RDY S^k);
  ^c_v(^k*2) == -(THI S^k)/(IND S^k);
END FOR
^c_v(^j*2-1) == ((IND S^j)-(IND S^j-1))/(RDY S^j);
^c_out == @gbrac(^c_v, (^j-^i+1)*2-1);
END FCT ^c_out
FCT @a(NUM ^i, NUM ^j) ! -------------- GGC (A)
FOR ^k ^i (^j-1) 1
  ^a_v(^k*2-1) == ((IND S^k)-(IND S^k-1))/(RDY S^k);
  ^a_v(^k*2) == -(THI S^k)/(IND S^k);
END FOR
^a_out == @gbrac(^a_v, (^j-^i+1)*2-2);
END FCT ^a_out
FCT @b(NUM ^i, NUM ^j) ! -------------- GGC (B)
^b_v(1) == -(THI S^i)/(IND S^i);
FOR ^k (^i+1) (^j-1) 1
  ^b_v(^k*2-2) == ((IND S^k)-(IND S^k-1))/(RDY S^k);
```


doi:10.6342/NTU201901098

```
  ^b_v(^k*2-1) == -(THI S^k)/(IND S^k);
END FOR
^b_out == @gbrac(^b_v, (^j-^i+1)*2-3);
END FCT ^b_out
FCT @d(NUM ^i, NUM ^j) ! -------------- GGC (D)
^d_v(1) == -(THI S^i)/(IND S^i);
FOR ^k (^i+1) (^j-1) 1
  ^d_v(^k*2-2) == ((IND S^k)-(IND S^k-1))/(RDY S^k);
  ^d_v(^k*2-1) == -(THI S^k)/(IND S^k);
END FOR
^d_v(^j*2-2) == ((IND S^j)-(IND S^j-1))/(RDY S^j);
^d_out == @gbrac(^d_v, (^j-^i+1)*2-2);
END FCT ^d_out
!! ============================================== End Code
```


doi:10.6342/NTU201901098

7.3 GGC Implementation into Zemax

The codes detailed in this section implements the ability to evaluate the GGC of the current optical system, and any arbitrary subsystems within, as a merit function operand in ZEMAX.

```
##==========================================================##
## Integration of GGC into ZEMAX
##==========================================================##
DECLARE gb_base_in, DOUBLE,1,4
DECLARE gb_in, DOUBLE,1,100

s1 = PVHX()
s2 = PVHY()
ggc_ind = PVPX()

IF ggc_ind==1
  GOSUB GGC_A
ENDIF
IF ggc_ind==2
  GOSUB GGC_B
ENDIF
IF ggc_ind==3
  GOSUB GGC_C
ENDIF
IF ggc_ind==4
  GOSUB GGC_D
ENDIF

OPTRETURN 0, out
END

#=================================================# Sub-Routines
SUB GGC_A
  FOR k,s1,s2-1,1
    ind1 = 2*(k-s1)+1
    ind2 = 2*(k-s1)+2
    gb_in(ind1) == ( INDX(k)-INDX(k-1) ) * CURV(k)
    gb_in(ind2) = -THIC(k) / INDX(k)
  NEXT
  gb_ind = 2*(s2-s1)
  GOSUB GBracket
  out = gb_out
RETURN

SUB GGC_B      # FCT   @b   (NUM ^i, NUM ^j)
  gb_in(1) = -THIC(s1) / INDX(s1);
```


doi:10.6342/NTU201901098

```
  FOR k, s1+1, s2-1, 1
    ind1 = 2*(k-s1)
    ind2 = 2*(k-s1)+1
    gb_in(ind1) = ( INDX(k)-INDX(k-1) ) * CURV(k)
    gb_in(ind2) = -THIC(k) / INDX(k)
  NEXT
  gb_ind = 2*(s2-s1)-1
  GOSUB GBracket
  out = gb_out
RETURN

SUB GGC_C
  FOR k,s1,s2-1,1
    ind1 = 2*(k-s1)+1
    ind2 = 2*(k-s1)+2
    gb_in(ind1) = ( INDX(k)-INDX(k-1) ) * CURV(k)
    gb_in(ind2) = -THIC(k) / INDX(k)
  NEXT
  ind3 = 2*(s2-s1)+1
  gb_in(ind3) = ( INDX(s2)-INDX(s2-1) ) * CURV(s2)
  gb_ind = 2*(s2-s1)+1
  GOSUB GBracket
  out = gb_out
RETURN

SUB GGC_D
  FOR k, s1+1, s2, 1
    ind1 = 2*(k-s1)-1
    ind2 = 2*(k-s1)
    gb_in(ind1) = -THIC(k-1) / INDX(k-1)
    gb_in(ind2) = ( INDX(k)-INDX(k-1) ) * CURV(k)
  NEXT
  gb_ind = 2*(s2-s1)
  GOSUB GBracket
  out = gb_out
RETURN

SUB GBracket
  gb_c1 = gb_in(1)
  gb_c2 = 1
  gb_flag = 0
  gb_n = 1
  IF gb_ind > 4;
    LABEL gb_flag_0
        gb_base_in(1) = gb_in(2*gb_n);
        gb_base_in(2) = gb_in(2*gb_n+1);
        gb_base_ind = 2
        GOSUB GB_Base
```


doi:10.6342/NTU201901098

```
      temp = gb_base_out
      gb_c1_temp = temp*gb_c1 + gb_in(2*gb_n+1)*gb_c2;
      gb_c2_temp = gb_in(2*gb_n)*gb_c1 + gb_c2;
      gb_c1      = gb_c1_temp;
      gb_c2      = gb_c2_temp;
      gb_n       = gb_n+1;
      det_gb_ind = gb_ind-(2*gb_n)
      IF det_gb_ind == 2;
        gb_flag  = 1;
          gb_base_in(1) = gb_in(2*gb_n)
          gb_base_in(2) = gb_in(2*gb_n+1)
          gb_base_in(3) = gb_in(2*gb_n+2)
          gb_base_ind = 3
          GOSUB GB_Base
          temp1 = gb_base_out
          gb_base_in(1) = gb_in(2*gb_n+1)
          gb_base_in(2) = gb_in(2*gb_n+2)
          gb_base_ind = 2
          GOSUB GB_Base
          temp2 = gb_base_out
        gb_out   = gb_c1*temp1 + gb_c2*temp2
      ENDIF
      IF det_gb_ind == 1;
        gb_flag  = 1;
          gb_base_in(1) = gb_in(2*gb_n)
          gb_base_in(2) = gb_in(2*gb_n+1)
          gb_base_ind = 2
          GOSUB GB_Base
          temp1 = gb_base_out
          gb_base_in(1) = gb_in(2*gb_n+1)
          gb_base_ind = 1
          GOSUB GB_Base
          temp2 = gb_base_out
        gb_out   = gb_c1*temp1 + gb_c2*temp2
      ENDIF
    IF gb_flag == 0
      GOTO gb_flag_0
    ENDIF
  ELSE
      gb_base_in(1) = gb_in(1)
      gb_base_in(2) = gb_in(2)
      gb_base_in(3) = gb_in(3)
      gb_base_in(4) = gb_in(4)
      gb_base_ind   = gb_ind
      GOSUB GB_Base
    gb_out = gb_base_out
  ENDIF
RETURN
```


doi:10.6342/NTU201901098

```
SUB GB_Base
  IF gb_base_ind == 0
    gb_base_out = 1
  ENDIF
  IF gb_base_ind == 1
    gb_base_out = gb_base_in(1)
  ENDIF
  IF gb_base_ind == 2
    gb_base_out = gb_base_in(1)*gb_base_in(2) + 1
  ENDIF
  IF gb_base_ind == 3
    gb_base_out = gb_base_in(1) + gb_base_in(3) +
                  gb_base_in(1)*gb_base_in(2)*gb_base_in(3)
  ENDIF
  IF gb_base_ind == 4
    gb_base_out =
       gb_base_in(1)*gb_base_in(2)*gb_base_in(3)*gb_base_in(4) +
       gb_base_in(1)*gb_base_in(4) + gb_base_in(3)*gb_base_in(4) +
       gb_base_in(1)*gb_base_in(2) + 1;
  ENDIF
RETURN
```


doi:10.6342/NTU201901098